AFOSR 65-1917

AF-AFOSR-812-65

OCT 14 1965

FIFTH RARE EARTH RESEARCH CONFERENCE

AUGUST 30, 31, SEPTEMBER 1, 1965

sponsored by Institute for Atomic Research, Iowa State University and Air Force Office of Scientific Research - Directorate of Chemical Sciences

CLEARINGHOUSE
FOR FEDERAL SCIENTIFIC AND
TECHNICAL INFORMATION
Hardcopy | Microfiche
$4.00 | 0.75 | 112 | as
ARCHIVE COPY

Book Two

Cycle 1

solid state session P-1

DISCLAIMER NOTICE

THIS DOCUMENT IS BEST QUALITY PRACTICABLE. THE COPY FURNISHED TO DTIC CONTAINED A SIGNIFICANT NUMBER OF PAGES WHICH DO NOT REPRODUCE LEGIBLY.

CONTENTS

Solid State Session P-1

Page

Initial Susceptibility Investigation of Magnetic Transitions in Several Rare Earth Metals: Thermal Hysteresis in Ferromagnetic Transitions
F. J. Jelinek, E. D. Hill and B. C. Gerstein 1

Distribution of Magnetic Moment Density in Tb
O. Steinsvoll, G. Shirane, R. Nathans..... 15

Magnetostriction in the Heavy Rare Earth Metals
B. F. DeSavage and A. E. Clark..... 23

Observation of Optical Absorption Bands Associated with Magnetic Order in Rare-Earth Metals
C. Chr. Schuler..... 35

Infrared Absorption Structure in Rare Earth Metals: Relationship to Spin Arrangement and Band Structure
B. R. Cooper and R. W. Redington..... 45

Electron-Spinwave Scattering in Gadolinium
B. Lüthi and H. Rohrer..... 55

Thermal Conductivity and Electrical Resistivity of Samarium at Low Temperatures
Sigurds Arajs and G. R. Dunmyre..... 63

Results of Augmented Plane Wave Calculations of the Band Structure of Cerium Metal
J. T. Waber and A. C. Switendick 75

Theoretical Results for Positron Annihilation in Rare Earth Metals
T. L. Loucks..... 89

High Pressure Polymorphism and Magnetic Ordering in Some Sm-Type Rare Earth Alloys and Samarium
A. Jayaraman, R. C. Sherwood, and E. Corenzwit 91

Valence Bond Formation in the Close-Packed Rare Earth Metals
Forrest L. Carter..... 103

INITIAL SUSCEPTIBILITY INVESTIGATION OF MAGNETIC TRANSITIONS IN SEVERAL RARE EARTH METALS: THERMAL HYSTERESIS IN FERROMAGNETIC TRANSITIONS*

F. J. JELINEK, E. D. HILL and B. C. GERSTEIN

Institute for Atomic Research and Department of Physical Chemistry
Iowa State University, Ames, Iowa
(Work performed in the Ames Laboratory of the U. S. A. E. C.)

ABSTRACT

Thermal hysteresis of magnetic transitions in polycrystalline Gd, Tb, Dy, Ho, Tm and Sm have been investigated by an a. c. mutual inductance magnetic susceptibility technique. A thermal hysteresis effect was observed in the ferromagnetic transitions of Tb, Dy, Ho and Tm. No thermal hysteresis was observed in the magnetic transitions of Gd and Sm.

I. INTRODUCTION

Magnetic susceptibility measurements were made on several polycrystalline rare earth metals of 99.8% purity using the low field a. c. mutual inductance technique described by Hartshorn[1] with the bridge and cryostat system described by Jennings[2] and Gerstein[3] respectively. Interest in the investigation of thermal hysteresis in these metals initially arose from the discrepancy between heat capacity work in this laboratory on Sm metal and that of Roberts.[4] Roberts reported a maximum in her heat capacity versus temperature curve at 13.8°K. The work in this laboratory showed a still rising Cp versus temperature curve at 12.7°K, the lower limit of these measurements. Thermal hysteresis of the magnetic ordering process occurring in the region of the heat capacity maximum was considered to be a possible explanation of this discrepancy.

In measuring the magnetization of solid materials using a. c. methods, one must consider both dispersion and absorption. The dispersion, χ'_m, is associated with the change in mutual inductance of the sample coils per mole of sample present, and the absorption, χ''_m, is related to the a. c. losses associated with the specimen. The a. c. measurement enables one to correlate the resistive changes of the bridge with these losses. Experimentally we have observed that χ''_m is zero for $T > T_N$, the antiferromagnetic ordering temperature, from which we infer that eddy current losses are negligible in all samples measured except samarium. The eddy current losses in samarium are believed to be due to the large sample size. The a. c. losses at $T < T_N$ are therefore primarily associated with magnetic losses. Thus at $T < T_N$ we are looking at an "effective" a. c. susceptibility and can merely correlate changes in this function with heat capacity and static susceptibility work. At $T > T_N$, χ'_m rapidly approaches zero, magnetic losses become negligible and there is reasonable agreement between our measured χ'_m and static susceptibility results.

The measurements were made at fields of 10 ± 1 oersted. The bulk magnetization below the Curie point (T_C) is attributed to reversible domain wall motion, such that domains with components in the direction of the external field are enlarged and the others are reduced. (5) The sample coil of the mutual inductance bridge was calibrated using a known paramagnetic salt, $Mn(NH_4)_2(SO_4)_2 \cdot 6H_2O$. This measurement yielded a numerical coil constant which permitted the conversion of resistive and inductive changes to χ''_m and χ'_m respectively. With the exception of Sm, the average sample size measured was approximately

2×10^{-3} moles. The sensitivity of the susceptibility measurement with this size sample was such that a value of $\chi'_m = 10^{-3}$ emu/mole could be detected to within one percent.

II. RESULTS AND DISCUSSION

1) Terbium: Koehler et al.[6] performed neutron diffraction studies on single-crystals and polycrystalline Tb. They observed a transition to an antiferromagnetic state at 230°K and a subsequent transition to a ferromagnetic state at 220°K. They also found that in the antiferromagnetic region the magnetic structure of Tb is helical and the transition from the antiferromagnetic to the ferromagnetic state is centered at 224°K. Jennings et al.[7] reported a sharp anomaly in the specific heat versus temperature curve at 227.7°K and an anomolous region near 220°K which was found to depend on the thermal history of the sample (Fig. 1).

The present results are shown in Fig. 1. The measurements indicated a transition to an ordered magnetic structure at 230.5°K, in agreement with other workers. In the region of ferromagnetic order we observed a four degree thermal hysteresis effect upon heating and cooling. Data taken while heating the sample showed a maximum in χ'_m at 219.9°K and data taken while cooling showed a maximum at 215.7°K. The maximum on cooling always occurred at the same temperature regardless of the time elapsed on cooling. The heating curve was reproduced only if the sample was cooled to 77°K and allowed to stand for several hours. Otherwise, various curves would be obtained, ranging from the original heating curve to the curve representing the

sample being cooled from room temperature. Above the Néel point at 230.5°K, the heating and cooling curves coincided. The thermal hysteresis effect was also observed in the χ''_m versus temperature curve in the region of ferromagnetic ordering. The minimum in the χ'_m curve at 224°K occurs in the small but finite temperature region where Koeler et al.[6] report that the interlayer turn angle remains constant.

An extrapolation of the $1/\chi'_m$ versus T°K curve above 230°K to $1/\chi'_m = 0$ yielded a paramagnetic Curie point of 235.6°K. The a-, b-axis crystals of Heglund et al.[8] yielded a paramagnetic Curie point of 239°K. From their plot of $1/\chi$ versus T°K for a-, b-axis crystals a molar susceptibility of 185×10^{-3} emu. was calculated at 300°K. Our results yielded a molar susceptibility at 300°K of 166×10^{-3} emu.

2) Dysprosium: The results of the present work are shown in Fig. 2. Also shown are the results of heat capacity measurements on Dy metal performed in this laboratory by Griffel et al.[9] In this heat capacity work two peaks are evident, the higher of which, at 174°K, was termed reproducible and did not exhibit thermal hysteresis. The lower peak at 83.5°K does exhibit a dependence on the thermal history of the sample. Our susceptibility measurements show a transition at 179°K, the temperature at which other workers find the onset of antiferromagnetic order. In the region of ferromagnetic order we observe a thirteen degree thermal hysteresis effect. Data taken while cooling the sample from room temperature exhibited a maximum in the susceptibility versus temperature curve at 70.5°K. This cooling maximum was reproducible regardless of what temperature above the ferromagnetic

ordering temperature cooling was started. Data taken while heating the sample from 4.2°K exhibited a maximum in the susceptibility versus temperature curve at 83°K. This curve was reproducible providing the sample was allowed to remain at 4.2°K for approximately one hour before heating. Above the Néel point at 179°K, the heating and cooling curves coincided. The susceptibility data above 179°K yielded a paramagnetic Curie point of 152.5°K which agrees closely with the results of Behrendt et al.[10] and Arajs and Colvin.[11] Our results also yielded a molar susceptibility at 300°K of 115×10^{-3} emu. The molar susceptibility calculated by Arajs and Colvin at 300°K was 100×10^{-3} emu.

3) Holmium: The results of this work and the heat capacity work of Gerstein et al.[12] are shown in Fig. 3. Ho exhibits two peaks in the heat capacity curve. The higher one at 131.6°K is reproducible and exhibits no dependence on the thermal history of the sample. The lower peak at 19.4°K does exhibit thermal hysteresis, in that the height of the peak varies depending on the thermal history of the sample. The interval which exhibited thermal hysteresis ranged from 17 to 21°K. The magnetic susceptibility measurements reported here also exhibited thermal hysteresis in the region of ferromagnetic order near 20°K. As shown in Fig. 3, the transition from the paramagnetic to the antiferromagnetic state was observed to occur at 129.3°K. From about 70° below and at all temperatures above this point, the heating and cooling curves coincided. The antiferromagnetic-ferromagnetic transition, however, exhibited a 2.7° thermal hysteresis effect between heating and cooling curves. Before heating, the sample was allowed to

remain at 4.2°K for at least one hour, thereby making the heating curves reproducible. The cooling curves, like those for Dy and Tb, were reproducible regardless of the time elapsed on cooling. The maximum in the cooling curve occurred at 18°K and the maximum upon heating occurred at 20.7°K. The plots of χ''_m versus T°K exhibited maximums at very nearly the same temperature as the corresponding χ'_m plot. χ''_m also approached zero much more rapidly in Ho than in the other metals studied.

An extrapolation of the $1/\chi'_m$ data to zero at temperatures considerably above the Néel point yielded a paramagnetic Curie point of 86°K. Strandberg et al.[13] calculated the magnetic susceptibility of polycrystalline Ho from susceptibility measurements on a- and c-axis crystals. The molar susceptibility at 200°K calculated from their data is 127×10^{-3} emu. Our a.c. measurements yielded a molar susceptibility at 200°K of 138×10^{-3} emu.

4) Thulium: Previous work on the magnetic and thermal properties of Tm indicate that the metal's behavior is out of the ordinary with respect to the preceeding metals investigated in this work, namely Tb, Dy and Ho. Neutron diffraction studies by Koehler et al.[14, 15] report that polycrystalline Tm undergoes a paramagnetic to antiferromagnetic transition at 53°K and a subsequent transition to a "ferrimagnetic" type of antiphase domain structure at 38°K. A simple oscillating z-component antiferromagnetic structure is said to exist between 38 and 53°K. In the "ferrimagnetic" state the net moment is reported to be parallel to the c-axis.

The results of this work are shown in Fig. 4. Heat capacity measurements by Jennings et al.[16] are included for comparison. It is interesting to note that the heat capacity exhibits no peak below 55°K. The plots of χ'_m versus T°K in Fig. 4(a) indicate that a paramagnetic to antiferromagnetic transition occurs at 57.5°K The heating and cooling curves above this temperature coincide and no thermal hysteresis is observed at the Néel point. This is in contrast to the lambda-type anomaly in the heat capacity at 55°K which was reported to exhibit thermal hysteresis. A 2.8° thermal hysteresis is observed, however, in the region of the antiphase domain structure. The cooling curve reaches a maximum in χ'_m at 27.8°K and the heating curve reaches a maximum in χ'_m at 30.6°K. As in the previous metals discussed, the heating and cooling curves were reproducible. Fig. 4(b) illustrates the thermal hysteresis effect in plots of χ''_m versus T°K. The elbow in the curve at 37.5°K agrees well with the onset of "ferrimagnetism" as reported by Koehler et al[14] in their neutron diffraction investigation.

An extrapolation of $1/\chi'_m$ to zero yielded a paramagnetic Curie point of 17.5°K. This is in close agreement with the results of Arajs.[17] Rhodes et al.[18] obtained a molar susceptibility at 100°K of approximately 95×10^{-3} emu. Our results yielded a molar susceptibility at 100°K of 92×10^{-3} emu.

Mutual inductance magnetic susceptibility measurements were also made on Gd and Sm. No thermal hysteresis was observed near the ferromagnetic ordering temperature (292.5°K) in Gd. Likewise no thermal hysteresis was observed in the maximum obtained at 14.8°K in Sm. It has been suggested that crystallographic distortion near the

Curie point in the metals exhibiting thermal hysteresis may account for these effects.[19] The extraordinarily large magnetostriction values reported for Dy tends to correlate with the large thermal hysteresis of this metal observed in this work.

III. ACKNOWLEDGMENTS

The authors wish to acknowledge Dr. Karl Gschneidner, Jr. and Dr. F. H. Spedding for valuable discussions pertaining to this work, and Dr. L. D. Jennings whose idea it was originally to perform the above measurements.

REFERENCES

1. Hartshorn, L., J. Sci. Instr. 2, 145 (1925).
2. Jennings, L. D., Rev. Sci. Instr. 31, 1269 (1960).
3. Gerstein, B. C., U.S.A.E.C. Rept. No. IS-331.
4. Roberts, L. M., Proc. Phys. Soc. (London) B70, 476 (1957).
5. Bozorth, R. M., Rev. Mod. Phys. 19, 29 (1947).
6. Koehler, W. C., Child, H. R., Wollan, E. O. and Cable, J. W. J. Appl. Phys. 34, 1335 (1963).
7. Jennings, L. D., Stanton, R. M. and Spedding, F. H., J. Chem. Phys. 27, 909 (1957).
8. Hegland, D. E., Legvold, S. and Spedding, F. H., Phys. Rev. 131, 158 (1963).
9. Griffel, M. Skochdopole, R. E. and Spedding, F. H., J. Chem. Phys. 25, 75 (1956).
10. Behrendt, J. F., Legvold, S. and Spedding, F. H., Phys. Rev. 109, 1544 (1958).
11. Arajs, S., Colvin, R. V., J. Appl. Phys. 32, 336S (1961).
12. Gerstein, B. C., Griffel, M., Jennings, L. D., Miller, R. E., Skochdopole, R. E. and Spedding, F. H., J. Chem. Phys. 27, 394 (1957).
13. Strandburg, D. L., Legvold, S. and Spedding, F. H., Phys. Rev. 127, 2046 (1962).
14. Koehler, W. C., Cable, J. W. Wollan, E. O. and Wilkinson, M. K., Phys. Rev. 126, 1672 (1962).
15. Koehler, W. C., Cable, J. W., Wollan, E. O. and Wilkinson, M. K., J. Appl. Phys. 33, 1124 (1962).

16. Jennings, L. D., Hill, E. D. and Spedding, F. H., J. Chem. Phys. 34, 2082 (1961).

17. Arajs, S., J. Appl. Phys. 31, 323S (1960).

18. Rhodes, B. L., Legvold, S. and Spedding, F. H., Phys. Rev. 109, 1547 (1958).

19. Darnell, F. J., Phys. Rev. 130, 1825 (1963).

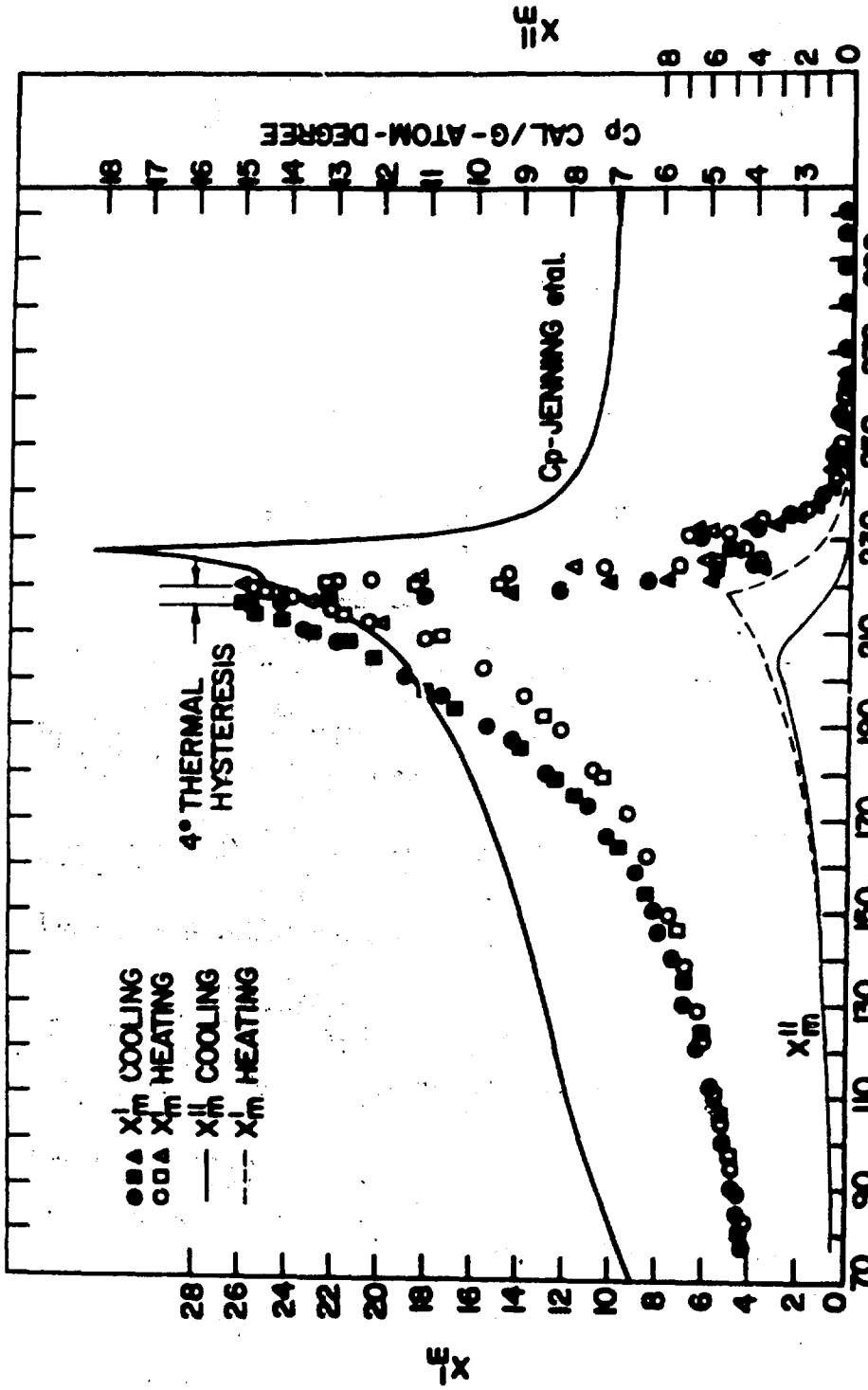

Fig. 1. χ'_m, χ''_m and C_p versus T°K for Tb metal.

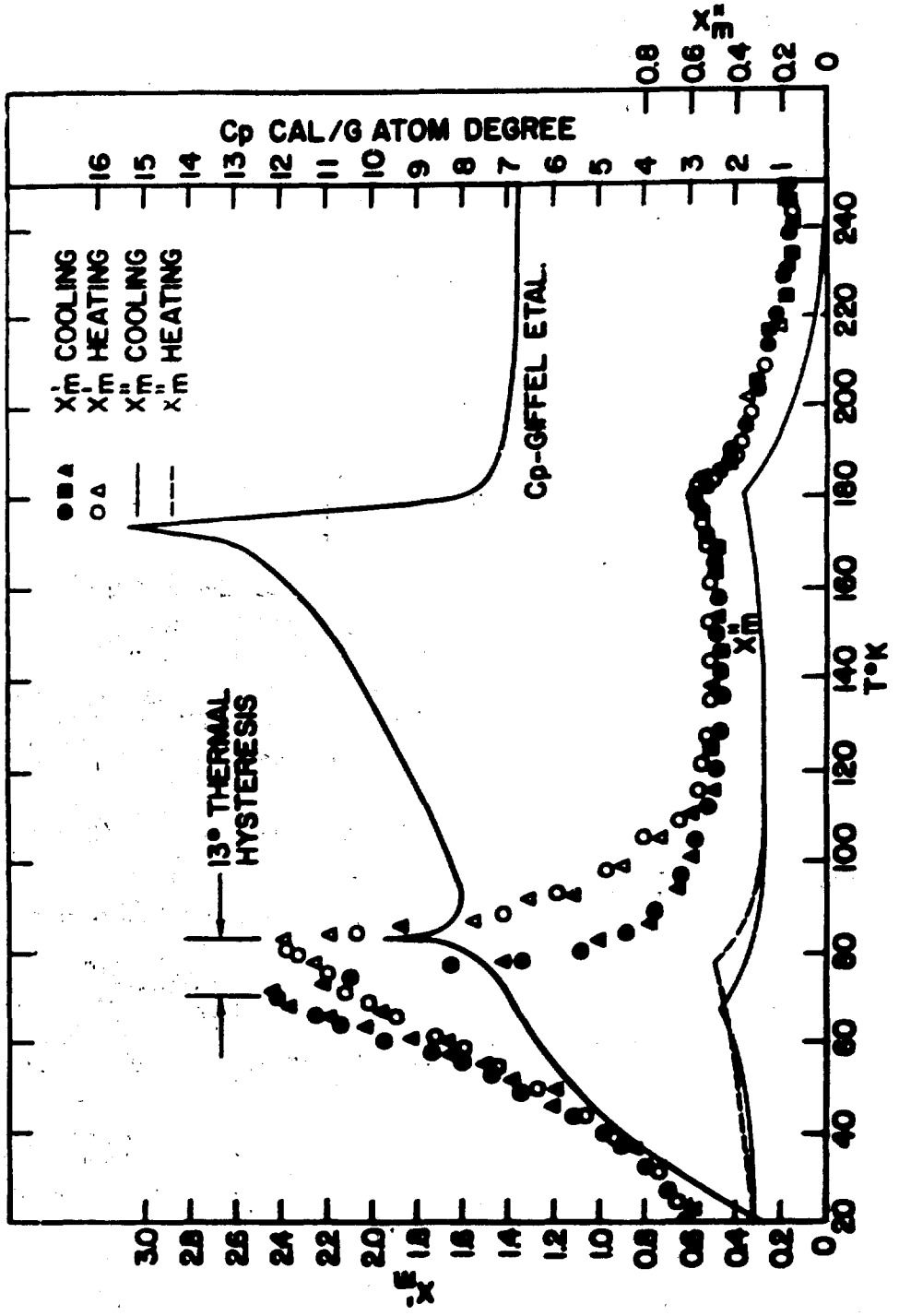

Fig. 2. X'_m, X''_m and C_p versus T°K for Dy metal.

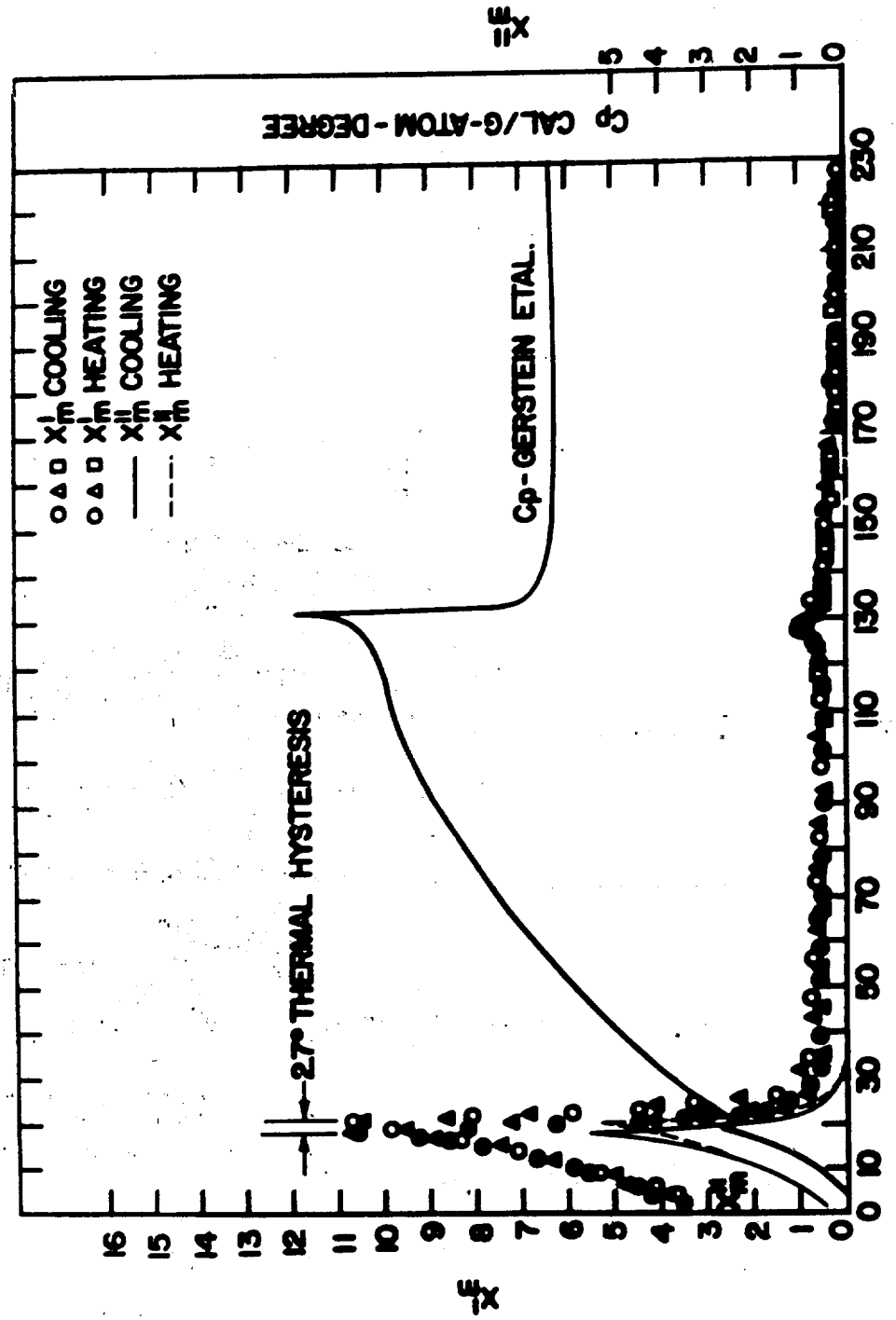

Fig. 3. χ'_m, χ''_m and C_p versus T°K for Ho metal.

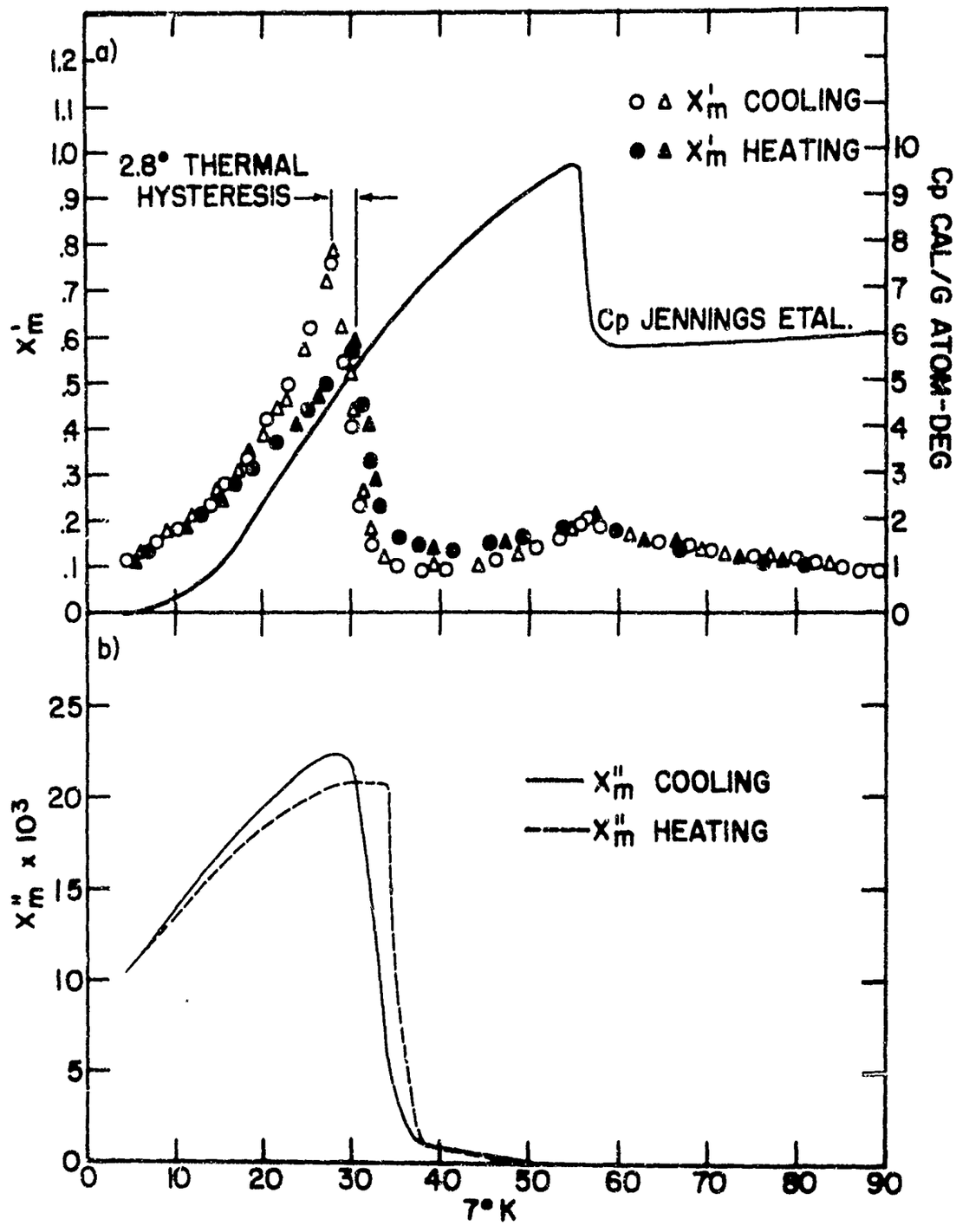

Fig. 4. a) χ'_m and C_p versus T°K for Tm metal.

b) χ''_m versus T°K for Tm metal.

DISTRIBUTION OF MAGNETIC MOMENT DENSITY IN Tb*

O. Steinsvoll†, G. Shirane, R. Nathans

Brookhaven National Laboratory, Upton, New York

H. A. Alperin and S. J. Pickart

U. S. Naval Ordnance Laboratory, Silver Spring, Maryland and

Brookhaven National Laboratory, Upton, New York

Abstract

The magnetic form factor of metallic terbium has been measured at $4.2^{\circ}K$ by scattering of polarized neutrons with wavelength $\lambda = 0.8\text{Å}$ from single crystal samples. Using a split coil superconducting magnet giving a field of 40K Oe across the crystal it was possible to magnetize the samples close to saturation along both the a- and the b-directions, the latter being the direction of easy magnetization. The over-all agreement with theoretical calculations for the Tb^{3+} ion form factor is satisfactory. The experimental points were found to lie on a smooth curve which is consistent with the theoretical prediction that the terbium magnetic moment density has a disc-shaped distribution normal to the resultant moment direction.

INTRODUCTION

The determination of the neutron magnetic form factors of the magnetic elements is of great value because their Fourier transforms will give information about the spatial distribution of the magnetic moment densities in the atoms. Much experimental and theoretical work in recent years has therefore been concerned with the determination of the magnetic form factor for ions of the transition elements. The form factors for the 3d metals have been measured with polarized

---

*Work performed under the auspices of the U.S.Atomic Energy Commission.

†Guest scientist from Kjeller Research Establishment,Kjeller,Norway.

neutrons with considerable accuracy. However, to date no comparable measurements have been performed on the rare earth metals. The difficulty in making such measurements is twofold. First, good single crystal samples must be available and secondly, a magnetic field strong enough to obtain saturation must be provided without depolarizing the incident neutron beam.

An excellent single crystal of the element terbium was put at our disposal by Prof. F. H. Spedding, Prof. S. Legvold, and Dr. L. Sill of the Ames Laboratory. A special superconducting magnet was constructed which provided a field of 40K Oe across the sample. The problem of depolarization of the neutron beam through this magnet was avoided by a method to be described below.

Metallic terbium crystallizes with a h.c.p. structure. Below 220°K it has an ordered ferromagnetic state with the b-axis the direction of easy magnetization. A moment of 9.34 μ_B at 4.2°K was found by D. E. Hegland et al[1] from magnetization measurements.

EXPERIMENTAL

The polarized neutron technique has been described in detail elsewhere.[2] Briefly, the experiment consists of measuring the ratio between two scattered intensities in the Bragg peaks from the sample when the neutrons are polarized parallel or antiparallel to the magnetic field. This so-called flipping ratio R is related to the ratio γ between the magnetic and nuclear scattering amplitudes, p and b respectively, in the following manner:

$$R = \left(\frac{1+\gamma}{1-\gamma} \right)^2 \qquad (1)$$

The magnetic scattering amplitude is proportional to the magnetic form factor of the atoms in the sample. Several corrections have to be applied to formula (1) in an actual experiment.

The original single crystal of terbium was cut into smaller

pieces which could be magnetized along different crystallographic directions. In addition, the small-sized crystals were needed in order to avoid secondary extinction effects. This will be discussed below. One piece 3mm x 3mm x 9mm in size was cut with its long dimension along the b-axis. Another smaller piece (1mm x 1.4mm x 4mm) had its long dimension in the a-direction. The measurements were performed at $4.2^{\circ}K$ with the crystals magnetized along their long dimensions to minimize demagnetization. A neutron wavelength of 0.8Å was used which permitted measurements of the form factor up to the value $\left(\frac{\sin\theta}{\lambda}\right) = 1.1\text{Å}^{-1}$.

A schematic view of the split coil superconducting magnet is shown in Fig. 1. A doughnut-shaped region in the space between the coils has a very strong depolarizing effect upon the neutron beam. This comes about because the magnetic field changes direction in this region, and over a short distance all magnetic components effectively go to zero. This depolarizing effect could be seen by studying the flipping ratio at different heights in the reflected beam from an analyzing crystal placed behind the magnet. The two coils have separate power supplies in order that the current in the coils can be adjusted independently. By letting the lower coil carry less current than the upper one (see figure 1b) this depolarizing region can be forced to move downwards and out of the collimated incident neutron beam. The polarization vector of the primary neutron beam still has to perform an adiabatic turn with the magnetic field in the region where the field changes direction between the coils above the bad spot. Here, however, a horizontal field component guides the neutron polarization across the turning region, and the polarization performs an almost perfect turn with the magnetic field. A polarization of 98% could be measured in the beam, after it had passed through the magnet. In fact, the polarization had then been turned twice.

If the sample is not completely saturated additional depolarization will occur in the crystal itself. A basic requirement in the experiment is that the sample be magnetized normal to the scattering

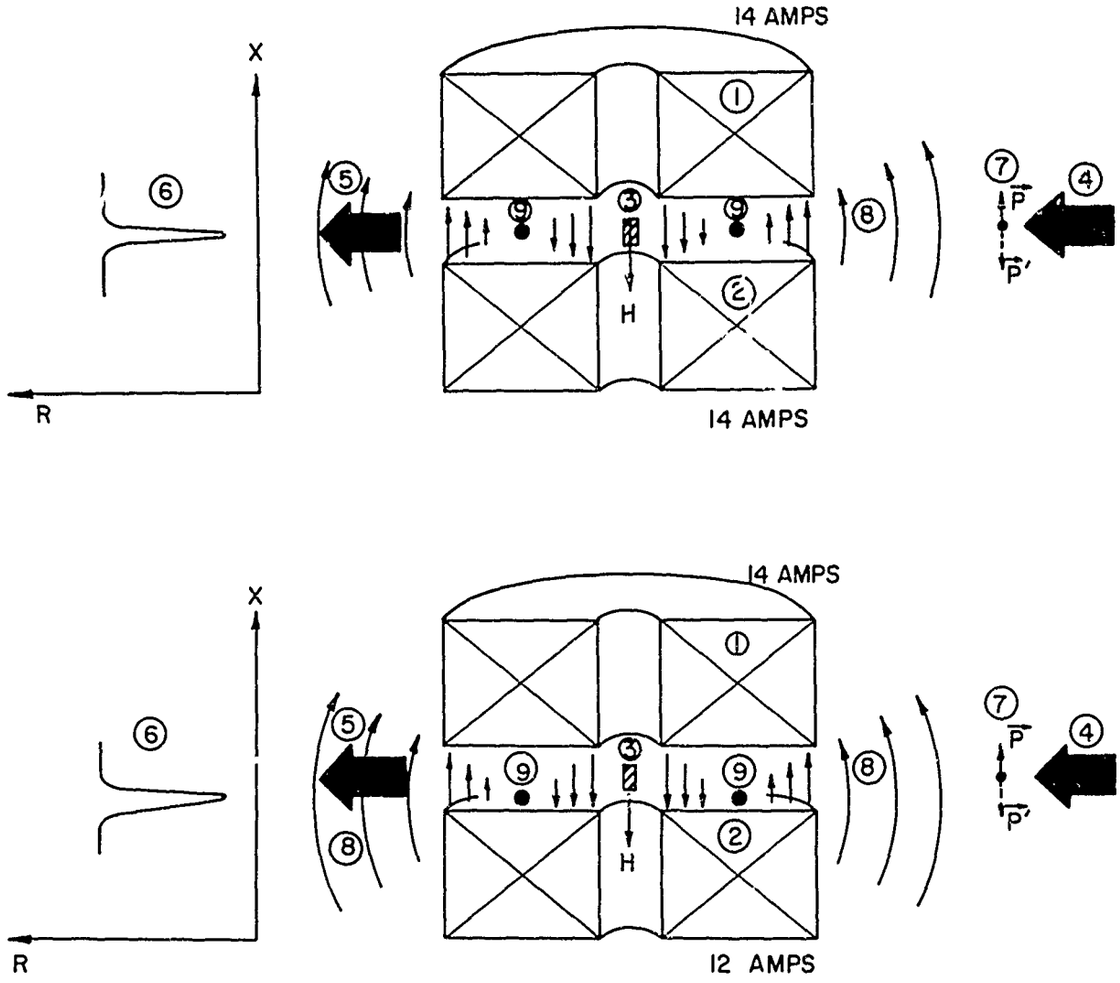

Figs. 1a and 1b: 1 and 2: Superconducting coils. 3: Crystal sample. 4: Incident neutron beam. 5: Scattered neutron beam. 6: Graph showing flipping ratio R when measured as a function of height across the neutron beam. 7: Polarization vector $\vec{P}$ of the neutron beam ($\vec{P}'$ polarization vector when the R. F. flipper is on). 8: Return field from the superconducting magnet. 9: Depolarizing region. Fig. 1a shows the situation when both coils carry the same current. The depolarizing region is situated in the middle between the coils. In Fig. 1b the two coils carry different currents, thus the depolarizing region is forced downwards.

vector. The strong field of the superconducting magnet made it possible to achieve a magnetization close to saturation along the a- and b- directions; the small depolarization still present reduced the effective beam polarization in the sample to 93%.

Intense reflections arising from the large magnetic scattering amplitude (2.51×10^{-12}cm in the forward direction) made it necessary to use two crystals of different sizes in order to eliminate the effect of secondary extinction. A small crystal (the a-axis crystal) was used to study the predominantly strong low angle reflections,while a larger b-axis crystal was used for the weaker high angle reflections. Integrated intensities measured on the a-axis crystal when plotted against calculated intensities showed no systematic trend indicative of secondary extinction. Since the (006) reflection measured on the b-axis crystal yielded a value of the flipping ratio in agreement with the same reflection measured on the extinction-free a-crystal it is therefore safe to conclude that the even weaker high angle reflections from the b-crystal must be free of extinction. Confidence in the final form factor measurements is sustained by noting that the strong reflections ((002), (004), (006), etc.) and the weak reflections ((100), (102), (200), etc.) all fall on the same smooth curve. The presence of simultaneous Bragg reflections was minimized by using long pillar-shaped samples.

RESULTS

The normalized magnetic form factor values were obtained using a value of the nuclear scattering amplitude of $b = 0.76 \times 10^{-12}$cm and a value of 9.34 μ_B for the moment on the Tb atoms. The results are given in Table I and Figure 2. For comparison the magnetic form factor computed by M. Blume[3] for the Tb^{3+} ion in an external magnetic field has also been drawn.

A comparison of the theoretical value for the saturation moment (S = 3, L = 3, so 2S+L = 9 Bohr magnetons) with the measured value leads one to conclude that the exchange energy is probably large compared to

TABLE

hkℓ	$\left(\frac{\sin\theta}{\lambda}\right)$ Å^{-1}	f	hkℓ	$\left(\frac{\sin\theta}{\lambda}\right)$ Å^{-1}	f
100	.160	.97 ± .02	224	.657	.183 ± .002
002	.175	.86 ± .02	008	.702	.148 ± .001
101	.182	.84 ± .02	118	.755	.119 ± .002
102	.237	.74 ± .03	226	.765	.115 ± .001
103	.308	.59 ± .03	330	.833	.080 ± .001
200	.320	.65 ± .02	332	.851	.075 ± .001
201	.332	.61 ± .01	0010	.878	.066 ± .001
004	.351	.56 ± .01	228	.895	.059 ± .001
203	.415	.46 ± .02	334	.904	.056 ± .002
105	.467	.39 ± .02	1110	.921	.053 ± .005
300	.481	.40 ± .03	336	.985	.035 ± .001
302	.512	.36 ± .03	2210	1.04	.022 ± .001
006	.527	.311 ±.006	1112	1.09	.016 ± .001
222	.582	.261 ±.005	338	1.09	.014 ± .001
116	.596	.239 ±.004	440	1.11	.012 ± .002

The values of the normalized magnetic form factor f have been computed from the experimental data assuming an effective polarization of 93% and a flipping efficiency of 99%.

the crystal field energy and thus Blume's calculation assumes no mixing of the $M_J = 6$ ground state with higher states. This results in a disc-shaped spatial distribution of the magnetic moment density which can be oriented by the external field, and justifies the plotting of the a-axis and b-axis data on one curve. The geometry of our experimental arrangement (scattering vector always perpendicular to the direction of the applied field) however, ensures that only the rotationally symmetric projection of the disc will be observed. This

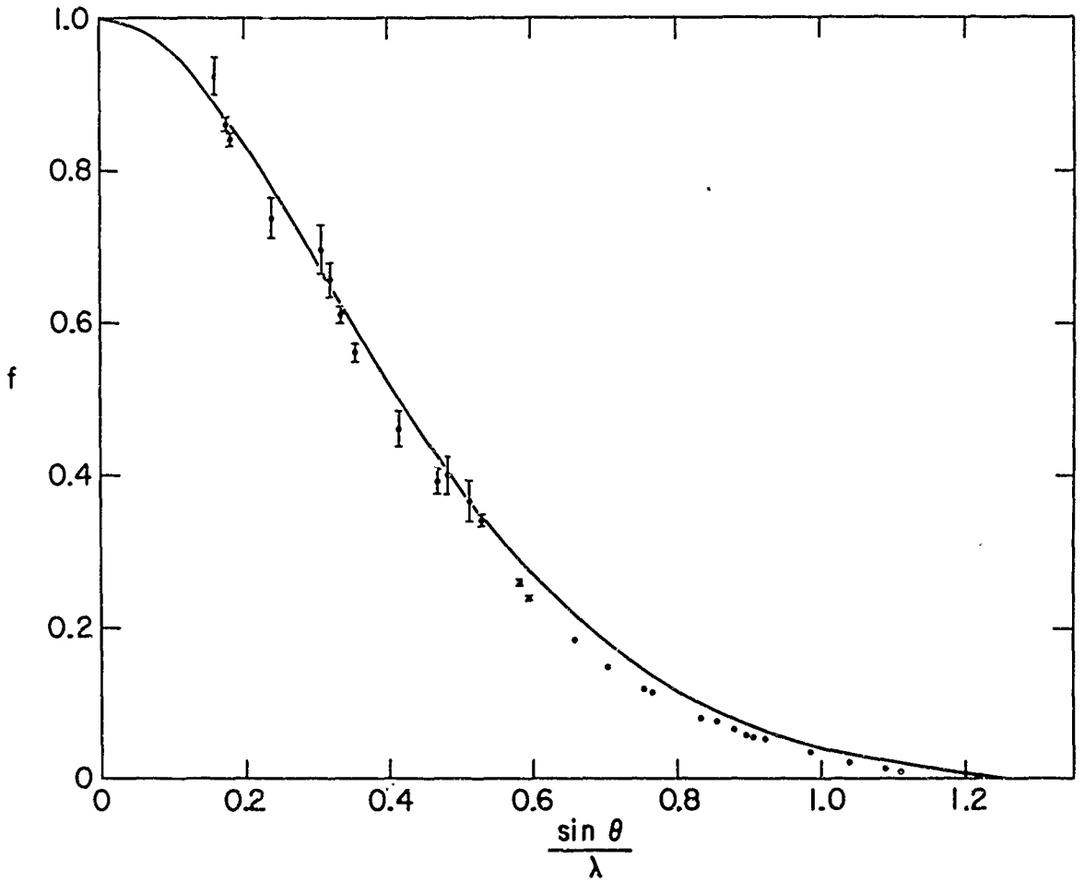

Fig. 2. The normalized form factor of metallic terbium as a function of $\left(\frac{\sin\theta}{\lambda}\right)$ Å^{-1}. The smooth curve is due to a calculation of M. Blume as described in the text.

prediction is confirmed by the fact that all experimental points for large values of $\sin\theta/\lambda$ lie on a smooth curve.

The experimental points are somewhat lower than the theoretical curve at high angles. This same tendency has also been noted for other rare earth ions when their magnetic form factors have been measured and compared with appropriate theoretical calculations.

These measurements for terbium metal lie somewhat higher than the values which can be obtained from paramagnetic scattering (to $\sin\theta/\lambda = 0.6$) by Atoji[7] on TbC_2.

The data were not accurate enough at small scattering angles to see any possible scattering effects due to polarized conduction electrons.

ACKNOWLEDGMENTS

The authors wish to express their gratitude to Prof. F. H. Spedding, Prof. S. Legvold and Dr. L. Sill of the Ames Laboratory who kindly provided them with the terbium crystal used for the experiments. They also wish to thank Dr. M. Blume and Dr. D. E. Cox for helpful discussions.

REFERENCES

1. D. E. Hegland, S. Legvold, and F. H. Spedding, Phys. Rev. 131, no. 1, 158 (1963).
2. R. Nathans, C. G. Shull, G. Shirane, and A. Andresen, Phys. Chem. Solids 10, 138 (1959).
3. M. Blume, private communication.
4. M. Blume, A. J. Freeman, and R. E. Watson, J. Chem. Phys. 37, no.6, 1245 (1962).
5. W. C. Koehler and E. O. Wollan, Phys. Rev. 92, 1380 (1953).
6. W. C. Koehler, E. O. Wollan, and M. K. Wilkinson, Phys. Rev. 110, 37 (1958).
7. M. Atoji, J. Chem. Phys. 35, 1950 (1961).

MAGNETOSTRICTION IN THE HEAVY RARE EARTH METALS

B. F. DeSavage and A. E. Clark

U. S. Naval Ordnance Laboratory, White Oak
Silver Spring, Maryland

ABSTRACT

We have found that the magnetostrictive strains in single crystals of the heavy rare earth metals Tb, Dy, and Er are extraordinarily large (10^{-3} to 10^{-2}) at low temperatures. When these strains are combined group theoretically with spin-operators which transform according to the irreducible representations of the hexagonal group, it is observed that the lowest order magnetostrictive strains arise primarily from single-ion terms in the interaction Hamiltonian and hence have a temperature and field dependence given by a simple function of the magnetic moment:

$$\lambda(T) = \lambda(0)\ \hat{I}_{5/2}\left\{\mathcal{L}^{-1}[m(T,H)]\right\}$$

Here $\mathcal{L}^{-1}[m(T,H)]$ is the inverse Langevin function of the moment and $\hat{I}_{\ell+\frac{1}{2}}$ is a reduced hyperbolic Bessel function of order $\ell + \frac{1}{2}$, where ℓ is the degree of the spin operators. Assuming the deformable-ion model, Tsuya, Clark, and Bozorth predict the 0°K values of these strains $\lambda(0)$ from the strained charge distribution of the conduction electrons. We find the extrapolated 0°K values of the

shear magnetostriction, taking Dy as 100, to be 117, 100, 28, and -44 for Tb, Dy, Ho, and Er, respectively, which are to be compared with the theoretical estimates of 115, 100, 36, and -33.

INTRODUCTION

Callen and Callen[1] have calculated the temperature dependence of the magnetostriction in crystals of hexagonal close packed symmetry. Their procedure is to write the Hamiltonian of the system for small strains as:

$$H = H_e + H_m + H_{me} \tag{1}$$

where H_e is the elastic energy, H_m is the magnetic energy of the unstrained crystal, and H_{me} is the magnetoelastic energy. Callen and Callen express H_{me} as:

$$H_{me} = \sum_{\mu,j,\ell} B_j^{\mu,\ell} \, e_i^{\mu,j} \sum_i K_i^{\mu,\ell}(S) \; . \tag{2}$$

In this expression $K_i^{\mu,\ell}(S)$ are polynomials of degree ℓ in spin S which transform according to the i^{th} basis function of the μ^{th} irreducible representation. $e_i^{\mu,j}$ are symmetry strain components and $B_j^{\mu,\ell}$ are temperature independent magnetoelastic coupling coefficients. The index j enumerates strains of the same irreducible representation.

Minimizing the free energy with respect to the strains and converting the symmetry strains to conventional strains referred to a cartesian coordinate system coinciding with the hexagonal a-, b-, and c-axes, the magnetostriction is

given by:[2]

$$\lambda = \sum_{i,j} e_{i,j}\,\beta_i\,\beta_j = \lambda_1^{\alpha,2}(\beta_x^2 + \beta_y^2)(\alpha_z^2 - \tfrac{1}{3}) + \lambda_2^{\alpha,2}\beta_z^2(\alpha_z^2 - \tfrac{1}{3})$$
$$+ \lambda^{\gamma,2}\left\{\tfrac{1}{2}(\beta_x^2 - \beta_y^2)(\alpha_x^2 - \alpha_y^2) + 2\beta_x\beta_y\alpha_x\alpha_y\right\} \qquad (3)$$
$$+ \lambda^{\epsilon,2}(\beta_x\alpha_x + \beta_y\alpha_y)\,\beta_z\alpha_z$$

the α's and β's are direction cosines of the magnetization direction and measurement direction, respectively. The coefficients $\lambda_j^{\mu,2}$ are temperature dependent coefficients which are given by:

$$\lambda_j^{\mu,2} = \lambda_j^{\mu,2}(0)\ \hat{I}_{5/2}\,[\mathcal{L}^{-1}(m)]. \qquad (4)$$

In this expression $\lambda_j^{\mu,2}(0)$ is the 0°K value of the magnetostriction and $\hat{I}_{5/2}\,[\mathcal{L}^{-1}(m)]$ is a hyperbolic Bessel function whose argument is the inverse Langevin function of the reduced magnetization. The function $\hat{I}_{5/2}$ reduces to m^3 at low temperatures and to $\frac{2}{5}m^2$ at high temperatures. The $\lambda_j^{\mu,2}(0)$'s are made up of a magnetoelastic coupling constant $B_j^{\mu,2}$ divided by an elastic modulus. The superscripts α, γ, and ϵ denote the three distinct modes of strain in a hexagonal system: α, a fully symmetric strain in which hexagonal symmetry is preserved, γ, a shearing strain in the basal plane, and ϵ, a shearing strain in a plane containing the c-axis. The coefficients subscripted 1 and 2 represent a change in the basal plane diameter and the c-axis length, respectively.

Equation (4) applies only to one-ion interactions in which there is coupling between the strain field and single spins. A two-ion theory has been derived by Callen and Callen,[1] however, it appears that for the heavy rare earths a single-ion theory is sufficient to predict the correct temperature dependence of the magnetostriction[2] components of Eq. (3). For two lower-order components not included in Eq. (3), the two-ion terms are required.

Tsuya, Clark, and Bozorth[3] have calculated the magnitudes of the magnetostriction in the heavy rare earth metals Tb, Dy, Ho, Er, and Tm on the basis of two mechanisms: (1), the distortion of the crystalline electric field due to strain induced change of position of the nearest neighbor positive ions, and (2), the distortion of the electric field arising from the strain-perturbed charge distribution of the conduction electrons. Using the equivalent operator method of Stevens they find:

$$B_j^{\mu,2} = \alpha J \left(J - \tfrac{1}{2}\right) \langle r_f^2 \rangle W_j^{\mu,2} \qquad (5)$$

In this expression α is a number calculated by Stevens[4] for each of the rare earths. J is the total angular momentum in units of $\hbar$, and $\langle r_f^2 \rangle$ is the average of the square of the radius of the 4f electron shell. $W_j^{\mu,2}$ is the model dependent part of the expression. In the first mechanism, $W_j^{\mu,2}$ is a lattice sum containing terms

of the form $P_2 = \sum_n (2Z_n^2 - X_n^2 - Y_n^2)/2R_n^5$ and

$P_4 = \sum_n (35Z_n^4 - 30Z_n^2 R_n^2 + 3R_n^4)/8R_n^7$. In the second mechanism, the magnetostriction is estimated using the deformable-ion model assuming a spherical charge density. Under these approximations[3]

$$2W_2^{\alpha,2} = \frac{1}{2}W^{\gamma,2} = \frac{1}{2}W^{\epsilon,2} \simeq \frac{e}{r^3}\int_0^{r_f}\rho(r_c)r_c^2\,dr_c$$

and $W_1^{\alpha,2} = 0$

where $\rho(r_c)$ is the charge density of the conduction electrons.

It is seen that the product $\alpha\ J(J-1/2)\ \langle r_f^3\rangle$ is common to all atomic mechanisms and since $W_J^{4,2}$ varies slightly with the number of 4f electrons, a good estimate of the relative magnitude of the magnetoelastic coupling constants in the rare earths is found by a comparison of the expression:

$$\alpha J\ (J - 1/2)\ \langle r_f^3\rangle$$

After introducing the appropriate elastic constants, the 0°K magnetoelastic constants of Eq. (3) become:

$$\lambda_1^{\alpha,2}(0) = \frac{3K}{D}(W_1^{\alpha,2} - \frac{1}{3}W_2^{\alpha,2})C_{33} - \frac{3K}{D}(W_1^{\alpha,2} + \frac{2}{3}W_2^{\alpha,2})C_{13}$$

$$\lambda_2^{\alpha,2}(0) = \frac{3K}{D}(W_1^{\alpha,2} - \frac{1}{3}W_2^{\alpha,2})(-2C_{13}) + \frac{3K}{D}(W_1^{\alpha,2} + \frac{2}{3}W_2^{\alpha,2})(C_{11}+C_{12})$$

$$\lambda^{\gamma,2}(0) = \frac{KW^{\gamma,2}}{2(C_{44}-C)};\quad K = \alpha\langle r_f^3\rangle J(J - \tfrac{1}{2}) \qquad (6)$$

$$\lambda^{\epsilon,2}(0) = \frac{KW^{\epsilon,2}}{4C_{44}};\quad D = C_{33}(C_{11}+C_{12}) - 2C_{13}^2$$

Estimating the elastic constants from the room temperature sound velocities in dysprosium,[5] we find:

$$\lambda_1^{\alpha,\beta}(0) = \frac{K}{64.1}\,(15.7W_1^{\alpha,\beta} - 12.66W_2^{\alpha,\beta})\,10^{-11}$$

$$\lambda_2^{\alpha,\beta}(0) = \frac{K}{64.1}\,(14.8W_1^{\alpha,\beta} + 24.8W_c^{\alpha,\beta})10^{-11} \qquad (7)$$

$$\lambda^{\gamma,\beta}(0) = KW^{\gamma,\beta}/9.14 \times 10^{11}$$

$$\lambda^{\epsilon,\beta}(0) = KW^{\epsilon,\beta}/9.76 \times 10^{11}$$

EXPERIMENT

We have sought to test this theory by measuring all of the magnetostriction coefficients in terbium in the paramagnetic region, where the magnetocrystalline anisotropy is negligible. This, together with previous measurements of the magnetostriction in Er,[3] Dy,[2] and Ho[6] should give an indication of the validity of the approximations made in the Tsuya-Clark-Bozorth theory.

We have used the conventional strain gage method to measure the magnetostriction in terbium. In order to separate the four coefficients experimentally, it was necessary to measure the strains along the a- and c-axes and a direction 45° between the two while the magnetic field was rotated from the measurement direction to a direction perpendicular. For example, $\lambda_2^{\alpha,\beta}$ is determined by measuring the change in length along the c-axis while rotating the field from the c- to the a-axis. The 0°K magnitude is found by extrapolating the experimental data

to 0°K according to the theoretical temperature dependence of Eq. (4). This procedure requires that our measurements be consistant with the dictates of the Callen and Callen theory, namely, that at each temperature, the magnetic moment be held constant during the measurement. In the paramagnetic region, the magnetic susceptibility along the c-axis is different from that along the a-axis. In order to maintain constant moment during measurement, the magnetic field must be changed during rotation if the initial and final directions have different susceptibilities, as for example in the measurements of $\lambda_1^{\alpha,2}$ and $\lambda_2^{\alpha,2}$. Figure 1 illustrates this point. The top curve is the temperature dependence of $\lambda_2^{\alpha,2}$ measured at constant moment. The experimental points agree well with the theoretical temperature dependence. The lower curve shows the magnetostriction measured at constant field and here $\Delta\ell/\ell$ is found to have the opposite sign and a different temperature dependence.

The temperature dependences of the four coefficients are shown in Fig. 2, which is a log-log plot of the λ's versus the function $\hat{I}_{5/2}[\mathcal{L}^{-1}(m)]$. Best agreement with the Callen and Callen theory is found with lines drawn through the data points having slopes of unity and intercepts at $T = 0°K$ $(\hat{I}_{5/2} = 1)$ of $\lambda_1^{\alpha,2}(0) = -0.26 \times 10^{-2}$, $\lambda_2^{\alpha,2}(0) = 0.9 \times 10^{-2}$, $\lambda^{\gamma,2}(0) = 1.0 \times 10^{-2}$, and

$\lambda^{\epsilon,2}(0) = 1.15 \times 10^{-2}$.

DISCUSSION

Table I compares the predicted and measured relative magnitudes of the magnetostriction in the heavy rare earths by making use of Eq. (5). The values of $\langle r_f^2 \rangle$ are taken from Freeman and Watson.[7] The magnetostriction λ is related to the magnetoelastic coupling coefficients B by $\lambda = - BC^{-1}$, where C is an elastic constant. The elastic constants have been measured only for Dy and in lieu of this, the ratio of the polycrystalline shear moduli have been used to calculate the magnetostriction.

Table I

Element	α	$\langle r_f^2 \rangle$ a.u.	λ_{th}	$\lambda_{exp}^{\gamma,2}$	polycrystal λ
Tb	-1/99	.756	115	117	+
Dy	-2/315	.726	100	100	+
Ho	-1/450	.696	36	28[a.]	+
Er	4/1575	.666	-33	-44	-
Tm	1/99	.638	-74	—	-

a. Legvold, Alstad, and Rhyne, Phys. Rev. Letters 10, 50 (1963)

The magnitude of λ as predicted by the theory is given relative to Dy taken arbitrarily as 100. The experimental determinations of $\lambda^{\gamma,2}(0)$ normalized to Dy are shown in the table along with the sign of the magnetostriction as

measured in the polycrystalline material. Good agreement between experiment and theory is observed for the signs and relative magnitudes. The predicted sign reversal between Ho and Er is observed in both single crystal and polycrystalline materials.

In Table II, our experimental results on Tb are compared to those calculated on the basis of the deformable-ion model (assuming a spherical charge density for the conduction electrons) and those calculated from the distortion of the crystalline field due to the field. As expected, because of the screening of the 4f electrons by the outer shells, the deformable-ion magnetostriction is too large. In the Table, we have normalized the theoretical value of $\lambda^{\gamma,2}$ to the experimental value of 0.010 by assuming the screening factor σ to be 0.75. This is consistent with the value of $\sigma \cong 0.8$ estimated by Freeman.[8] Excellent agreement is found between theory and experiment for the coefficient $\lambda_2^{\alpha,2}$; the other two coefficients, $\lambda_1^{\alpha,2}$ and $\lambda^{\epsilon,2}$, are of the correct sign and order of magnitude. On the other hand, the magnetostriction calculated from the crystalline field is too small and predicts the wrong sign for $\lambda^{\epsilon,2}$ and incorrect ratios for $\lambda_1^{\alpha,2}/\lambda^{\gamma,2}$ and $\lambda_2^{\alpha,2}/\lambda^{\gamma,2}$. Hence it appears that the crystal field plays a minor role in the magnetostriction of the rare earths and that the dominant mechanism is the interaction between the conduction electrons and the 4f electrons.

Table II

λ	Experiment	Deformable Ion	Crystal Field
$\lambda_1^{\alpha,2}$	-.0026	-.0045	-.0017
$\lambda_2^{\alpha,2}$	.009	.0088	.0033
$\lambda^{\gamma,2}$	.010	.010	.0006
$\lambda^{\epsilon,2}$	.0115	.0094	-.0023

REFERENCES

1. E. R. Callen and H. B. Callen, to be published in Phys. Rev.
2. A. E. Clark, B. F. DeSavage, and R. M. Bozorth, Phys. Rev. 138, A216 (1965).
3. N. Tsuya, A. E. Clark, and R. M. Bozorth, International Conference on Magnetism, Nottingham, England, 1964.
4. K. W. H. Stevens, Proc. Phys. Soc. 65, 209 (1952).
5. A. E. Clark, unpublished data.
6. S. Legvold, J. Alstad, and J. Rhyne, Phys. Rev. Letters 10, 50 (1963).
7. A. Freeman and R. Watson, Phys. Rev. 127, 2058 (1962).
8. A. Freeman, private communication.

Released by the Commander,
U. S. Naval Ordnance Laboratory
Silver Spring, Maryland

26 MAY 1965 Frank Nichta
Technical Information Office

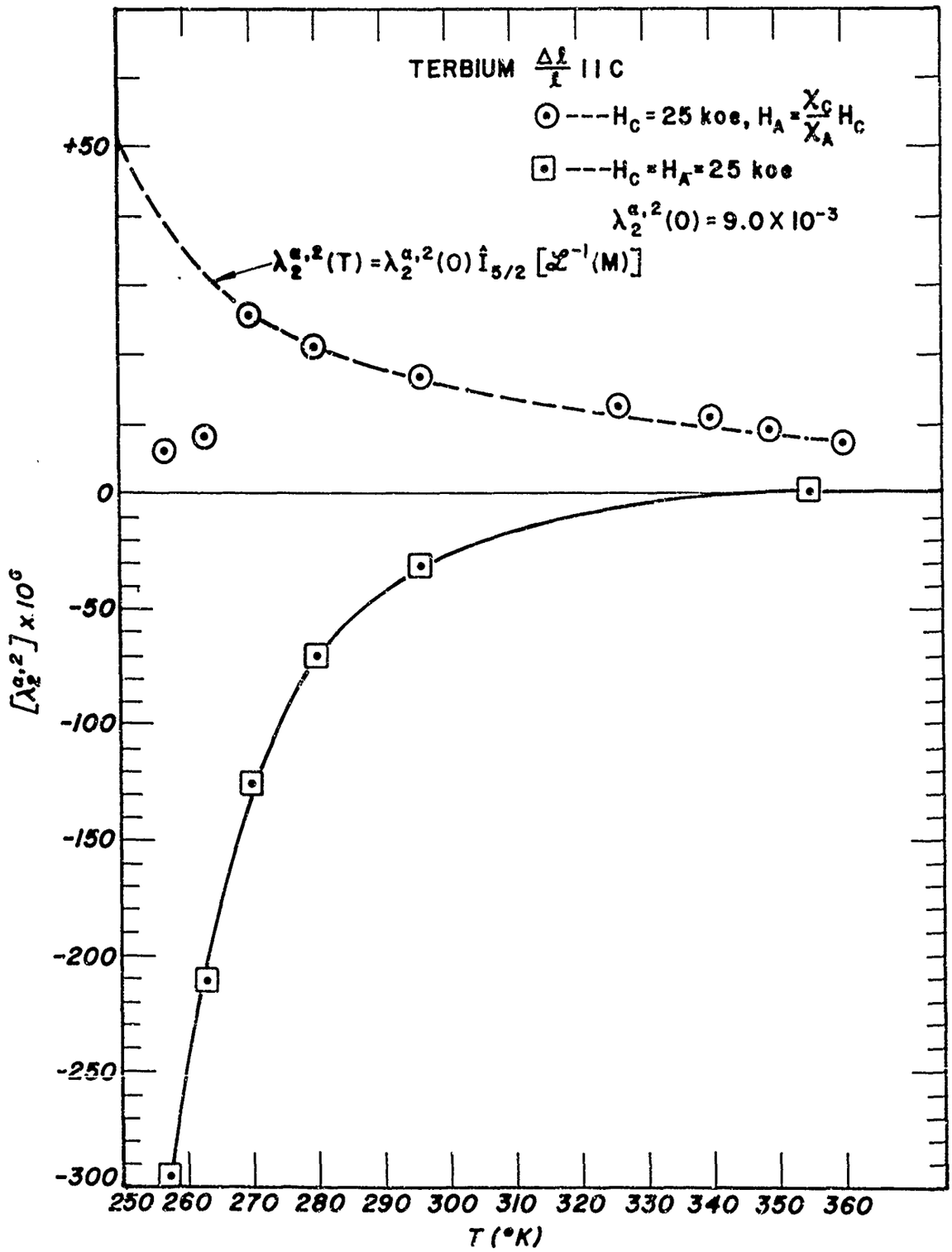

Fig. 1. Temperature dependence of the magnetostriction coefficient $\lambda_2^{\alpha,2}$ at constant moment and field.

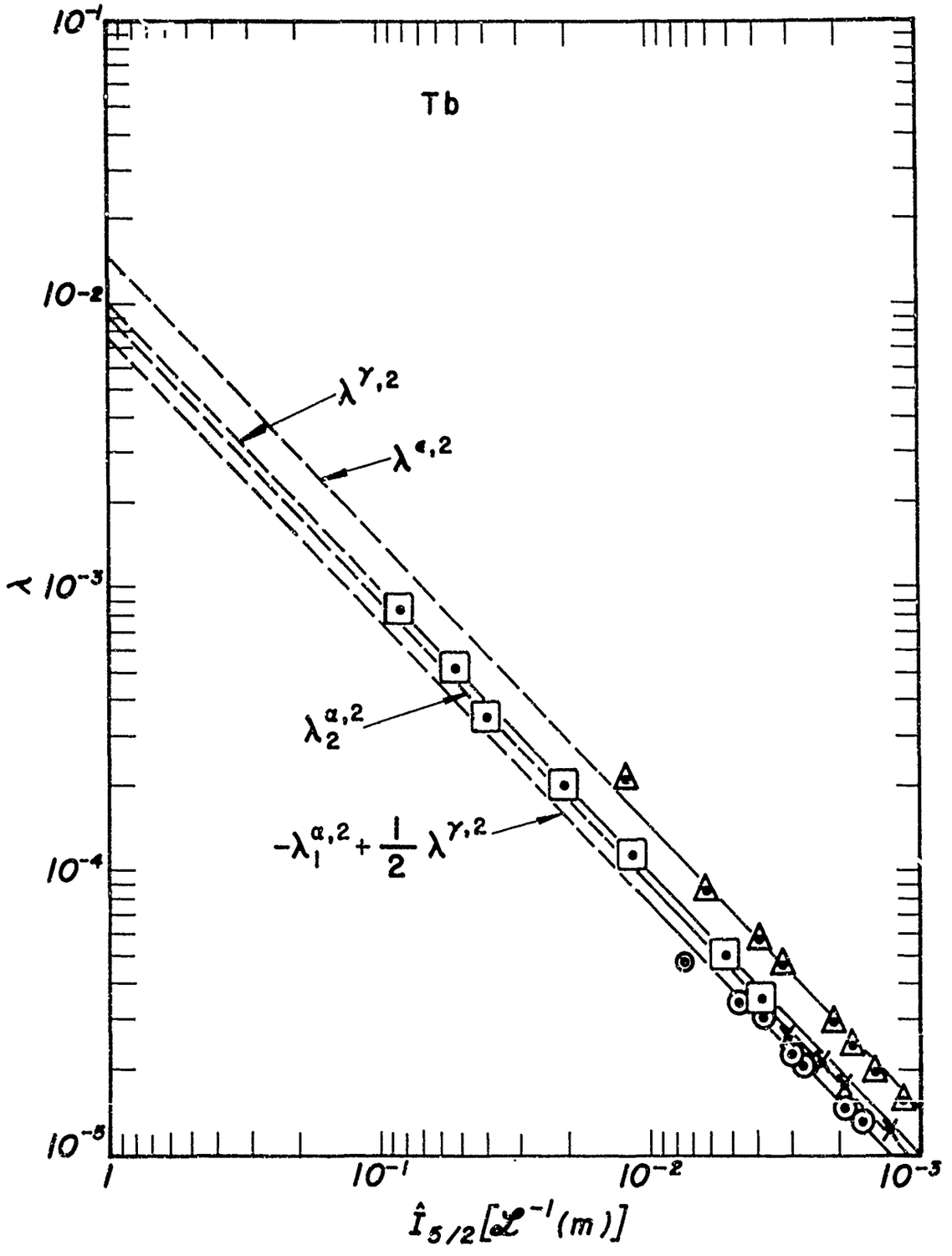

Fig. 2. Magnetostriction coefficients of Tb vs. $\hat{I}_{5/2}$ [$\mathcal{R}^{-1}$(m)].

OBSERVATION OF OPTICAL ABSORPTION BANDS ASSOCIATED WITH MAGNETIC ORDER IN RARE-EARTH METALS.

C. Chr. Schüler

IBM Zurich Research Laboratory
Rüschlikon, Zurich, Switzerland

ABSTRACT

Spectroscopic studies of Gd-metal reflexion methods have revealed an absorption band in the infrared , centered at 0.4 eV, which appears in the ferromagnetically ordered state below 289° K. The strength of the absorption increases with increased order as the temperature is lowered.

A similar band is present in Dy-metal in the spiral-phase below 178° K and persists into the ferromagnetic phase below 85° K.

The nature of these extra absorptions is not jet understood. An earlier explanation on the basis of magnetic superzones present in the antiferromagnetic phases of Dy and Ho must now be abandoned, since it does not apply to ferromagnetic order.

INTRODUCTION

Optical spectroscopy of metals yields valuable information on the properties of conduction electrons and electronic energy bands. As part of a more extended investigation of the optical properties of rare-earth metals, this paper reports on experimental results which are concerned with a special aspect of this work : the influence of magnetic order on the reflectivity of Gd, Dy and Ho.

The original purpose of the studies to be reported was to verify theoretical predictions by Miwa (1962). He noticed that optical absorp-

tion bands should be observable, associated with periodic spin order which is found in many rare earth materials.

It had been observed earlier that the electrical resistivity of Tb, Dy, Ho and Er shows profound anomalies in the antiferromagnetic phases of these metals, which are characterized by periodic spin arrangements. In order to explain these anomalies, Mackintosh (1962) and Miwa (1962) suggested the following model :

The periodic arrangement of localized ion spins interacts with the conduction electrons through the well-established s-f exchange interaction. Since the periodicity is different from that of the lattice, additional Brillonin zones are formed, and new energy-gaps are introduced into the conduction band. The resulting change in Fermi surface is reflected by a striking increase in electrical resistivity.

Calculations on the basis of this model by Miwa and in more detail by Elliott and Wedgwood (1963, 1964) are in good agreement with the experimental data. Superzone boundaries should, however, not only influence the electrical resistivity but also give rise to optical absorption from electron transitions across the new gaps. The gaps are of the order $Eg = VS\, M(T)\, |F(\tau)|$ where V is an effective exchange energy, S the ion spin, M(T) the temperature-dependent, relative magnetisation and $|F(\tau)|$ a structure factor. Inserting numerical values and taking M(T) not close to zero, Eg becomes a few tenths of an eV, which corresponds to optical absorption in the near infrared. Our first reflectivity measurements on Ho did indeed reveal an absorption band with a peak at 0.35 eV for the magnetic spiral phase below 132°K (Schüler, 1964), which seemed to fit the predictions rather well.

Further extension of this work to Dy and Gd, will now be presented, which calls for some modifications of the original ideas.

EXPERIMENTAL

All measurements were done on vacuum deposited, polycrystalline films, about 3000 Å thick, which provided the necessary optical surfaces in a convenient manner. In order to obtain film samples with electrical and magnetic properties close to those of bulk material, all depositions were carried out under ultra-high vacuum conditions. This, together with an annealing procedure, produces films of the required quality, as we have demonstrated earlier (Schüler, 1963). The samples were kept in the same vacuum throughout the measurements so that no problem with surface contamination arose. A dewar finger to which the substrates were attached allowed cooling of the specimen down to 78°K.

Reflectivity at nearly normal incidence was determined by comparing with a silver film deposited simultaneously and close to the rare-earth film. The vacuum chamber was fitted with a sapphire window so that measurements between 0.25 and 5 eV of photon energy were possible.

RESULTS

First the reflectivity R of the sample at room temperature was found by comparing with the reflection from the Ag film for which very accurate absolute reflectivity data are available from the work of Bennet et. al (1965). Afterwards, reflexion vs. temperature curves were taken for a large number of fixed photon energies between 0.25 and 2 eV.

Figure 1 shows an R vs. T plot for Dy. One notices an increase in R with decreasing temperature. This corresponds to a reduction in phonon scattering for the conduction electrons which dominate the optical properties in this energy range. At 179° K, the ordering temperature for the magnetic spiral structure, there is a sudden change in slope, and R now decreases as the temperature is lowered further, indicating

additional absorption. Similar curves were found earlier for Ho.

It is rather surprising, however, that there is no evidence of a discontinuity accompanying the transition to the ferromagnetic state at $T_c = 85^{\circ}$ K. This is in contrast to the behaviour of the electrical resistivity, where a distinct drop at T_c indicates that the superzone boundaries and energy gaps vanish.

An obvious choice for an experiment which can clarify this point is Gd, which is only simple ferromagnetic.

The result of measurements identical to that on Dy was rather unexpected.

An R vs. T curve is shown in Fig. 2 It is essentially of the same nature as for Dy except for the different ordering temperature of $T_c = 289^{\circ}$ K.

This seems to indicate that magnetic order, regardless of its periodicity, plays the dominant role in this effect.

More support is lent to this point by comparing the spectral dependence of the anomaly, which is plotted in Figs. 3 and 4. As previously for Ho, a resonance-like dispersion is found with a peak in the 0.3 to 0.4 eV range. It is remarkable that there are only minor differences between the curves for the ferromagnetic state of Gd and the spiral state of Dy.

An important aspect of the absorption bands is the temperature dependence of their position. It can be seen from Figs. 3 and 4 that little shift towards lower energies is observed for higher temperatures in Dy, none for Gd. Such a shift should however occur for an energy gap which varies with M(T). Only the magnitude of the anomaly increases with magnetic order.

DISCUSSION

An explanation of the observed effect on the basis of magnetic superzones must obviously be abandoned in view of the results on Gd. The observation of an almost temperature independent position of the band, unfortunately also renders unlikely an association with energy gaps produced by band-splitting into spin-up and spin-down bands due to magnetic order, since such gaps, too, are expected to be proportional to M(T).

An even simpler explanation one might think of, is an influence of spin-disorder scattering of the conduction electrons which has a pronounced effect on the electrical resistivity and is almost equally reduced by periodic and ferromagnetic order.

However, our observations show that, above the ordering point, reduction in phonon scattering at lower temperatures leads to an increase in reflectivity. So we would expect even more increase in reflectivity upon additional reduction of spin disorder scattering by magnetic order. Instead, less reflectivity is found in the ordered state, which indicates rather more absorption.

In addition, the resonance like behaviour in the dispersion makes spin-disorder an even more unlikely cause of the effect.

We can only conclude that, so far, we have been unable to suggest a plausible explanation for our observations. Further studies are in progress, using single crystal films and polarized radiation in order to take the large anisotropy of transport phenomena in the rare-earth metals into account, which we have neglected so far. It is hoped to obtain some clues from this extension of the work.

REFERENCES

Bennet, Jean, M., and Ashley E.J., 1965, Appl. Optics 4, 221.

Elliott, R.J., and Wedgwood F.A., 1963, Proc. Phys. Soc. 81, 846.

Elliott, R J., and Wedgwood F.A., 1964, Proc. Phys. Soc. 84, 63.

Mackintosh, A.R., 1962, Phys.Rev. Letters 9, 90

Miwa, H., 1962, Progr. Theor. Phys. Japan 28, 208.

Schüler, C.Chr., 1963, Z Angew. Physik 15, 218.

Schüler, C.Chr., 1964, Phys. Letters 12, 84.

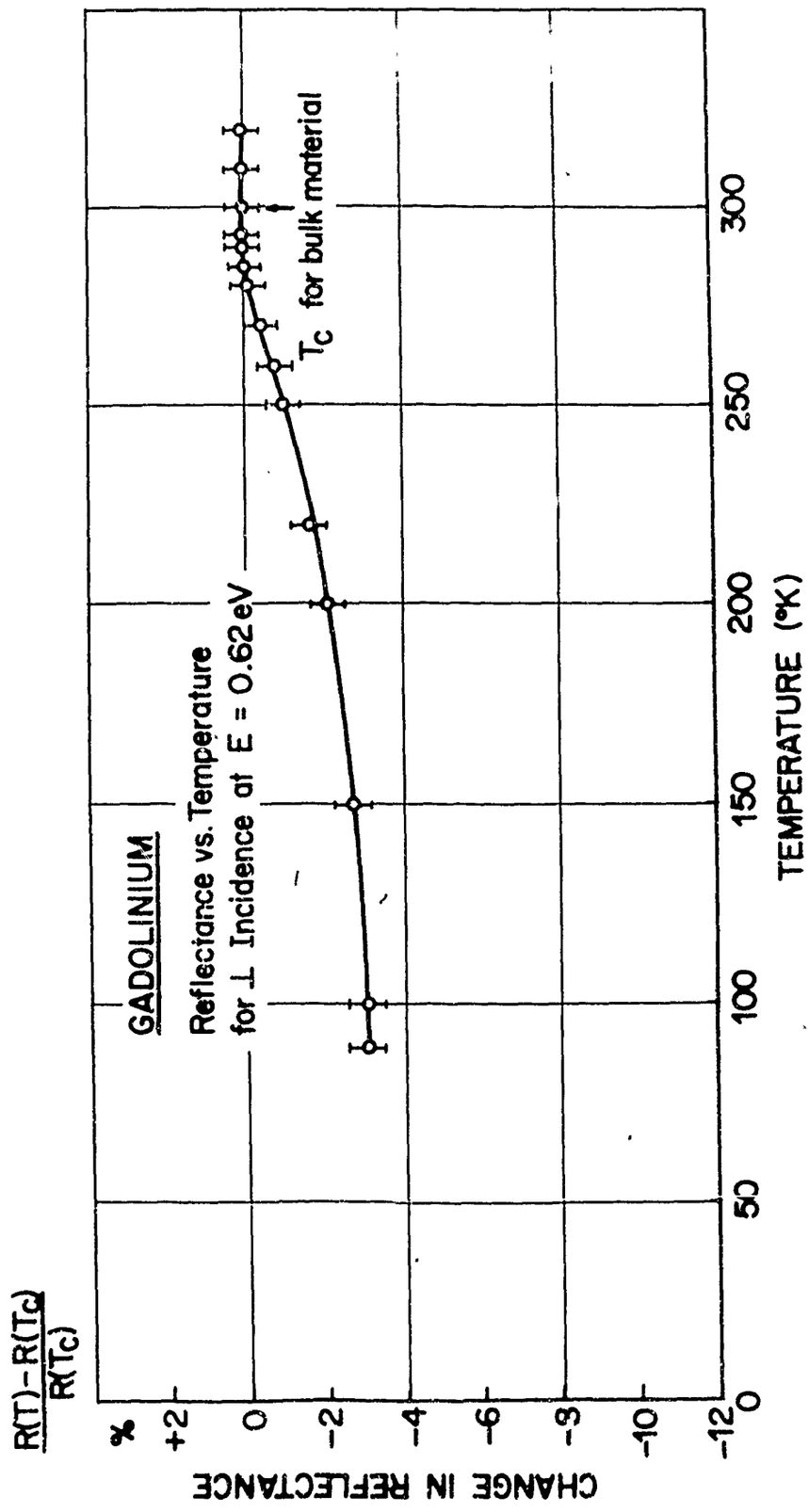
GADOLINIUM
Reflectance vs. Temperature
for ⊥ Incidence at E = 0.62 eV
T_c for bulk material
CHANGE IN REFLECTANCE
$\frac{R(T)-R(T_c)}{R(T_c)}$
%
+2
0
-2
-4
-6
-8
-10
-12
0
50
100
150
200
250
300
TEMPERATURE (°K)

Fig. 1

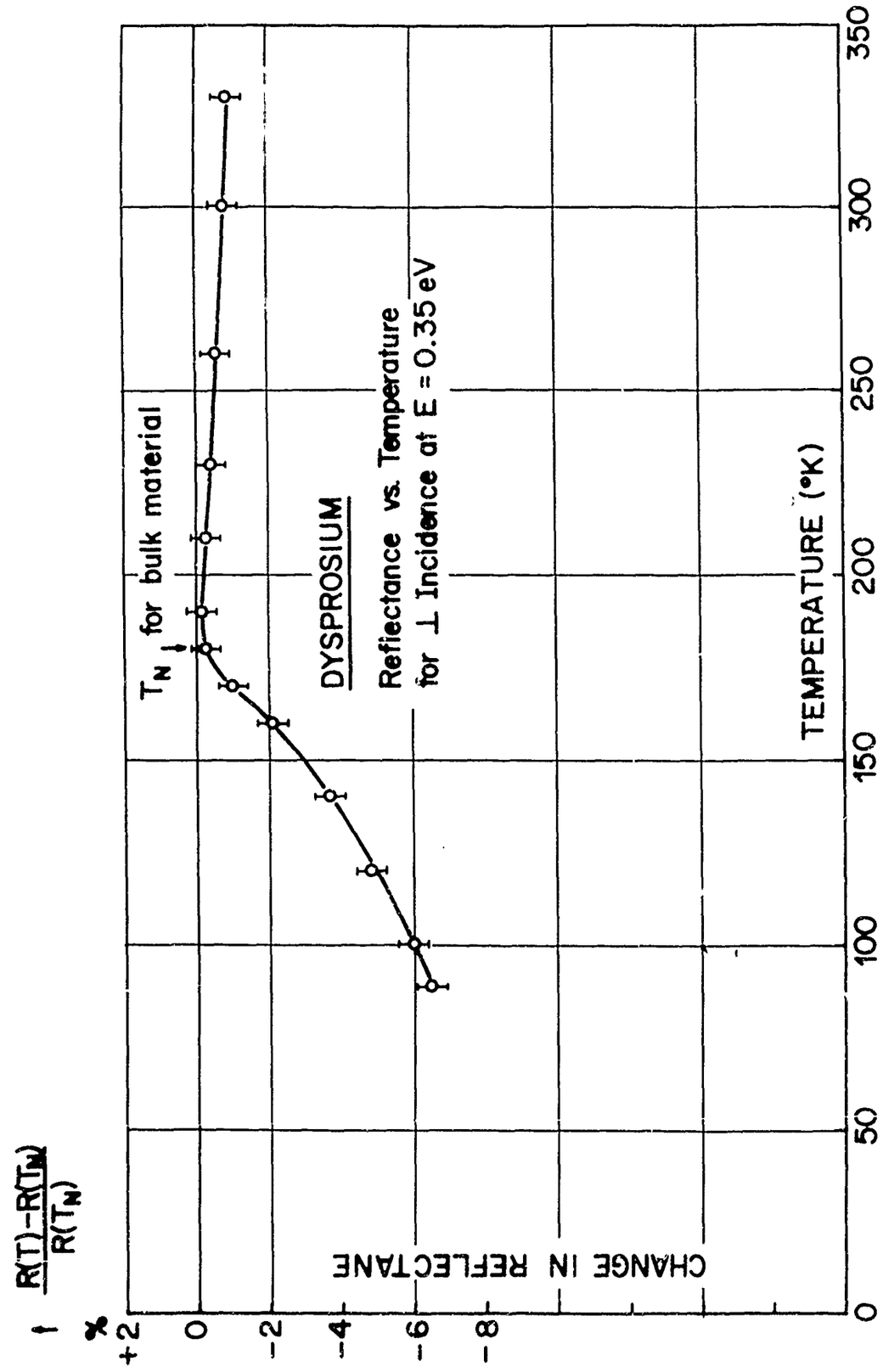
DYSPROSIUM
Reflectance vs. Temperature
for ⊥ Incidence at E = 0.35 eV
T_N for bulk material
CHANGE IN REFLECTANE
$\frac{R(T)-R(T_N)}{R(T_N)}$ %
+2
0
-2
-4
-6
-8
0
50
100
150
200
250
300
350
TEMPERATURE (°K)

Fig. 2

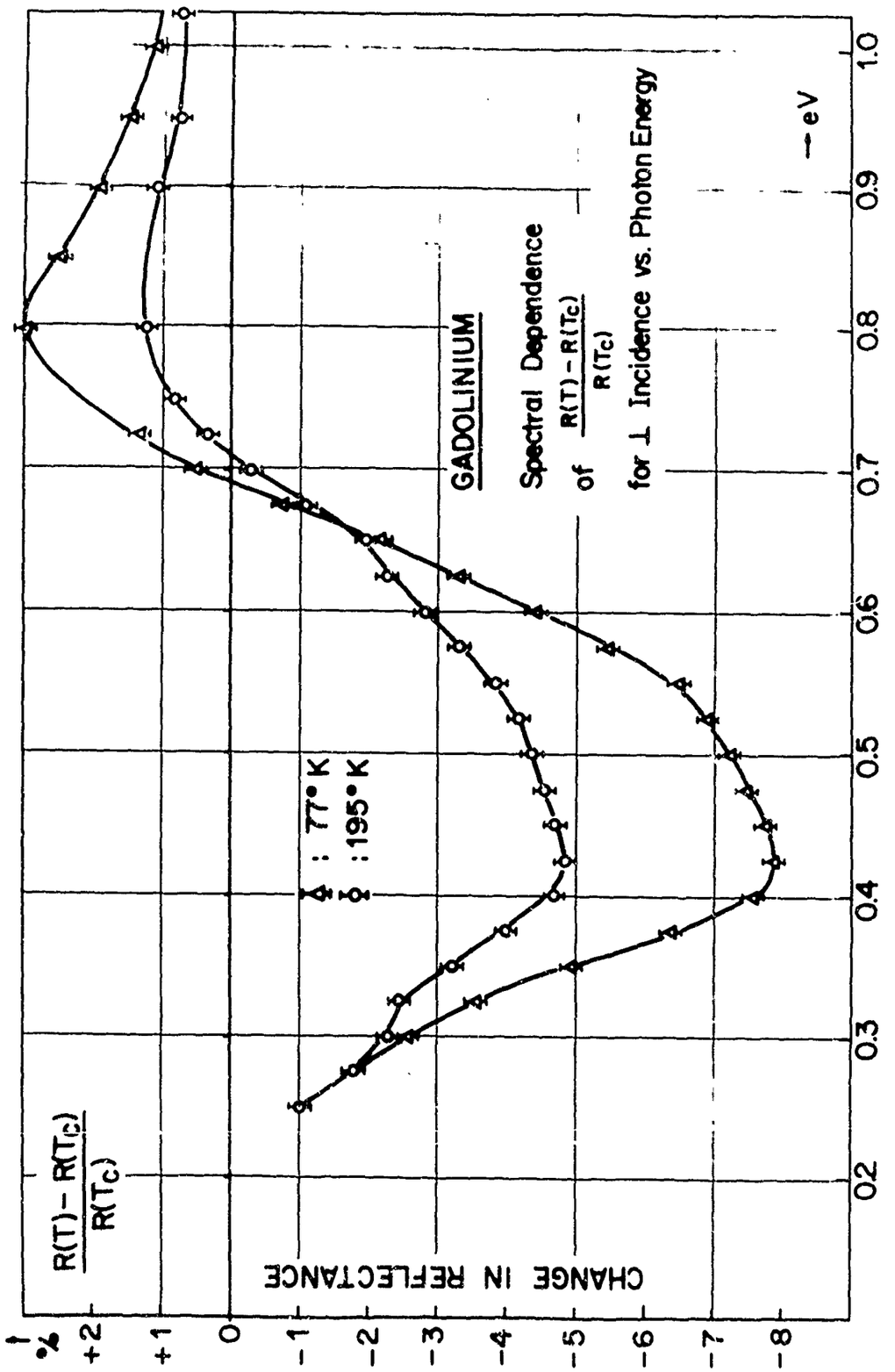
GADOLINIUM
Spectral Dependence
of $\frac{R(T)-R(T_C)}{R(T_C)}$
for ⊥ Incidence vs. Photon Energy
Δ : 77° K
○ : 195° K
CHANGE IN REFLECTANCE
$\frac{R(T)-R(T_C)}{R(T_C)}$
%
+2
+1
0
-1
-2
-3
-4
-5
-6
-7
-8
0.2
0.3
0.4
0.5
0.6
0.7
0.8
0.9
1.0
— eV

Fig. 3

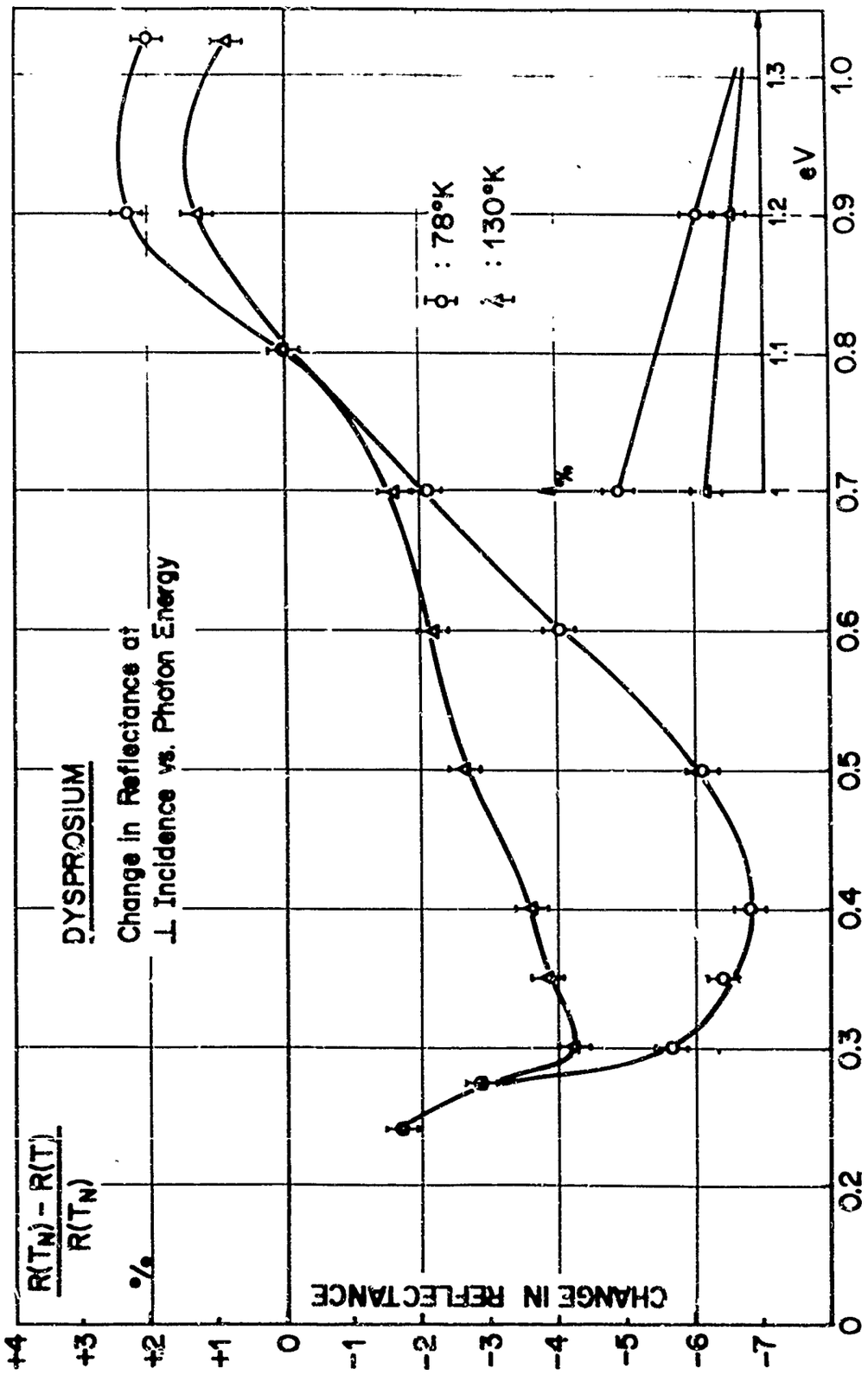
DYSPROSIUM
Change in Reflectance at
⊥ Incidence vs. Photon Energy
$\frac{R(T_N) - R(T)}{R(T_N)}$ %
CHANGE IN REFLECTANCE
Φ : 78°K
Δ : 130°K
eV
+4
+3
+2
+1
0
-1
-2
-3
-4
-5
-6
-7
0
0.2
0.3
0.4
0.5
0.6
0.7
0.8
0.9
1.0
1
1.1
1.2
1.3

Fig. 4

INFRARED ABSORPTION STRUCTURE IN RARE EARTH METALS: RELATIONSHIP TO SPIN ARRANGEMENT AND BAND STRUCTURE

B. R. Cooper and R. W. Redington

General Electric Research Laboratory
Schenectady, New York

ABSTRACT

This note points out (1) that there is a definitive experiment for distinguishing whether any part of the infrared absorption (from 0.25 to 0.85 eV) for the heavy rare earth metals is associated with the spiral periodicity, (2) that, as reported below, this experiment shows that for dysprosium the infrared absorption is completely independent of any periodicity associated with the spiral, and (3) that in the light of recent band calculations, there is an alternative explanation for the occurrence of low frequency optical structure for the heavy rare earth metals.

Recently Schüler[1] reported the appearance of structure at about 0.35 eV in the infrared reflectivity for a holmium film in the temperature range where holmium has a spiral spin arrangement with periodicity along the c axis. Following the ideas of Miwa,[2] Schüler suggested that the structure observed is due to the optical absorption corresponding to energy gaps in the conduction bands at the magnetic Brillouin zone boundaries associated with the spiral periodicity. It is the purpose of the present note to point out (1) that there is a definitive experiment for distinguishing whether this structure or indeed any part of the infrared absorption for the heavy rare earth metals is associated with the spiral periodicity, (2) that, as reported below, this experiment shows that for dysprosium,

which also has spiral spin structure, the infrared absorption is completely independent of any periodicity associated with the spiral, and (3) that in the light of recent band calculations[3,4] there is an alternative explanation for the occurrence of such low frequency structure for the heavy rare earth metals.

The definitive experiment for seeing whether the infrared structure is associated with the spiral periodicity rests on the fact that the application of a magnetic field in the plane of the spiral can be used to change the spin arrangement to one differing only slightly from ferromagnetic alignment along the field. This change occurs quite sharply[5] at a critical field H_c. In general H_c is not very large. If the infrared structure is due to the extra spiral periodicity, this structure can be extinguished by applying a field greater than H_c in the plane of the spiral. This effect will occur very sharply as a function of field. Therefore one need only examine the change in reflection or absorption at a given temperature in the spiral regime on applying a field $H > H_c$. Dysprosium is particularly suitable for such a study since H_c is less than 10 kilogauss throughout most of the spiral temperature region.[6] We have therefore examined transmission through Dy films for a range of frequency between 0.25 eV and 0.85 eV.

The measurements were made in a cryostat with calcium fluoride windows and special pole pieces which allowed a field of 22 kilogauss to be applied perpendicular to the light path and in the plane of the film. The films studied

had transmissions in the region of interest of a few percent, and were a few thousand Angstroms thick. They were prepared by evaporation on sapphire substrates in a separate vacuum system. For protection during the transfer to the cryostat the films were given a protective evaporated layer of silicon monoxide 2000 to 3000 Å thick, which was present during the measurements. This would not cause any change in the measured absorption since silicon monoxide is transparent in the range of the present measurements. Electrical measurements on auxiliary samples indicated that such a coat was effective in preserving the metallic nature of the dysprosium film. No change was observed in the film properties in several days in the cryostat. However, after one to two weeks' exposure in air the transmission increased several times. As a final check on the experimental technique, the difference in transmission between a thick film and a thin film was studied and this showed the same absorption as indicated in the figure. A triangular five-point smooth was used on the raw data.

The results obtained on cooling below the Néel temperature, T_N = 179°K, are shown in Fig. 1. The figure shows the transmission at a given temperature normalized to that at 182°K (just above T_N). There is a distinct dip in the transmission for the 87°K curve at about 0.44 eV and at a somewhat lower frequency for 123°K. (The lowest temperature shown, 87°K, is quite close to that, ≈ 85°K, at which bulk dysprosium has a thermal transition to a ferromagnetic phase.) Such structure is clearly absent for the 235°K

curve where Dy has no magnetic ordering. (Structure is also absent in the corresponding room temperature curve which lies between 1.3 and 1.5 on the scale of Fig. 1 for photon energies between 0.3 eV and 0.8 eV.) It is difficult to clearly distinguish whether there is structure in the frequency range observed at 138°K. For the spiral mechanism suggested by Schüler the absorption structure should go to zero frequency at T_N, while for the mechanism based on the band structure of the conduction electrons discussed below it will probably shift to very low frequencies as temperature increases toward T_N. As the structure shifts to lower frequencies for temperatures increasing toward T_N, it is increasingly obscured by the free carrier contribution to the absorption. This probably accounts for the difficulty in observing any well defined structure at 138°K.

There is no measurable change in the curves shown in Fig. 1 when a field of 22 kilogauss is applied in the plane of the film. Ideally the experiment would be done with single crystals. However, the use of a polycrystalline film presents no great obstacle. For a polycrystalline sample, any given crystallite will have its c axis at some angle θ to H. The main effect of the applied field is to produce an effective field $H\sin\theta$ in the plane of the spiral which can distort the spiral.[7] Then crystallites with $\theta > \theta_c$ are essentially ferromagnetic, while those with $\theta < \theta_c$ are spirals. Here

$$\theta_c = \sin^{-1} (H_c/H). \qquad (1)$$

Then the fraction of crystallites having a ferromagnetic arrangement for a given field is

$$f = \int_{\theta_c}^{\pi/2} \sin\theta d\theta \Big/ \int_{o}^{\pi/2} \sin\theta d\theta = (H_c/H)\left[(H/H_c)^2 - 1\right]^{1/2} \quad \ldots(2)$$

f increases rapidly for $H>H_c$. For example, f = 0.87 for $H = 2H_c$. For T = 123°K, for dysprosium[6] H_c is about 5 kilogauss. Thus for an applied field of 22 kilogauss, $H/H_c \gtrsim 4$, giving $f \gtrsim 0.97$. Thus in Dy, through most of the spiral region, one can obtain almost complete ferromagnetic alignment with a field such as the 22 kilogauss used in the present experiment. Then just as for single crystals, one should be able to obtain almost complete extinction of any optical structure associated with the spiral periodocity by applying a field of this magnitude. The fact that there is no change in the infrared transmission structure upon application of the field clearly shows that the structure does not depend on the spiral periodicity and the resulting presence of magnetic Brillouin zone boundaries.

There is an alternative explanation for the occurrence of such low frequency structure for the heavy rare earth metals. Recent work of Dimmock, Freeman and Watson[3,4] indicates that the conduction electron bands for the heavy rare earth metals closely resemble those of transition metals rather than being free electron like. This leads to a large density of states at the Fermi level. The behavior for the rare earth metals from Gd to Tm is expected to be similar in this regard. Since the situation for the heavy rare

earths is closely analogous to that in nickel and iron with flat d like bands lying close to the Fermi energy, it is quite reasonable to expect the same sort of low frequency optical structure as occurs for nickel[8-10] and iron.[10] Indeed the frequency at which the structure occurs for Dy and Ho is quite similar to that for nickel and iron. The optical structure in nickel is attributed to transitions from a flat d band to the s band in the vicinity of the Fermi energy.[8,11-13] If a similar mechanism is the cause of the low frequency optical structure in Dy and Ho, similar structure should occur for all the heavy rare earths including gadolinium which is an ordinary ferromagnet. One would expect the structure to appear from very low frequencies on cooling below T_N as the d band for minority spin electrons in the ordered magnetic state is driven increasingly above the Fermi energy by the exchange with localized f electrons. The structure would shift to higher frequencies until the maximum d band exchange splitting is obtained with thermal saturation of the magnetization. We also note that there is an indication of an additional dip in the relative transmission curves for 87°K and 123°K at about 0.6 eV. As in the case of nickel,[12,13] additional structure at such frequencies would be quite reasonable for the model just discussed. To conclude we point out that the application of a magnetic field in the way done in the present experiment would be expected to have virtually no effect on the infrared structure for such a model. Thus our present observations on Dy are completely consistent with what one expects by considering the recent band calculations[3,4] for

the heavy rare earth metals and the known behavior[8-12] of Ni.

Acknowledgements

The authors are grateful to Dr. W. Engeler and Dr. M. Garfinkel for the use of their cryostat, magnet and associated equipment. They also wish to acknowledge interesting conversations with Dr. H. R. Philipp.

References

1. C. Chr. Schüler, Phys. Letters 12, 84 (1964).
2. H. Miwa, Progr. Theor. Phys. 29, 477 (1963).
3. J. O. Dimmock and A. J. Freeman, Phys. Rev. Letters 13, 750 (1964).
4. A. J. Freeman, J. O. Dimmock, and R. E. Watson, Bull. Amer. Phys. Soc. 10, 376 (1965).
5. T. Nagamiya, K. Nagata, and Y. Kitano, Progr. Theor. Phys. 27, 1253 (1962).
6. D. R. Behrendt, S. Legvold, and F. H. Spedding, Phys. Rev. 109, 1544 (1958).
7. B. R. Cooper and R. J. Elliott, Phys. Rev. 131, 1043 (1963).
8. H. Ehrenreich, H. R. Philipp, and D. J. Olechna, Phys. Rev. 131, 2469 (1963).
9. G. S. Krinchik and G. M. Nurmukhamedov, Zh. Eksperim. i Teor. Fiz. 48, 34 (1965).

10. D. H. Martin, S. Doniach, and K. J. Neal, Phys. Letters 9, 224, (1964).
11. B. R. Cooper and H. Ehrenreich, Solid State Communications 2, 171 (1964).
12. B. R. Cooper, H. Ehrenreich, and L. Hodges, Proc. Intern. Conf. on Magnetism, Nottingham, England (September, 1964).
13. B. R. Cooper, to be published in Phys. Rev.

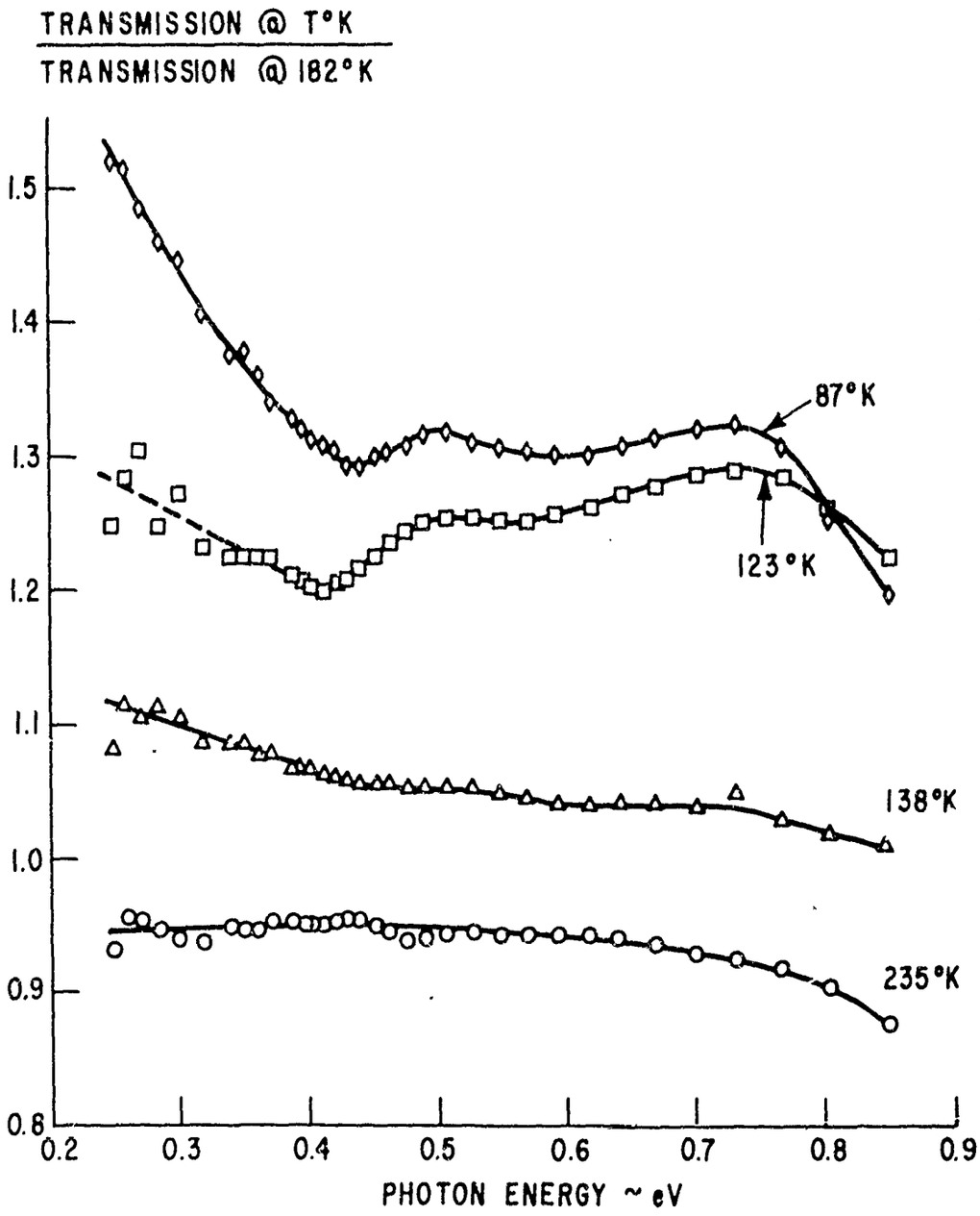

Fig. 1. Relative transmission for dysprosium films above and below the Neel temperature (179°K).

ELECTRON-SPINWAVE SCATTERING IN GADOLINIUM

B. Lüthi and H. Rohrer

IBM Zurich Research Laboratory
Rüschlikon, Zurich, Switzerland

ABSTRACT

The electrical resistivity due to magnetic scattering in polycrystalline gadolinium has been determined in the temperature range between 4.2° K and 25° K. The part of the resistivity due to scattering by domains and magnetic impurities is practically independent of temperature, whereas that due to spinwave scattering follows a $T^{3.1 \pm 0.2}$ law and is considerably smaller than the resistivity due to phonon scattering. The temperature dependence of the latter varies between $T^{2.8}$ and $T^{3.5}$.

Results are presented here of an experiment which determines directly that part of the electrical resistivity due to magnetic scattering of conduction electrons. By applying a sufficiently high magnetic field, the magnetic excitations will be frozen-out and the magnetic contribution, ρ_m, to the electrical resistivity will disappear. Up till now, a Grüneisen function for the phonon resistivity was usually subtracted from the total resistivity in order to obtain the magnetic part. It will be shown that this is incorrect at temperatures below 25° K. The experiment was performed on Gd because it is a rare earth metal where the s-f exchange mechanism stands on somewhat firm grounds, and because it has a low anisotropy field of about 1 kG at helium

PRECEDING PAGE BLANK

temperature. Six polycrystalline samples of different origin were studied with a pulsed magnetic field technique in the temperature range between 4 and 25° K. In addition, the magnetoresistance was measured in a longitudinal field in order to keep the demagnetizing field and the ordinary magnetoresistance low. Supplementary magnetization measurements in this geometry do indeed show a saturation already at about 1 kG.

Figure 1 shows typical experimental results. Here, the measured magnetoresistance is plotted against the applied field. The initial decrease of the electrical resistivity is due to the freezing-out of the magnetic scattering processes and the following increase comes from ordinary longitudinal magnetoresistance. At low temperatures, the magnetic resistance $\Delta\rho_m$ will saturate in relatively low fields ($\sim$ 40 kG) so that the normal magnetoresistance $\Delta\rho_n$ can be determined easily. By application of the Kohler-rule[1], the magnetic resistivity for higher temperatures can then be obtained, and is shown by the dotted lines in Figure 1. It should be mentioned, that the Kohler-rule, unfortunately, could not be used to compare the ordinary magnetoresistance of different samples, because most specimens showed a pronounced texture.

At higher temperatures, saturation is no longer reached in our fields and an extrapolation procedure has to be applied in order to determine the total magnetic resistivity. For high fields, a simple exponential dependence with the spinwave energy-gap is expected because normally only one-spinwave processes will be important. Such an exponential plot of $\Delta\rho_m$ does indeed give straight lines, and the total magnetic resistivity ρ_m can then be determined immediately. An additional weak field-and temperature-dependence to the exponential one, would give no noticeable changes.

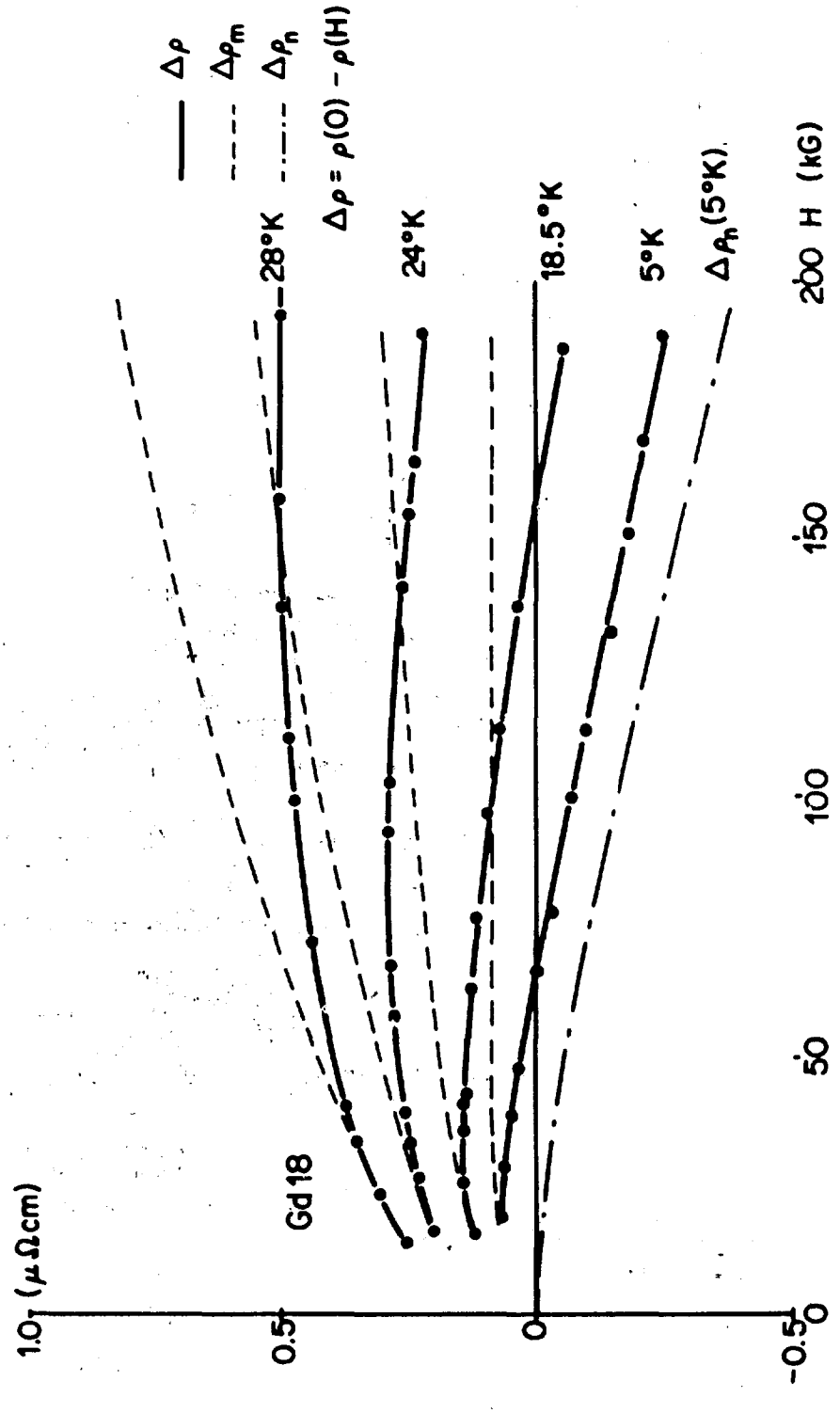

Figure 1 Magnetoresistance of Gd 18
Δρ : measured magnetoresistance Δρn : ordinary magnetoresistance
Δρm : magnetoresistance due to magnetic scattering

In Figure 2, the total magnetic resistivity for the different specimens is shown as a function of temperature. It exhibits two important features: First, the magnetic resistivity shows, similarly to the total electrical resistivity, a temperature independent contribution which is a sensitive function of the material. We attribute this residual magnetic resistivity partly to domain effects and partly to magnetic impurities. Second, the remaining, temperature-dependent part, is roughly the same for all samples and is, therefore, attributed to the scattering by spinwaves.

It is unfortunate that in the temperature region below 15° K, which is the most easily accessible region for theory, nothing can be said about the electron-spinwave scattering for the following two reasons. First, the temperature dependence of the magnetic resistivity is approximately within the experimental accuracy, and second, the magnetic impurity scattering term can also have a slight temperature dependence and can, therefore, no longer be separated from the spin wave scattering term.

A summary of the results is given in Figure 3. From Figure 3a the temperature dependence of the total resistivity is seen to vary between a $T^{3.5}$ law and a T^{3} law. In order to get the phonon resistivity, we have to subtract the magnetic part, which is plotted in Figure 3b. This phonon part is then shown in Figure 3c. Two things can be seen immediately. The temperature dependence is not at all a Grüneisen T^{5} law but varies between $T^{2.8}$ and $T^{3.5}$. Second, in our temperature range, the phonon part is considerably larger than the magnetic part, contrary to what is obtained by subtracting a Grüneisen T^{5} law from the total resistivity. A temperature dependence different from a T^{5} law can be expected if Umklapp-processes are important as will be the case in a polyvalent metal such as Gd.

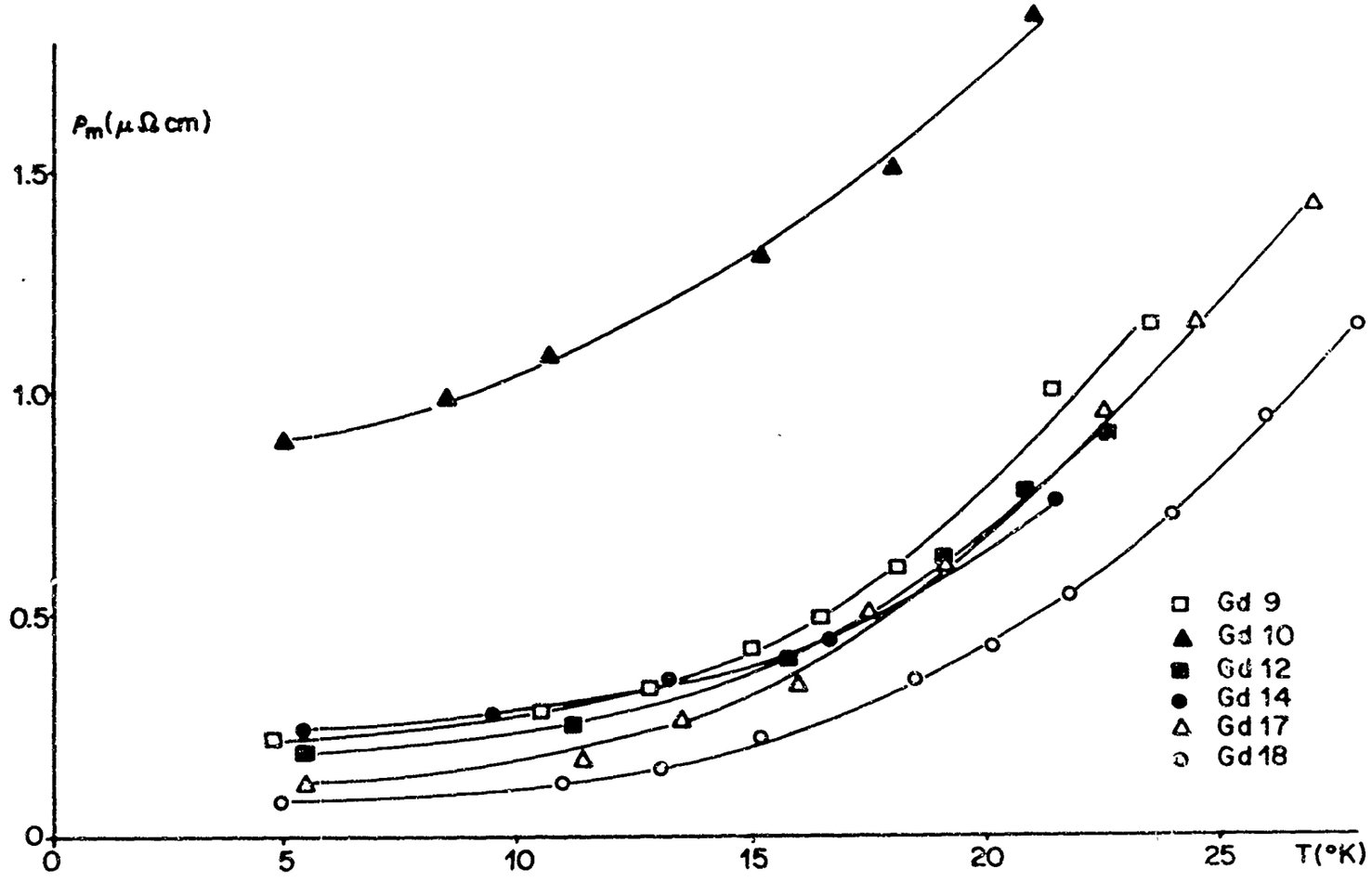

Fig. 2 Total magnetic resistivity as function of temperature.

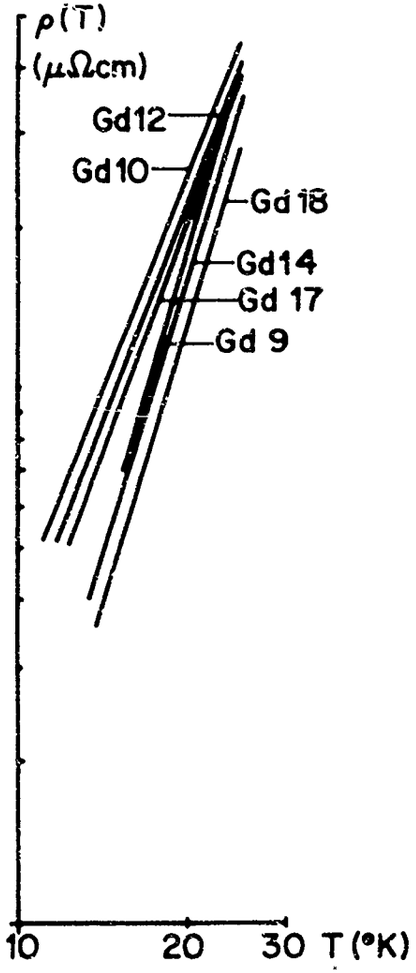

Fig. 3a Total electrical resistivity

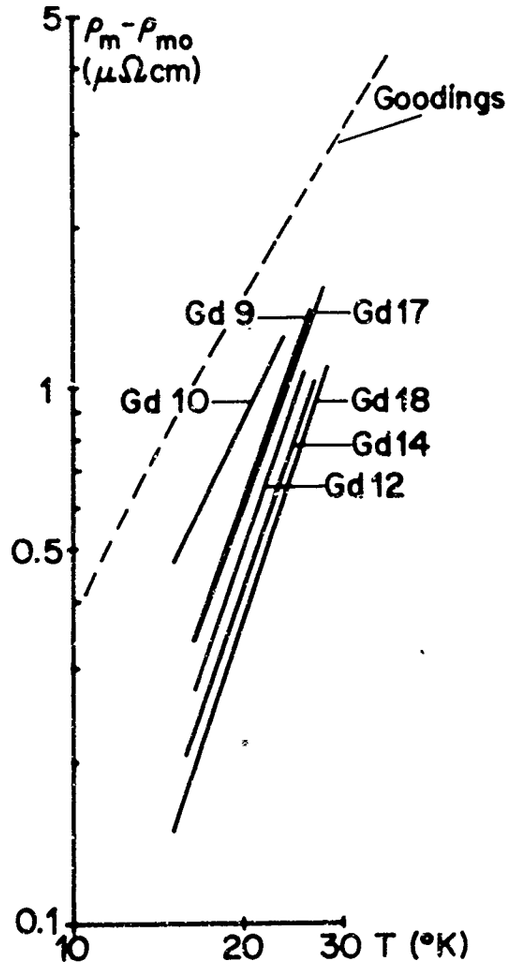

Fig. 3b Resistivity due to spinwave-scattering

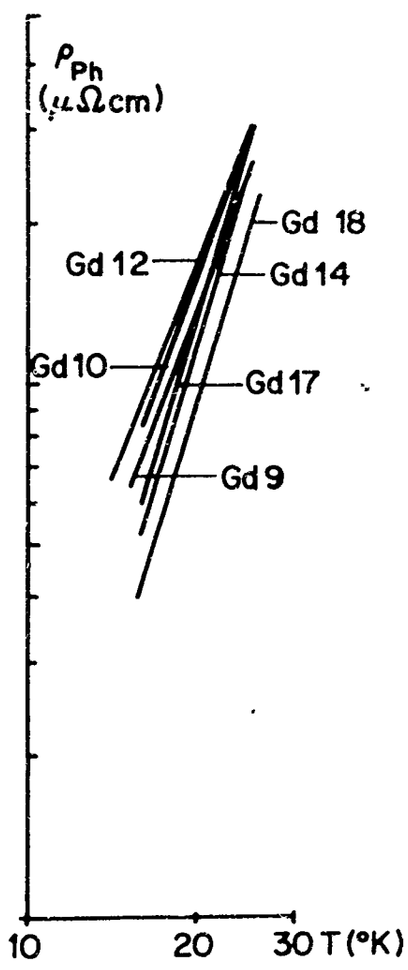

Fig 3c Resistivity due to phonon-scattering

The difference in magnitude of the phonon resistivity in various samples is due to different textures in the polycrystalline samples, which was confirmed by X-ray measurements.

The resistivity arising from the scattering by spinwaves is plotted in Figure 3b. With the exception of Gd 10, the spinwave resistivity follows roughly a $T^{3.1}$ law. Gd 10 showed an extremely high residual magnetic resistivity. An additional, weak temperature dependence of the scattering by magnetic impurities and domains could, therefore, lead to the rather large temperature dependent part of the magnetic scattering at low temperatures. The difference of the spinwave resistivity for various amples is also attributed to the different texture of the specimens.

As already mentioned above, we cannot determine the magnetic resistivity at low temperatures accurately enough to check the well-known Kasuya-T^2 law valid for a free electron gas. Little is known of the band structure of the rare earth metals. Recently, Kasuya[2] suggested a model which leads to highly anisotropic energy bands and spinwave spectra. In view of the qualitative character of this model, it is too early to predict anything about the magnetic resistivity. The only quantitative calculation in our temperature range was made by Goodings,[3] which is shown by the dotted line. He considered the spinwave induced s-d scattering. Considering the many approximations he uses, the agreement or disagreement with our results should not be taken too seriously.

REFERENCES

1. M. Kohler, Ann. Phys. 32, 211 (1938).
2. T. Kasuya, to be published in "Magnetism" edited by G. T. Rado and H. Suhl.
3. D. A. Goodings, Phys. Rev. 132, 542 (1963).

THERMAL CONDUCTIVITY AND ELECTRICAL RESISTIVITY OF SAMARIUM AT LOW TEMPERATURES

Sigurds Arajs and G. R. Dunmyre

Edgar C. Bain Laboratory
For Fundamental Research
United States Steel Corporation
Research Center
Monroeville, Pennsylvania

ABSTRACT

Thermal conductivity and electrical resistivity of samarium have been measured from 5 to 200°K and from 5 to 300°K, respectively. Two anomalies, one at 12 ± 1°K and another at 106 ± 1°K, are observed, resulting from an order-order magnetic transformation and an antiferromagnetic-paramagnetic transition, respectively. The Lorenz function is found to be larger at any temperature than that expected for pure electronic thermal conductivity. This implies that there is some phonon and possibly also some magnon thermal conductivity in samarium at low temperatures. The magnetic moment disorder electrical resistivity of samarium is determined to be 39.0 ± 0.5 μΩ cm, in fair agreement with the value to be expected from theoretical considerations.

Introduction

According to studies of the magnetic susceptibility[1], specific heat[2,3], electrical resistivity[4-6], and thermoelectric power[7], polycrystalline samarium exhibits two (magnetic) transitions at low temperatures. One occurs at about 12 ± 1°K and the other at

PRECEDING PAGE BLANK

106 ± 1°K. Neutron diffraction investigations have not yet been done on samarium. Thus, the nature of these transitions is not clearly understood at the present time. However, on the basis of the behavior of the above-mentioned physical properties, it appears that the transition at 106°K is the Néel point, i.e., a transition from an antiferromagnetic state to the paramagnetic state. The low temperature transition is quite likely a magnetic order-order transition. Recently we have found[8-11] that the changes in the magnetic state in gadolinium dysprosium, terbium, and erbium, whose detailed moment arrangements have been determined by the neutron diffraction techniques[12-15], exhibit noticeable influence on the heat conductivity of these metals. Since thermal transport studies have not yet been done on the light rare earth metals, we decided to perform such measurements. In this paper we present the results of thermal conductivity and electrical resistivity of samarium and discuss their significance.

Experimental Considerations

The sample of samarium, whose electrical resistivity and thermal conductivity were measured as a function of temperature, was prepared in the following manner. The initial stock of distilled samarium was obtained from Research Chemicals. According to the supplier a partial analysis showed the following impurities in weight %: Eu - 0.05, Ca - 0.02, Mg - 0.01, Gd - 0.01, and Si - 0.005. The metal was arc melted for 10 minutes in 100 Torr argon atmosphere. After the melting, a rod of 0.479 cm diameter and about 6 cm length

was machined from the ingot. Swaging of samarium ingots resulted in fracture, and it was therefore impossible to use this method to produce a good polycrystalline structure. The electrical resistivity of this sample at 4.17°K was found to be 6.73 μΩ cm. The electrical resistivity and thermal conductivity data were obtained using the equipment described elsewhere[16,17].

Results and Discussion

The electrical resistivity of samarium from liquid helium temperatures to 300°K is shown in Fig. 1. One clearly can observe two anomalies at low temperatures: one at 12°K and the other at 106°K. The detailed temperature variation of the electrical resistivity in the neighborhood of these temperatures is shown in Figs. 2 and 3, respectively. Since the temperature coefficient of the electrical resistivity, defined by

$$\alpha = (1/\rho)(d\rho/dT), \qquad (1)$$

where ρ is the total electrical resistivity at a temperature T, is a particularly sensitive function for the magnetic transitions, we also have plotted this quantity in Figs. 2 and 3. From these plots the above-given transition temperatures were determined.

The electrical resistivity of samarium changes almost linearly with temperature below 300°K. At about 106°K the resistivity decreases much more rapidly with decreasing temperatures than above this temperature. This behavior strongly suggests that above 106°K the magnetic moments, resulting from the localized 4f electrons in samarium, are disordered and give rise to considerable

moment disorder resistivity[18]. We estimate this from the experimental data to be 39.0 ± 0.5 μΩ cm. If one neglects the transfer of energy between the conduction electrons and the magnetic moment system, the moment disorder electrical resistivity is given by[20,21]

$$\rho_{md} = \frac{3\pi N m^*}{2\hbar e^2 E_F} G (g-1)^2 J(J+1), \qquad (2)$$

where N is the number of atoms per unit volume, m* the effective mass of a conduction electron, e the electronic charge, E_F the Fermi energy, g the Landé g-factor, J the quantum number associated with the total angular momentum of the magnetic moment, and $\hbar = h/2\pi$, h being the Planck constant. The symbol G in Equation (2) represents a coupling constant with the dimensions of energy times volume. Since the quantity in front of $(g-1)^2 J(J+1)$ in Equation (2) is expected to be approximately the same for all trivalent rare earth metals, one predicts that ρ_{md} should be proportional to $(g-1)^2 J(J+1)$. Since this factor is 4.46 and 4.50 for samarium and holmium, respectively, resistivity should be approximately equal for these two rare earth metals. This, indeed, is in accordance with the experimental results: for holmium[19] ρ_{md} = 32.3 μΩ cm which should be compared with ρ_{md} = 39.0 μΩ cm for samarium.

The thermal conductivity of samarium, also shown in Fig. 1, exhibits two maxima at low temperatures: one at about 9°K and another at 32°K. The first maximum and the following minimum at 13°K results from the low temperature magnetic order-order transformation. The observed thermal conductivity behavior is qualitatively consistent

with the electrical resistivity behavior, i.e., the rapid increase in the resistivity above 10°K causes a decrease in the thermal conductivity. The second maximum is, of course, of the conventional type observed in all pure metals. This maximum, qualitatively can be understood if one recalls that at low temperatures ($T \ll \Theta$, where Θ is the Debye temperature) the electronic thermal conductivity, limited by the impurity scattering, is proportional to T. At higher temperatures ($T \approx \Theta$) the electron-phonon scattering causes the electronic thermal conductivity to follow approximately T^{-2} dependence. Thus, a maximum in the λ vs. T curve results.

The thermal conductivity change at the Néel point, which according to the electrical resistivity data is 106°K, is not abrupt but gradual. However, the general increase in the thermal conductivity, when the magnetic moment becomes disordered, is in agreement with the results on the other rare earth metals[8,10,11] above their Néel temperatures.

In principle, the total thermal conductivity of a rare earth metal, possessing an ordered magnetic structure, should be written as

$$\lambda = \lambda^{e} + \lambda^{\ell} + \lambda^{m} , \qquad (3)$$

where the superscripts, e, ℓ, and m imply that the heat is carried by electrons, phonons, and magnons, respectively. For pure electronic thermal conductivity at low temperatures ($T \ll \Theta$), where the scattering processes can be considered elastic, one would expect

that the Lorenz function

$$L = \rho\lambda/T \qquad (4)$$

should be equal to the Lorenz number

$$L_o = \pi^2k^2/3e^2 = 2.445 \times 10^{-8}[V^2{}^oK^{-2}]. \qquad (5)$$

In this equation k is the Boltzmann constant and e the electronic charge. If some heat is also transported by phonons and magnons, then L should be larger than L_o.

Figure 4 shows the function L for samarium between 5 and 200°K. Although the Lorenz function was not determined from simultaneous measurements of ρ and λ (these properties were measured during separate runs using the same potential contacts) it is believed that L is sufficiently accurate to clearly establish that the experimental L is considerably larger than L_o at any temperature. This implies that there is some heat conduction by phonons and also possibly magnons. This aspect of the quantity L for samarium is similar to the behavior found in dysprosium[8], gadolinium[9], terbium[10], and erbium[11]. Since the present theoretical understanding of the role of magnons in the total heat conductivity of a magnetically ordered metal is quite poor, it is difficult at this moment to separate the terms λ^{ℓ} and λ^{m} from the measured values of λ. We are planning in the near future to perform thermal conductivity measurements on the above-mentioned rare earth metals (and also other ferromagnets) in the presence of strong magnetic fields (up to 60 KOe) in order to learn more about the magnitude and temperature dependence of λ^{m}.

Finally, we like to remark that recently accurate thermal

conductivity measurements on rare earth metals at 291°K have been made by Powell and Jolliffe[22]. For samarium they find $\lambda = 0.133$ W cm^{-1} °K^{-1} and $L = 4.2$ V^2°K^{-2}. These values appear to be consistent with our measurements when extrapolated from 200°K to 291°K. We did not perform thermal conductivity studies on samarium above 200°K because of serious difficulties experienced with radiation connections. For this reason our previous data on other rare earth metals[8-11] above liquid nitrogen temperatures now appear to be higher than the true values as can be concluded by the work of Powell and Jolliffe.

Acknowledgments

The authors are thankful to G. P. Wray for his technical assistance with the investigation, and to D. S. Miller for his critical review of this paper.

References

1. J. M. Lock, Proc. Phys. Soc. (London) B70, 566 (1957).
2. L. M. Roberts, Proc. Phys. Soc. (London) B70, 434 (1957).
3. L. D. Jennings, E. D. Hill, and F. H. Spedding, J. Chem. Phys. 31, 1240 (1959).
4. M. A. Curry, "Electrical Resistivity of Sm, Eu, Tm, Yb, and Lu", M. S. Thesis, Iowa State University of Science and Technology, Ames, Iowa (1958).
5. C. E. Olsen, "The Electrical Resistivity of Samarium and Europium between 1.4°K and 300°K, Los Alamos Scientific Laboratory Report LA-2406, Los Alamos, New Mexico (1960).

6. J. K. Alstad, R. V. Colvin, S. Legvold, and F. H. Spedding, Phys. Rev. 121, 1637 (1961).
7. H. J. Born, S. Legvold, and F. H. Spedding, J. Appl. Phys. 32, 2543 (1961).
8. R. V. Colvin and S. Arajs, Phys. Rev. 133, A1076 (1964).
9. S. Arajs and R. V. Colvin, J. Appl. Phys. 35, 1043 (1964).
10. S. Arajs and R. V. Colvin, Phys. Rev. 136, A439 (1964).
11. S. Arajs and G. R. Dunmyre, "Thermal Conductivity, Electrical Resistivity, and Lorenz Function of Polycrystalline Erbium between 5 and 200°K" (To be published in Physica).
12. W. C. Koehler, E. O. Wollan, M. K. Wilkinson, and J. W. Cable, "Magnetic Structure Properties of Rare Earth Metals", in Rare Earth Research (The Macmillan Company, New York, 1961), p. 149.
13. M. K. Wilkinson, W. C. Koehler, E. O. Wollan, and J. W. Cable, J. Appl. Phys. 32, 485 (1961).
14. J. W. Cable, E. O. Wollan, W. C. Koehler, and M. K. Wilkinson, J. Appl. Phys. 32, 495 (1961).
15. W. C. Koehler, H. R. Child, E. O. Wollan, and J. W. Cable, J. Appl. Phys. 34, 1335 (1963).
16. S. Arajs, R. V. Colvin, and M. J. Marcinkowski, J. Less-C Common Metals 4, 46 (1962).
17. R. V. Colvin and S. Arajs, Phys. Rev. 133, A1076 (1964).
18. B. R. Coles, Adv. Phys. 7, 40 (1958).
19. R. V. Colvin, S. Legvold, and F. H. Spedding, Phys. Rev. 120, 741 (1960).
20. P. G. de Gennes and J. Friedel, J. Phys. Chem. Solids 4, 71 (1958).
21. A. J. Dekker, J. Appl. Phys. 36, 906 (1965).
22. R. W. Powell and B. W. Jolliffe, Physics Letters 14, 171 (1965).

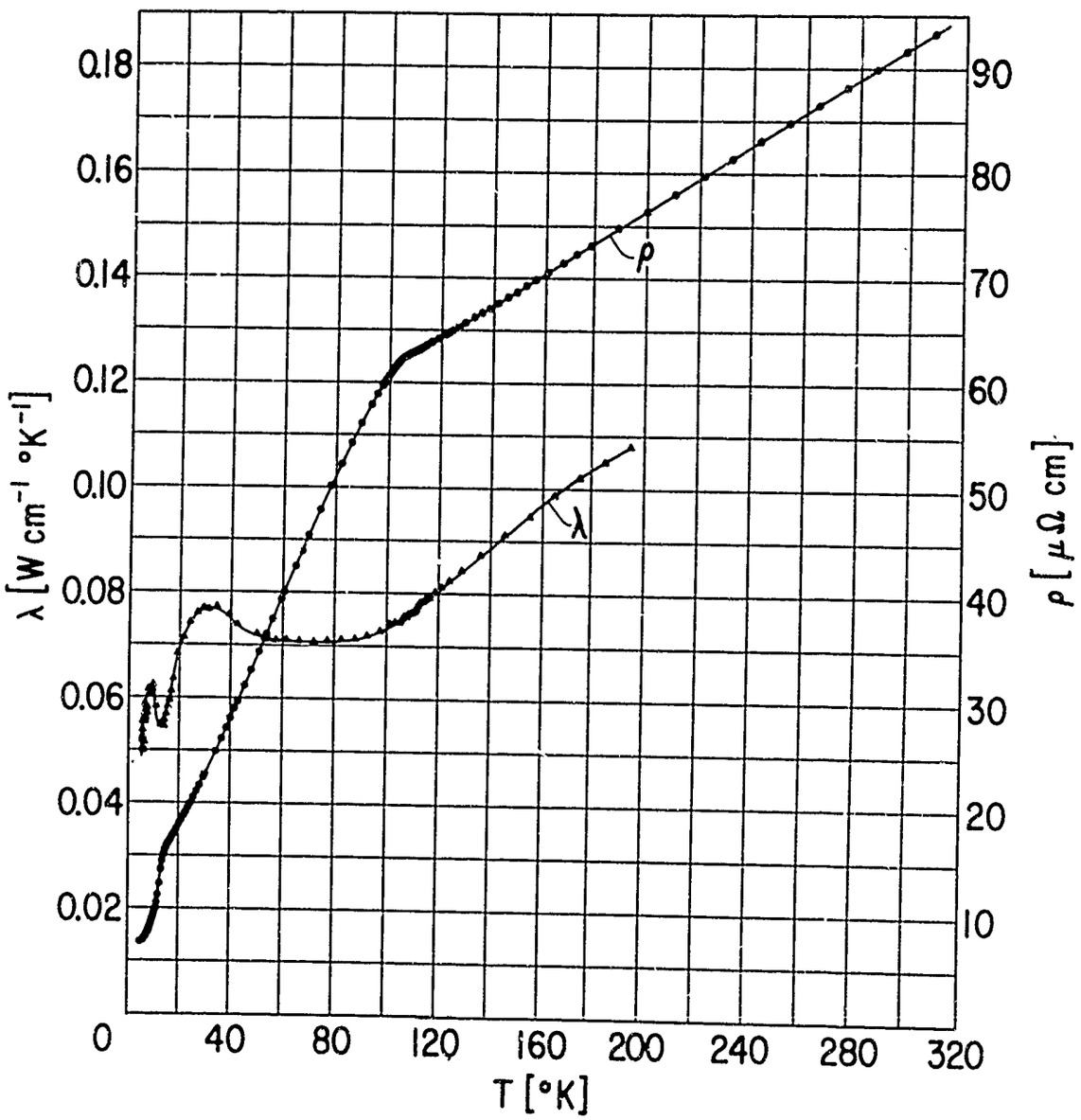

FIG. 1--ELECTRICAL RESISTIVITY AND THERMAL CONDUCTIVITY OF SAMARIUM AS A FUNCTION OF TEMPERATURE.

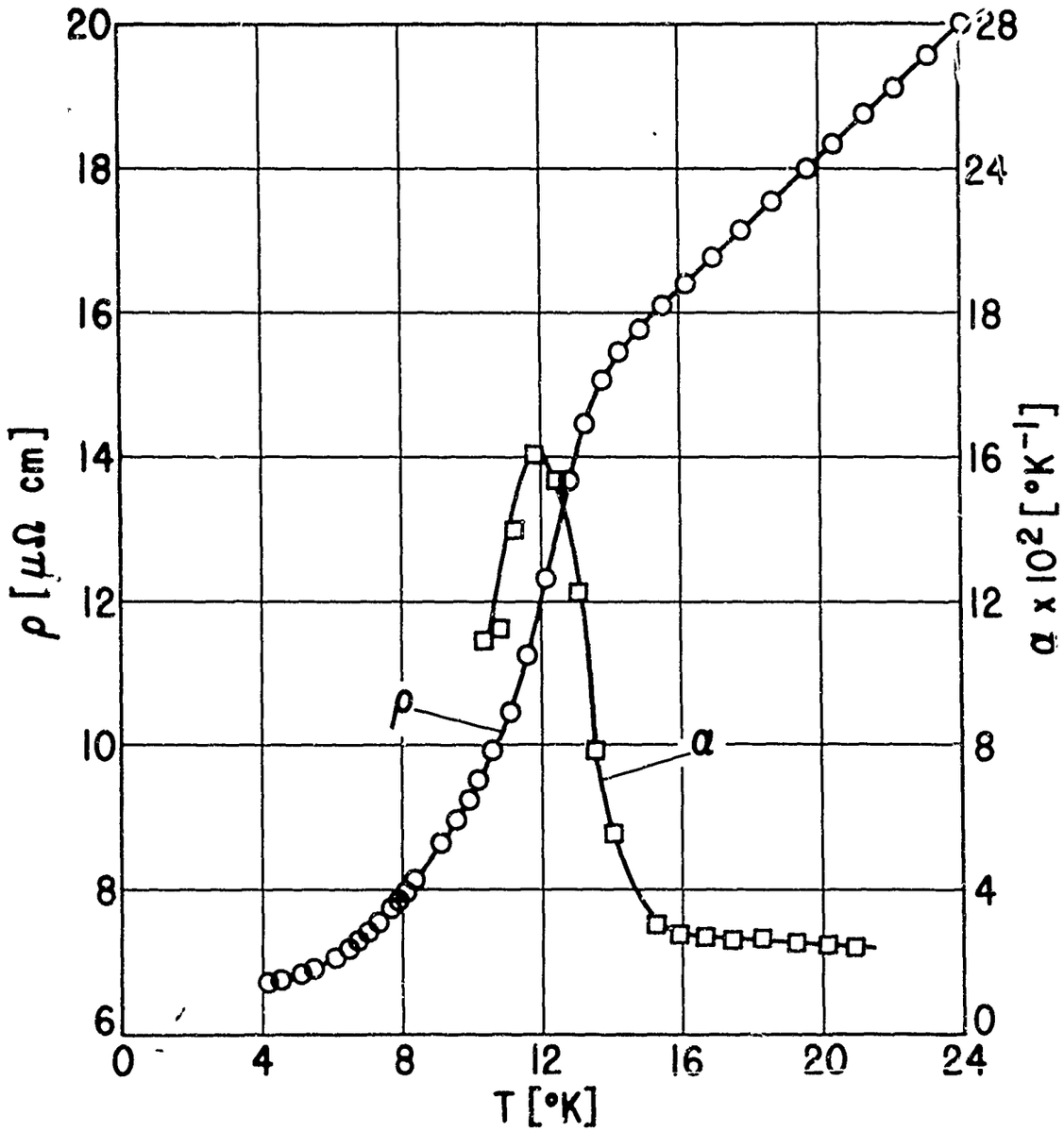

FIG. 2--ELECTRICAL RESISTIVITY OF SAMARIUM AND ITS TEMPERATURE COEFFICIENT.

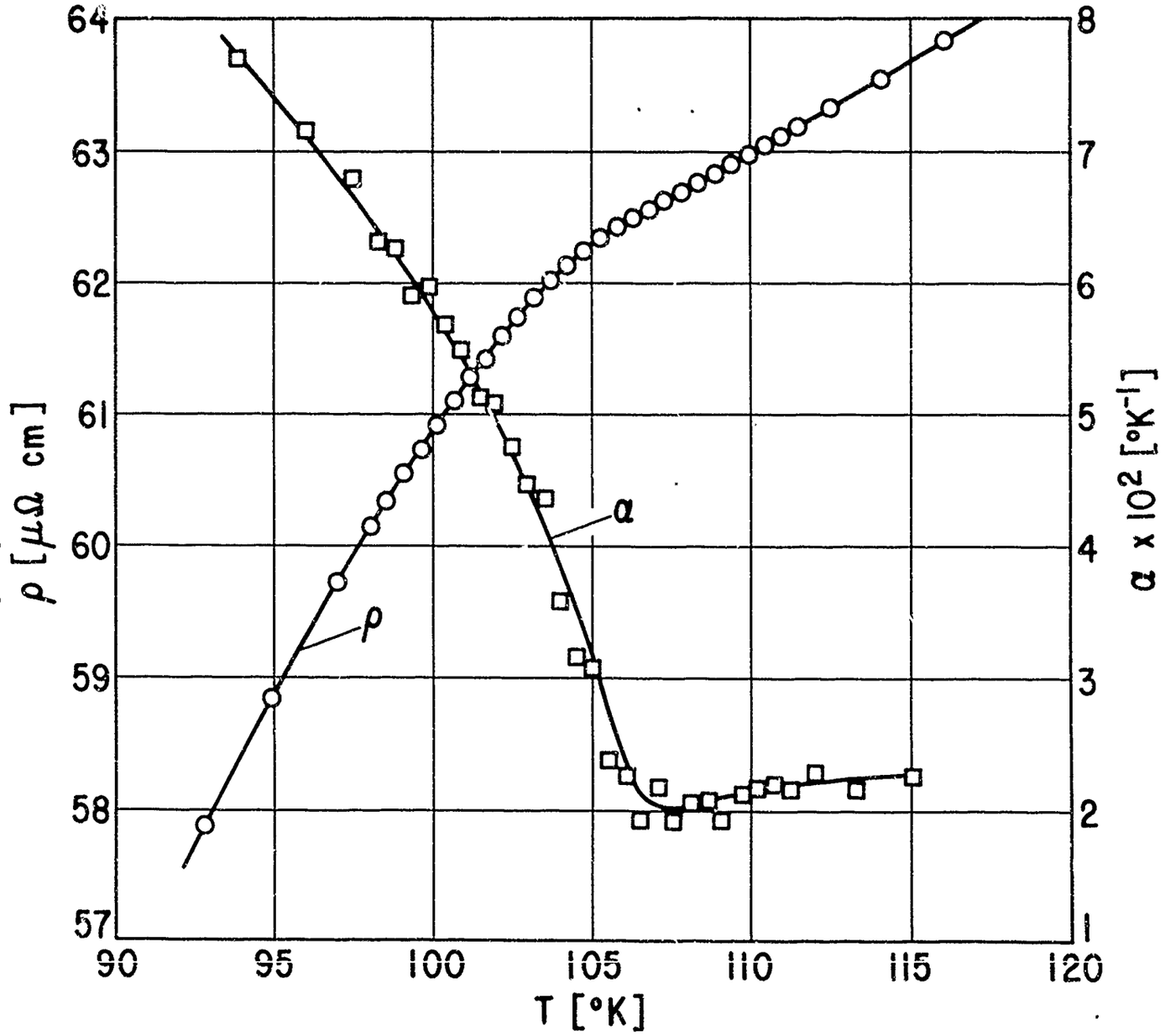

FIG. 3--ELECTRICAL RESISTIVITY OF SAMARIUM AND ITS TEMPERATURE COEFFICIENT.

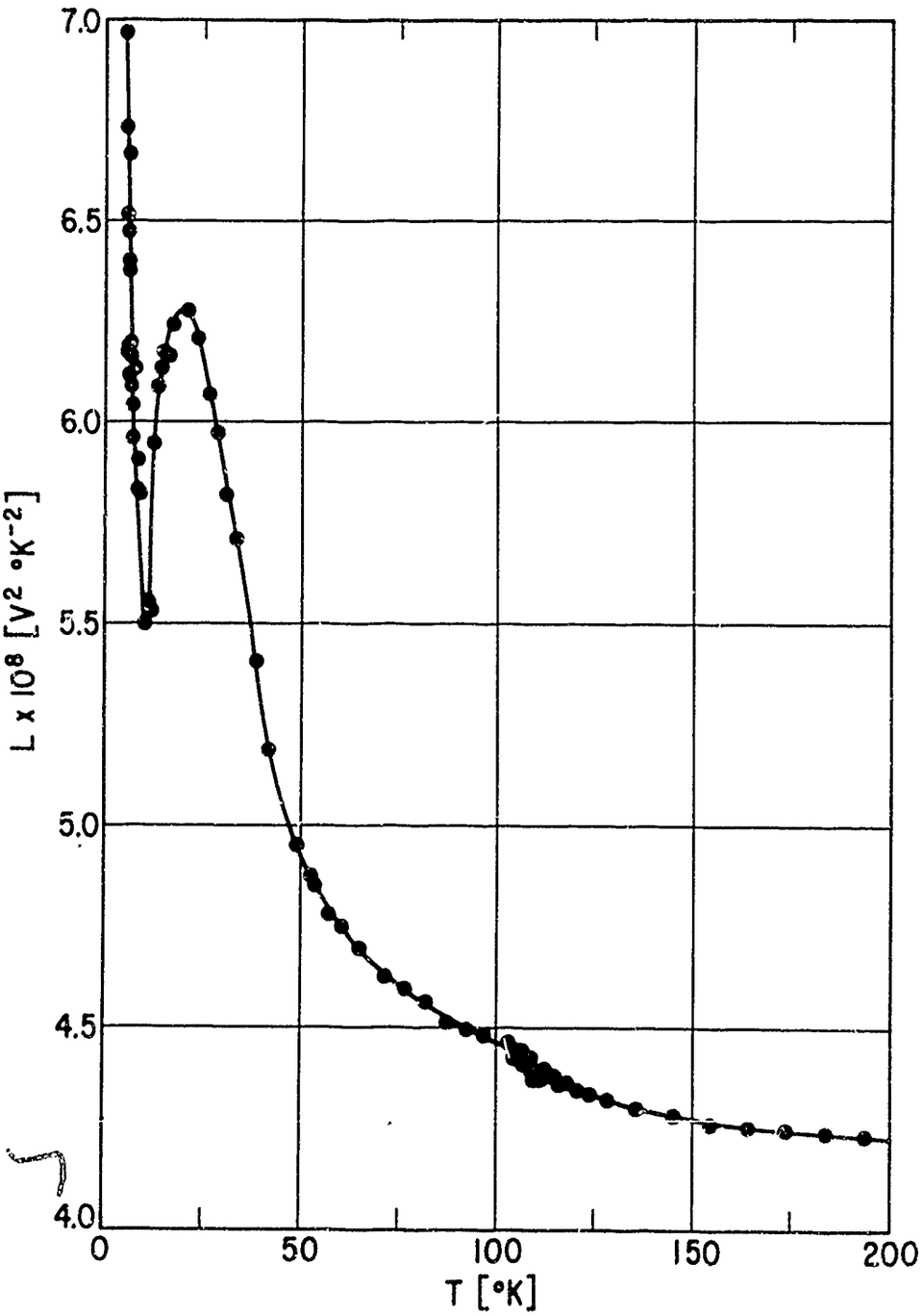

FIG. 4--LORENZ FUNCTION OF SAMARIUM AT LOW TEMPERATURES.

RESULTS OF AUGMENTED PLANE WAVE CALCULATIONS OF THE BAND STRUCTURE OF CERIUM METAL*

J. T. Waber† and A. C. Switendick‡

†University of California
Los Alamos Scientific Laboratory, Los Alamos, New Mexico
‡Sandia Laboratory, Albuquerque, New Mexico

ABSTRACT

Ten sets of electronic band structure calculations were performed for cerium metal by using the augmented plane wave method for five configurations of the type $6s^2 5d^x 4f^{2-x}$ and the lattice constants appropriate to the FCC gamma and FCC alpha phases. It is shown that the location of the f band is strongly dependent on the atomic configuration assumed in starting the calculation. The relation of these results to previous atomic calculations is discussed.

It is believed that the bands should not be occupied to a common energy level according to a simple Fermi-Dirac distribution, but rather that the 4 electrons outside the xenon core should be arranged in the f as well as in the s and d bands so as to be reasonably consistent with the configuration assumed. As a consequence the f-band location is dependent on the degree to which it is occupied. The two-electron calculations by Waber, Liberman and Cromer of the total energy for a cerium atom confined to a Wigner-Seitz sphere lend further support to this assignment hypothesis.

*This work was supported by the U. S. Atomic Energy Commission.
Reproduction in whole or in part is permitted for any purpose of the U. S. Government.

Introduction

Cerium metal, because of its several allotropic forms, offers the interesting opportunity of investigating how the electronic band structure of a metal changes with the arrangement and spacing of neighboring atoms. The band structure of iron in the body-centered and face-centered cubic forms was studied by Wood.[1] Such an investigation apparently has not been done for any other metal. The explanation given by Pauling[2] and by Zachariasen[3] for the transformation of cerium from the FCC gamma form to the "collapsed" FCC alpha form is that a 4f electron is promoted into the conduction band when the alpha phase is formed. To date the only study of the effect of configuration on band structure was done by Mattheiss[4] for vanadium. Even though only a portion of the bands was calculated, sensitivity to assumed configuration was indicated. For these reasons cerium is an interesting metal to study in some detail. The band structures of the double HCP beta and the BCC delta phase of cerium will not be discussed.

The only rare-earth metal for which a band calculation has been done to date is gadolinium, studied by Dimmock and Freeman.[5] They assumed the configuration to be $4f^7 5d^1 6s^2$. They found that the narrow f bands were approximately 0.8 Rydberg below the s and d bands. Rather than permitting the three conduction electrons to occupy this f band, they argued that to regard gadolinium as being in a configuration f^{10} would substantially raise the total energy. Thus from their experience with Hartree-Fock calculations (which are of a two-electron nature) they chose a configuration before solving the one-electron band structure problem. Apparently, however, no numbers were presented to justify their plausible approach.

Raynor and his colleagues[6-9] have attempted to elucidate the change in the metallic valence of cerium dissolved in different metals. Assuming that the valence of a metal can be directly related to its metallic diameter they deduce, from the apparent atomic diameter, that cerium acquires (or approaches) the valence of the solvent metal. The operative mechanism they postulate is the variation of strain energy with

the size of the hole into which the solute is placed.

No proposed electronic configuration for cerium metal has been universally accepted. Gschneidner and Smoluchowski[10] concluded on the basis of a variety of experimental data that one 4f electron is in a localized atomic state in gamma cerium and approximately 0.4 of a 4f electron in the alpha phase. In the present study, no a priori division of electrons was made. Certain conclusions can nevertheless be made.

Previous Studies of Atomic Configuration

Larson and Waber[11] presented the results of one-electron Hartree calculations for the free cerium atom at the Third Rare Earth Conference. The binding energy of the 4f electrons in the general atomic configuration $6s^2 5d^x 4f^{2-x}$ was shown to increase with the occupancy of the 5d orbitals. From the total energy of the free atom in this Hartree approximation they concluded that the probable configuration of the free atom was $6s^2 5d^{1.5} 4f^{0.5}$; the total energy E_T was approximately -16,794 Rydbergs.

As a more reasonable approximation, Waber, Liberman and Cromer[12] studied for the Fourth Rare Earth Conference the behavior of a cerium atom with the same general configuration confined to a Wigner-Seitz sphere of radius R_{ws}. In place of the non-relativistic self-consistent field (SCF) Hartree functions, they used the relativistic SCF Dirac-Slater wave functions,[13] which include exchange. The strong dependence of the one-electron energy eigenvalues on the occupancy of the 5d orbitals is shown in Fig. 1. Curves are shown for two radii, namely the Wigner-Seitz radii appropriate to the alpha (dotted) and gamma (full) phases.

This graph leaves the impression that the most stable configuration is $6s^2 5d^2$, since each of the eigenvalues is more negative for x = 2.0. When two-electron effects are included, this conclusion is modified. The total energy E_T was computed by the method of Snow, Canfield and Waber.[14] Results for different radii R_{ws} and different configurations are shown in Fig. 2. One concludes that the most stable configuration depends on the size of the Wigner-Seitz sphere, i.e. on the pressure.

It will be shown below that in the band structure calculations the location of the bands depends on the assumed electronic configuration. The f-like bands depend strongly on x, the occupancy of the d bands.

Method of Calculation

The augmented plane wave method was first proposed in 1937 by Slater.[15] The principal computational details of this method have been given by Wood.[1] In the present work, the Bloch function was expanded in terms of spherical harmonics with angular momenta $\ell \leq 13$. In general, the maximum value of the wave vectors retained in the set was $6\pi/a_o$. With this set, convergence was indicated to be better than 0.003 Rydberg.

Ern and Switendick[16] have discussed how to obtain the charge density associated with a particular angular momentum from the symmetrized APW crystal eigenfunctions.

The crystal potential was constructed by the method of Mattheis.[17] Namely, atomic overlap contributions were computed by Löwdin's alpha expansion method.[18] Contributions to the electronic charge densities were added out to the set of fourth nearest neighbors, in the present study, and spherically averaged. Dirac-Slater wave functions were used for each configuration. Slater's $\rho^{1/3}$ method[19] was employed to incorporate exchange by using the summed and spherically averaged charge density ρ.

Since the APW program available to us used the "telescoping" linear presentation mesh of Herman and Skillman,[20] values of the potential were interpolated at appropriate radii from the logarithmic radial mesh that Liberman, Waber and Cromer[13] used in calculating the Dirac-Slater wave functions.

The constant or muffin tin potential in the region between the APW sphere and the Wigner-Seitz sphere was obtained by spherically averaging the summed potentials and the exchange contribution. It was found that this potential increased linearly with x, the 5d occupancy, in both the gamma and alpha size spheres. The numbers are tabulated in Figs. 3 and 4.

Results

The band structure curves have been obtained for two sizes of the lattice constant and for five electronic configurations in each size. The complicated energy dependence $E(\vec{k})$ was obtained at 256 points in the Brillouin zone, namely at points $(\frac{m}{2}, \frac{n}{2}, \frac{p}{2})$ of the reciprocal lattice. Because of the narrowness of the f bands, it was necessary to evaluate the secular determinant at energy intervals as small as 8×10^{-5} Rydberg or 9 cm^{-1}. The results reported here may be regarded as preliminary since it was difficult to obtain all 13 eigenvalues (for s, d and f-like bands) associated with certain low symmetry or general wave vectors.

The over-all behavior of the bands as a function of configuration is shown in Figs. 3 and 4. For convenience and clarity, only the direction Γ to X (along Δ) is shown for each graph. The APW method partially incorporates the effect of the crystal field in lifting the degeneracy of states having a given angular momentum. For example,* the seven f-like atomic states (either spin) are separated into a non-degenerate Γ_{2*} and the two triply degenerate Γ_{15} and Γ_{25} states. Similarly, the 5d atomic states are split into the triply degenerate Γ_{25*} (t_{2g}) and doubly degenerate $\Gamma_{12}(e_g)$ states. Comparing Fig. 3 for the gamma-phase size with Fig. 4 for the collapsed or alpha phase, one sees that the crystal field splitting is larger in the latter case. In addition, one observes that the band width is larger, presumably because of increased overlap.

The pattern of the s and d bands, such as is typical of a 3d transition metal, is clearly discernible at the far right-hand side of these figures where it is assumed that no 4f states are occupied. This premise is unjustified because the calculations yield low-lying f states. At the far left-hand side, the f bands, which are shown as a cross-hatched region, interact with the s and d bands and the result is a more

---

*The notation used is substantially the same as that of Bouckaert, Smoluchowski and Wigner[21] except that the primed states are designated by asterisks to facilitate reading of the graphs.

complicated picture. Although the configuration $6s^2 4f^2$ is assumed, the f states are too high and would not be occupied; that is, the lower lying states which will hold four electrons have predominantly s and d character. For intermediate configurations such as $6s^2 5d^{1.5} 4f^{0.5}$ one, on the basis of the usual one-electron band picture, would put the four available electrons into the low-lying f states, despite the assumed configuration with a large d-character. Thus, one is led to conclude that an intermediate value of x, the d-orbital occupancy, is more reasonable.

The Schrödinger equation, as solved in any band structure calculation made to date, involves an average one-electron potential. That is, all solutions are obtained in the field of a single assumed charge distribution. One calculates E(k) curves which show crystal eigenstates of the assumed potential. These states are occupied by the valence electrons in accordance with Fermi-Dirac statistics, and occupancies are usually found which are reasonably consistent with the assumed configuration. In contrast, if one finds, as we do in cerium, a derived occupancy which is in conflict with the assumed one, other methods of assigning the occupancy should be studied. The simple Fermi-Dirac distribution may have to be modified. The reason is that, in the latter model, the energy states are assumed to be independent of the occupancy whereas our results clearly show the opposite.

When one calculates the E(k) curves for states lying above the Fermi energy, what he does in analogy to the atomic SCF calculations is to compute the eigenvalue for an unoccupied orbital. This often is a reasonable approximation to the correct eigenvalue. However, in a more correct treatment, if he were to take an electron from a normal valence state and put it into an excited orbital such as 5g and then complete an SCF calculation, he would find a different potential due to the new charge distribution. Consequently all of the one-electron eigenvalues would be changed. The 1s electrons would be affected only slightly and their charge distribution would be virtually unaltered. However, for the valence electrons, both their charge distribution and their eigenvalues

would be strongly affected. The rearrangement energy or shifts in eigenvalues corresponding to occupancy of higher states, or states not initially assumed, are not usually considered in band structure calculations. The present study, as do the atomic calculations, shows that the rearrangement energies due to reassignment of the occupancy need not be small. For cerium, rearrangement energies play an important role. A similar situation, although not as drastic, has been found in the study of the band structure of nickel by Snow, Switendick and Waber.[22]

When empty, the f states are very well bound as Fig. 1 shows. However, when they are filled to a reasonable extent, the electrostatic repulsion between orbitals increases sharply, and their eigenvalues rise above those of possible competing s and d states. Thus, it is suggested that a balance occurs, which results in an intermediate number of occupied states. These general remarks apply to band as well as to atomic calculations.

Generally the shape of the E(k) curves is relatively insensitive to the assumed electronic configuration, but this need not always be true. In the case of cerium, as the f bands move through the region of the s and d bands considerable modification occurs because of interaction between bands.

Kittel[23] in his appendix N shows that the partial molar free energies (or chemical potentials μ) of transferring electrons from phase i to phase j must be equal. In equilibrium the Fermi level must be the same in the two phases in contact. This argument can easily be extended to two competing bands. The partial molar free energy or the chemical potential for transferring an electron from the s and d bands to the f bands, or vice versa, also involves the energy shift due to the rearrangement of occupancies. Thus the energy which would be gained by the transfer of an electron into a partially filled f band is partially offset by the increased electrostatic interactions and the relocation of the f band. Such interactions are not embraced in the usual framework of Fermi-Dirac statistics. Thus we believe that each band does not have to be occupied to the same level, but rather that partial molar free

energies must be equal. Because of the effect of occupancy in the f bands on their location, we believe that the most appropriate band calculation to be used in estimating physical properties is one which is most nearly consistent with the assumed configuration or occupancy. In the present calculations, intermediate values of x between 1.0 and 1.5 in the general configuration $6s^2 5d^x 4f^{2-x}$ appear to meet this criterion.

Certain trends are clearly indicated by the present study. One of these is the effect of pressure. If we look at the $6s^2 5d^1 4f^1$ configuration for both the gamma and alpha phases, we see that, for alpha cerium, the f bands are contiguous to the s and d bands, whereas in gamma cerium about 0.1 Rydberg separates the f band from the s and d bands. Despite being labeled as f states, there is considerable mixing and a considerable amount of d-character when they are near the d band.* Thus one would conclude that a consistent assignment of occupancy would include more d-like electrons in the collapsed alpha phase than in the gamma.

The present results indicating an intermediate value of x, the d orbital occupancy, and a larger value of x in the alpha phase are in reasonable agreement with the two-electron cellular calculations of Fig. 2. Further, the results are not inconsistent with the assignment which Gschneidner and Smoluchowski[10] made, namely $6s^2 5d^{1.05} 4f^{0.95}$ for gamma and $6s^2 5d^{1.54} 4f^{0.46}$ for alpha cerium.

One of the inferences of this investigation is that a satisfactory and self-consistent band structure of a general metal cannot be achieved until the two-electron interactions are incorporated into the analysis. As a first step, it appears to be reasonable to calculate the electrostatic $< ij|\frac{1}{r_1 - r_2}| ij >$ and the exchange $< ij|\frac{1}{r_i - r_2}| ji >$ contributions. It is an interesting point that use of the one-electron APW method yields results similar to those found by the two-electron total energy calculation, namely an intermediate value of x is a more consistent

*On the basis of our charge density calculations we find less than two s-like electrons in the conduction band. This result is also usually found for the transition metals.

picture of occupancy of cerium in the solid.

To sum up, a large but reasonable sensitivity of the location of s, d and f bands to electronic configuration assumed for cerium atoms has been demonstrated. Because of new questions raised by this result, it is premature to assign a definite configuration to metallic cerium from these ab initio calculations.

Acknowledgments

The very great courtesy of Professors John Slater and John Wood in making the APW program available to us and their interest in this problem is deeply appreciated. Fruitful discussions with Drs. Arthur Freeman and Edward Kmetko are gratefully acknowledged. The computational staff of Los Alamos Scientific Laboratory has been of considerable assistance. Finally, we would like to acknowledge the patient and pleasant cooperation of Edward Snow and Mrs. Margaret Prince.

References

1. J. H. Wood, Phys. Rev., 126, 517 (1962).
2. L. Pauling, J. Amer. Chem. Soc., 69, 542 (1947).
3. W. H. Zachariasen quoted by A. Lawson and T. Tang, Phys. Rev., 76, 301 (1949).
4. L. F. Mattheiss, Phys. Rev., 134, A970 (1964).
5. J. O. Dimmock and A. Freeman, Phys. Rev. Lett., 13, 750 (1964).
6. R. T. Weiner, W. E. Freeth and G. V. Raynor, J. Inst. Metals, 86, 185 (1957-58).
7. D. S. Evans and G. V. Raynor, J. Nucl. Mater., 5, 308 (1962); also J. Less Common Metals, 4, 181 (1962).
8. I. R. Harris and G. V. Raynor, J. Less Common Metals, 6, 70 (1964), also ibid, 7, 1 (1964).
9. J. T. Waber, I. R. Harris and G. V. Raynor, Trans. Met. Soc. AIME, 230, 148 (1964).
10. K. Gschneidner and R. Smoluchowski, J. Less Common Metals, 5, 372 (1963).
11. A. C. Larson and J. T. Waber, Proc. 3rd Rare Earth Conference (Clearwater 1963) (Gordon and Breach, New York, 1964) p. 351.
12. J. T. Waber, D. Liberman and D. T. Cromer, Proc. 4th Rare Earth Conference (Phoenix 1964) (Gordon and Breach, New York) in press.
13. D. Liberman, J. T. Waber and D. T. Cromer, Phys. Rev., 137, A27 (1965).
14. E. C. Snow, J. M. Canfield and J. T. Waber, Phys. Rev., 135, A969 (1964).
15. J. C. Slater, Phys. Rev., 51, 846 (1937).
16. V. Ern and A. C. Switendick, Phys. Rev., 137, A1927 (1965).
17. L. F. Mattheiss, Phys. Rev. 133, A1399 (1964).
18. P. O. Löwdin, Advan. Phys., 5, 1 (1956).
19. J. C. Slater, Phys. Rev., 81, 385 (1951).
20. F. Herman and S. Skillman, Atomic Structure Calculations (Prentiss Hall, New York, 1963) p. 5-3 et seq.
21. L. P. Bouckaert, R. Smoluchowski and E. Wigner, Phys. Rev. 50, 58 (1936).
22. E. C. Snow, A. C. Switendick and J. Waber (unpublished results).
23. C. Kittel, Introduction to Solid State Physics (Wiley, New York, 1956) 2nd ed., p. 590.

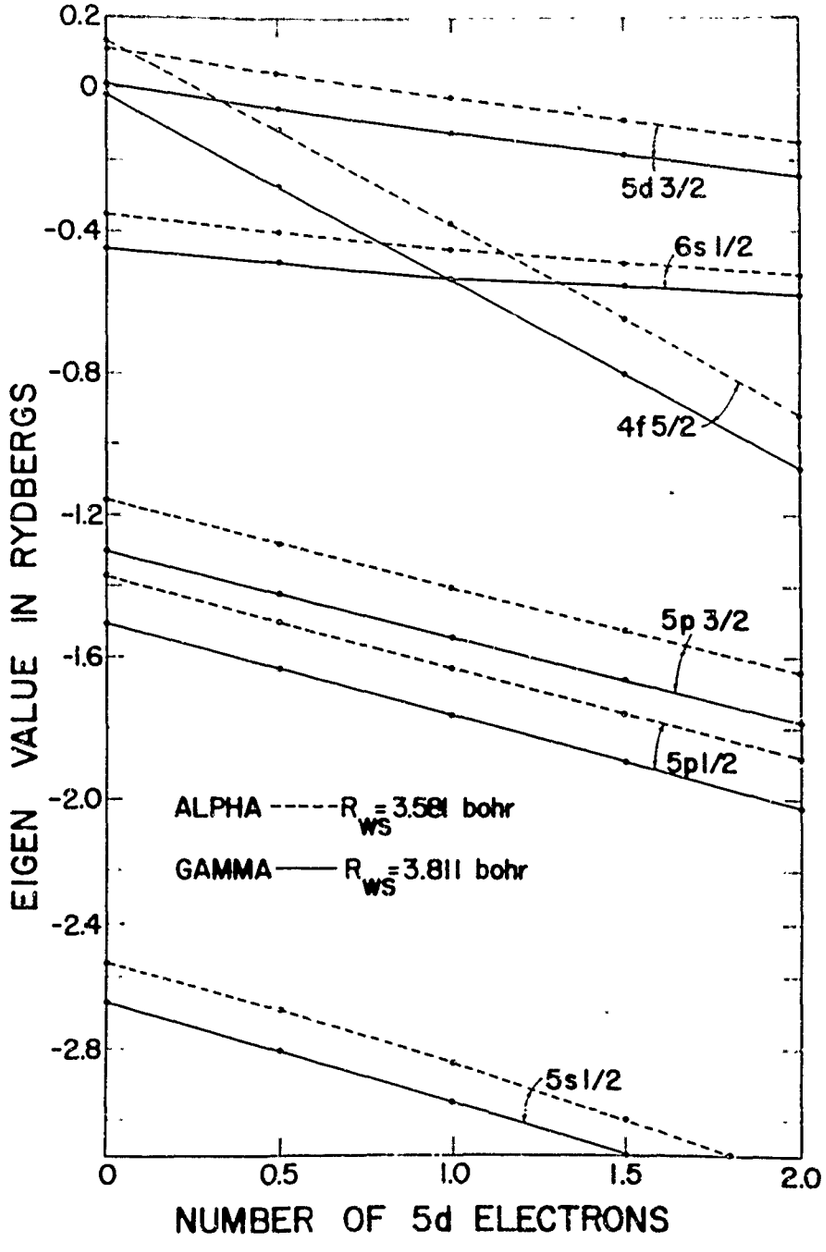

Fig. 1. Effect of the assumed configuration and sphere radius R_{ws} on the Dirac-Slater one-electron eigenvalues of alpha and gamma cerium. The j-values of the $(n\ell j)$ orbitals are indicated.

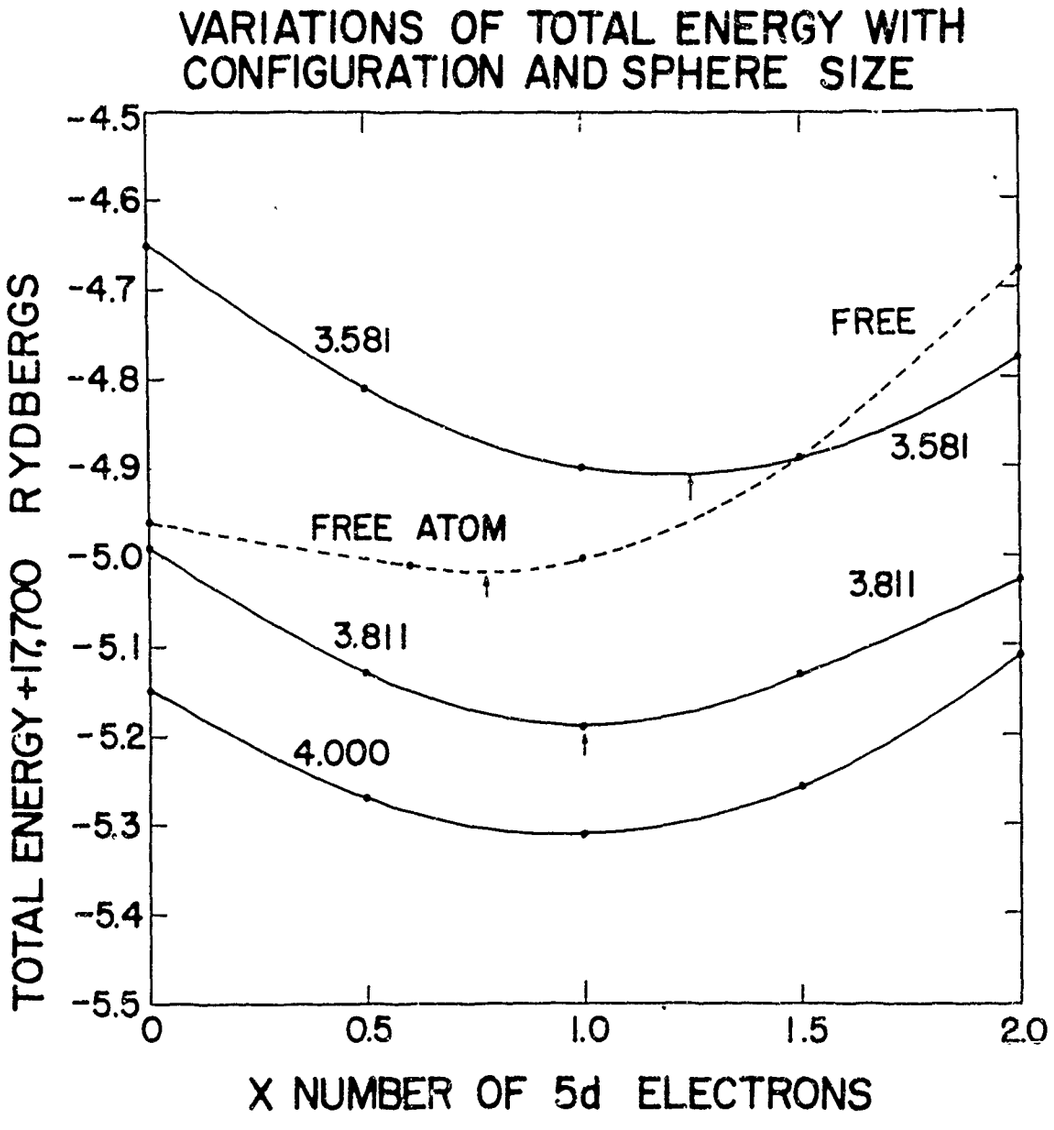

Fig. 2. Effect of assumed configuration and sphere size on the two-electron total energy of the confined cerium atom.

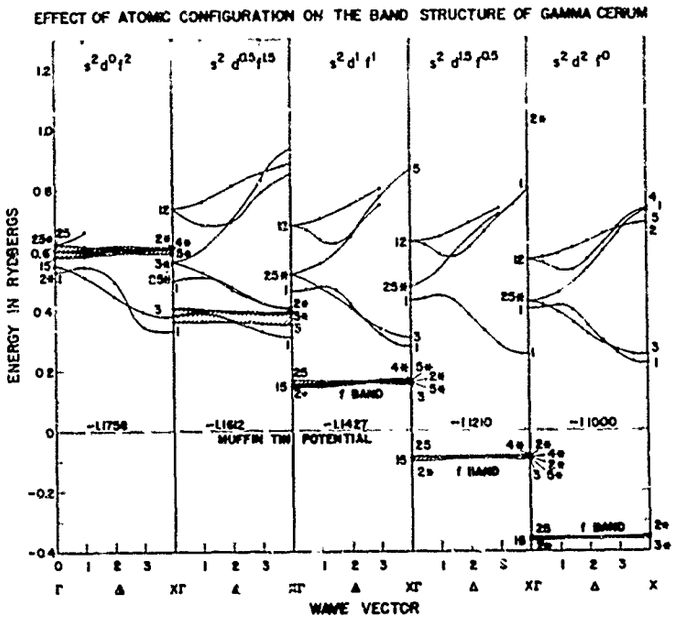

Fig. 3. Effect of the assumed configuration on the band structure of gamma cerium.

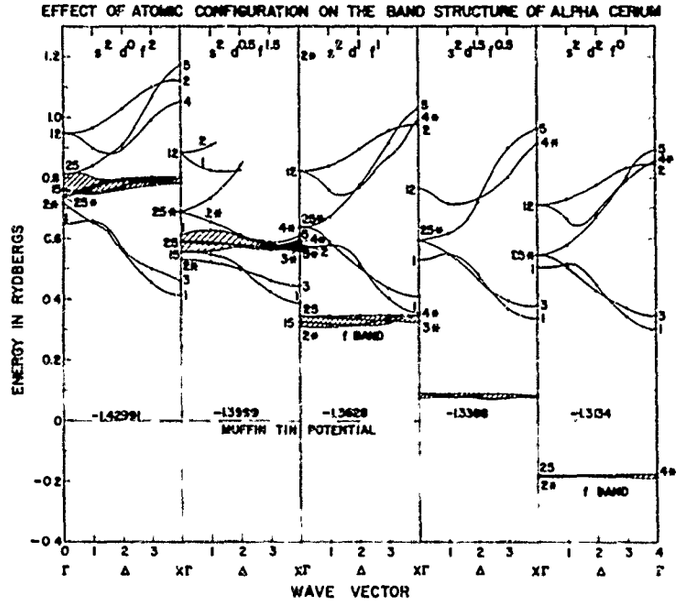

Fig. 4. Effect of the assumed configuration on the band structure of alpha cerium.

THEORETICAL RESULTS FOR POSITRON ANNIHILATION IN RARE EARTH METALS*

T. L. Loucks

Institute for Atomic Research and Department of Physics
Iowa State University, Ames, Iowa

ABSTRACT

The angular correlation of the photons from two-quantum positron annihilation has recently been measured in single crystals of holmium at 300°K and 70°K.[1] These results exhibit some very interesting structure as compared to the usual free-electron parabola, and they show clearly that the Fermi surface of holmium is highly anisotropic. An attempt is being made to reproduce these results theoretically; the method of calculation will be discussed in this paper.

The model is based on the muffin-tin potential and Augmented Plane Wave method (APW) of Slater.[2] The potential for the electrons (including free-electron exchange based on the local charge density in the crystal) is constructed from self-consistent-field atomic calculations. A similar potential (with opposite sign) is constructed for the positron with exchange excluded. The wave function for the positron is taken to be constant outside the APW spheres and is determined numerically inside the spheres using the positron potential and requiring zero slope at the sphere radius. The electronic wave function is taken to be a linear combination of APW's. The expansion coefficients are determined by finding the crystal eigenvalues from the secular equation and

PRECEDING PAGE BLANK

solving the coupled equations which result from the variational expression for the energy.

The probability that a photon pair will be produced with z-component of momentum P_z is proportional to

$$N(P_z) = \int_{-\infty}^{\infty} \int_{-\infty}^{\infty} dP_x dP_y \; \rho\,(P_x, P_y, P_z)$$

where

$$\rho(\underset{\sim}{P}) = \sum_{\underset{\sim}{k}} \left| \int \psi_{\underset{\sim}{k}}(\underset{\sim}{r})\; \psi_{+}(\underset{\sim}{r})\; \ell^{-i\underset{\sim}{P}\cdot\underset{\sim}{r}}\, d\tau \right|^2$$

An expression for N(Pz) has been developed using the above muffin-tin model for the electron and positron wave functions. Since it is based on the APW method it will have application not only to free-electron metals but also to transition and rare-earth metals. The results of this method should be very useful as an aid in the interpretation of positron annihilation experiments since these depend in a very complicated way on both the topology of the Fermi surface and the wave functions of the annihilating particles.

---

*Work performed in the Ames Laboratory of the U. S. A. E. C.

1. A. R. Mackintosh and R. W. Williams (to be published).

2. J. C. Slater, Phys. Rev. 51, 846 (1937).

HIGH PRESSURE POLYMORPHISM AND MAGNETIC ORDERING IN SOME Sm-TYPE RARE EARTH ALLOYS AND SAMARIUM

A. Jayaraman, R. C. Sherwood, and E. Corenzwit

Bell Telephone Laboratories, Incorporated
Murray Hill, New Jersey

ABSTRACT

The rare earth alloys LaY, PrY, NdY, NdTm and $LaGd_3$ all of which crystallize in the Sm-type structure undergo a pressure-induced phase change to the double hexagonal close packed structure (La-type); the high pressure phase is metastably retained at atmospheric pressure. However, under similar pressure and temperature treatment CeY decomposes to the elements. Magnetic data are presented for the normal and high pressure phases of NdTm, $LaGd_3$ and Sm; in the latter case the data are from earlier measurements. The significance of the breakdown of CeY and the anomalies in the low temperature magnetization data of $LaGd_3$, NdTm and Sm are discussed.

INTRODUCTION

A pressure-induced phase transformation to the double hexagonal close packed structure has been reported in Sm-metal.[1] The high pressure phase (dhcp) is retained metastably at atmospheric pressure and undergoes antiferromagnetic ordering at 27°K, about 12° higher than the Néel temperature observed for the normal form of Sm. Many rare earth binary alloys involving a lighter rare earth element than Sm, and a heavier rare earth element or Y, crystallize in the Sm-type structure,[2,3,4,5] near the equiatomic proportion. In some systems as for instance La-Gd, the

Sm-type structure is stable near the composition $LaGd_3$. It occurred to us that these alloys might undergo a pressure-induced structural transformation, similar to that found in the Sm metal. We have investigated LaY, CeY, PrY, NdY, NdTm and $LaGd_3$ in the present study. The magnetic behavior of NdTm and $LaGd_3$ was studied both in the normal as well as in the high pressure form. The results will be presented and discussed in this paper.

EXPERIMENTAL

The alloys were prepared by arc-melting in an argon atmosphere appropriate amounts of the metals. They were then heat treated at about 500°C for several days, in sealed evacuated quartz glass tubes. X-ray powder patterns revealed that the annealed samples were single phase materials and had the Sm-type structure. High pressure and temperature treatment was carried out in a piston cylinder apparatus. Samples were normally subjected to 40 kbar and 500°C for about 5 hours. After this treatment temperature was reduced to ambient and pressure released. The X-ray patterns of the specimens were then recorded. Magnetic susceptibility measurements were carried out with a pendulum magnetometer[6] down to 1.4°K.

RESULTS

All the alloys except CeY transformed to dhcp structure (La-type) and the high pressure phase is retained on release of pressure. Under similar pressure and temperature treatment, CeY broke down to the elements. In Table I the pertinent crystallographic data are presented. Although no attempt was made to locate the transition pressures precisely, it would seem from the results that the transition pressure increases in the sequence LaY < PrY < NdY. With NdY conversion to dhcp was only

Table I. Crystallographic Data

	Sm-Type Phase		La-Type Phase	
	a(Å)	c(Å)	a(Å)	c(Å)
$LaGd_3$	3.65±.02	26.33±.01	3.63±.02	11.79±.01
LaY	3.70±.02	26.65±.01	3.69±.02	11.85±.01
PrY	3.65±.02	26.25±.01	3.62±.02	11.68±.01
NdTm	3.60±.02	26.00±.01	3.60±.02	11.50±.01

partial under the experimental conditions stated above. Preliminary studies on NdHo and NdGd which have also the Sm-type structure indicate that a transformation to the dhcp structure (La-type) takes place in these.

The results of magnetization measurements are presented in Figs. 1 (Sm-form) and 2 (dhcp-form) for $LaGd_3$ and Figs. 3 (Sm-type) and 4 (dhcp-type) for NdTm. In the case of $LaGd_3$ a kink in the curve occurs at about 120°K for the Sm-form (See Fig. 1). The curve for NdTm shows a peak for the Sm-form at about 32°K (See Fig. 3). In either case, the curves for the dhcp form appear to be smooth. Fig. 5 is the data for Sm taken at 15300 oersteds and represents our earlier measurements.[1] Curve 1 is the data for the dhcp phase and 2 for the normal form of Sm. The latter has a kink in the curve at about 110°K and the dhcp form shows a very much enhanced anomaly at about 100°K. A sharp peak in magnetization occurs at 14.8°K for the normal phase of Sm and at 28°K for the dhcp phase.

DISCUSSION

Crystal structure and size relationship

In the rare earth metals pressure induced phase transformations have been shown to occur in the sequence hcp → Sm-type → dhcp → fcc.[1] The results of the present study indicate that the intra-rare earth alloys also fit into this sequence; the Sm-type invariably transforming to the

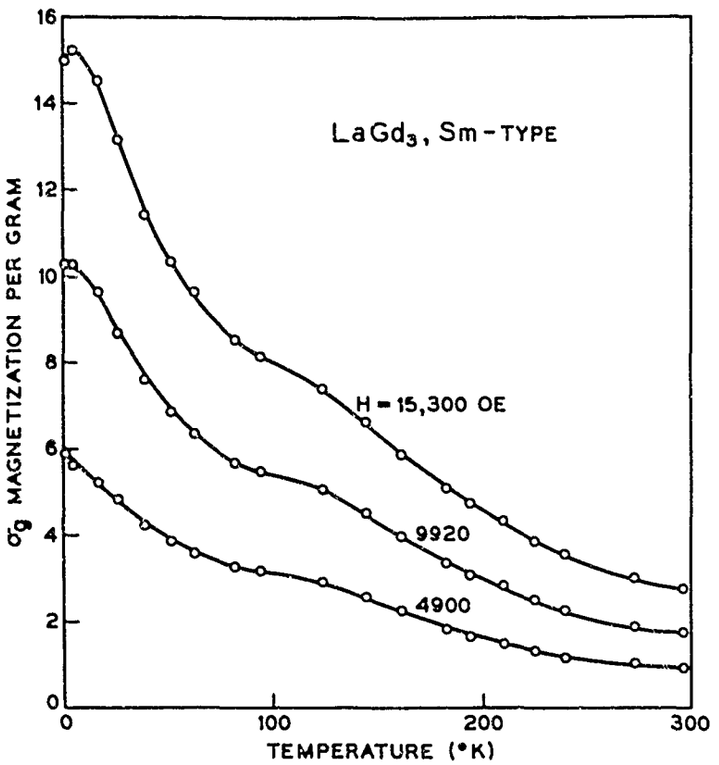

Fig. 1 Magnetic data for Sm-form of $LaGd_3$.

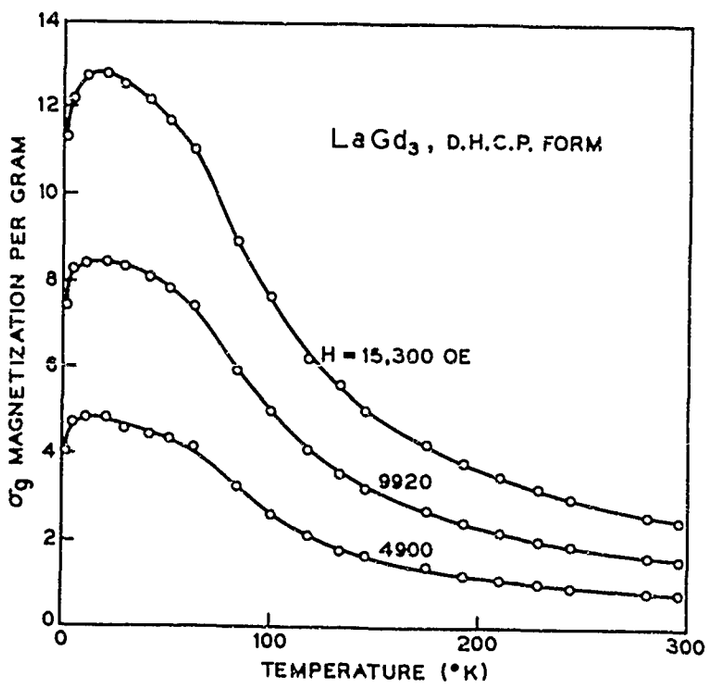

Fig. 2 Magnetic data for dhcp $LaGd_3$.

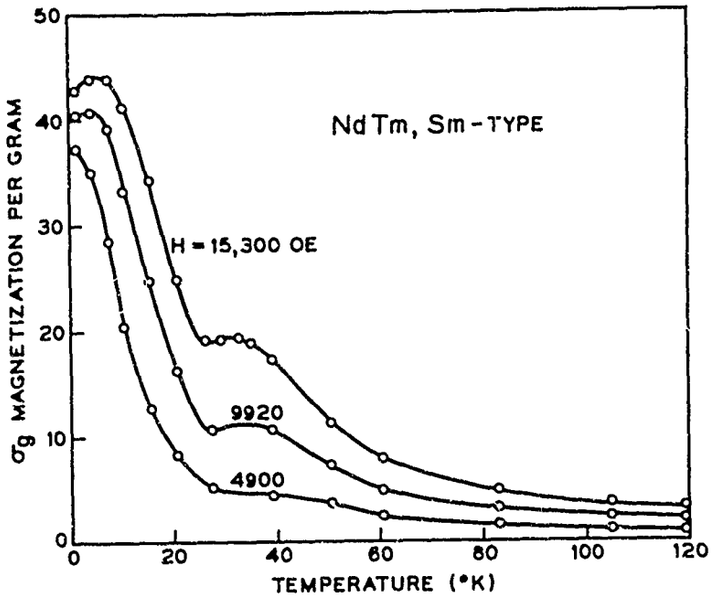

Fig. 3 Magnetic data for Sm-form of NdTm.

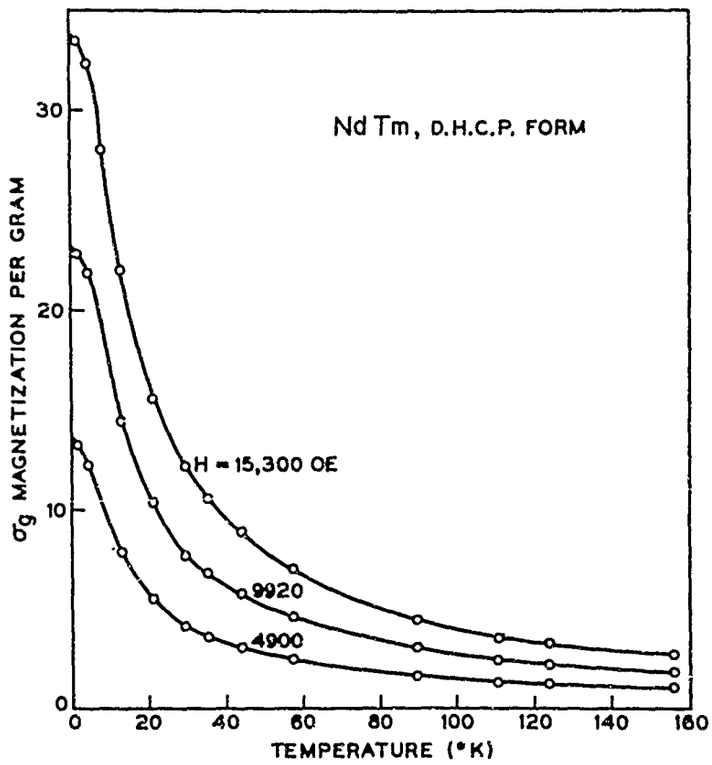

Fig. 4 Magnetic data for dhcp NdTm.

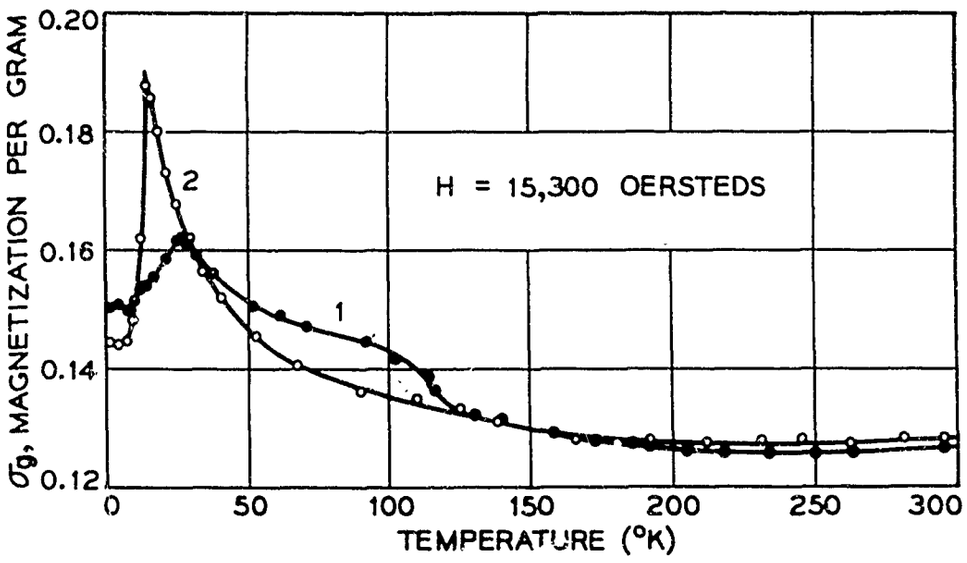

Fig. 5 Magnetic data for Samarium.

dhcp structure (La-type) under pressure.

The behavior of CeY can be rationalized as follows. Gschneidner et al.[8] have investigated the effect of the addition of Y on the γ to α-Ce transformation and find that the transition pressure rises with the addition of Y. In the γ to α-Ce transition the metallic radius of Ce changes from 1.824 Å to 1.71 Å.[10] It is suggested that the Ce atoms in CeY undergo this reduction in radius under pressure, resulting in a drastic change in the Ce to Y radius ratio. It must be that this change in radius ratio is incompatible with the stability of the Sm-type structure and causes the breakdown of the Sm-type CeY to the elements. In Table II are tabulated the radius ratio

Table II. Radius Ratio For the R.E. Alloys

	La	Ce^{3+}	Ce^{4+}	Pr	Nd
Y	1.06	1.026	0.956	1.032	1.028
Tm	-	-	-	-	1.034
Ho	1.053	1.02	-	-	1.022
Gd	1.041	1.008	-	-	1.01

(metallic radius) of the lighter rare earth to the heavier R.E. element or Y for several alloys crystallizing in the Sm-type structure. For Gd which transforms under high pressure and temperature (~35 kbar and 350°C) to the Sm-type structure[11] and for Sm, this ratio is unity. In the case of Ce^{4+} the radius ratio would be substantially lower than unity and is the only exception (See Table II). Thus it appears that the stability of the Sm-type structure in the intra-rare earth alloys is controlled by the size of the constituent atoms and apparently for a radius ratio less than unity, neither the Sm-type structure nor the dhcp structure is stable.

Magnetic behavior

The magnetic behavior of Gd-La and Gd-Y alloys has been studied by Thoburn, Legvold and Spedding.[12] According to these authors $LaGd_3$ has a poorly defined antiferromagnetic maximum at about 130°K. In our measurements on $LaGd_3$ (Sm-type), an anomaly in the magnetization curve is evident at about 120°K. The Sm form undergoes probably some kind of ordering at this temperature. In the magnetization curve for the dhcp form any such anomaly is not evident. The effective moment per Gd calculated from the susceptibility data in the paramagnetic region yields 8.45 and 8.8 Bohr magnetons for the Sm and dhcp forms of $LaGd_3$ respectively. At 4.2°K the magnetization increases with the field and at 80 kilo gauss, Gd is contributing 1.82 and 1.62 Bohr magnetons to the moment in the Sm-form and dhcp form respectively and the magnetization curves show very definitely some remanence in both forms. It is therefore believed that at very low temperatures (4.2°K) both forms are in all probability ferrimagnetic. Another possibility is that a very large crystal anisotropy prevents the attainment of a higher moment and in both forms, $LaGd_3$ is ferromagnetic. Lacking single crystal data we are unable to be more definite on this. In the Gd-Y alloys[12] an alloy of composition 95% Gd and 25% Y is ferromagnetic and Gd contributes its full moment 7.63 μ_β at a field of 17.5 k-oersteds. However the Gd-Y alloys are hcp in the entire compositional range and apparently have low crystal anisotropy.

Davis and Bozorth[13] studied Tm metal and reported a maximum in the susceptibility curve indicative of antiferromagnetic ordering at about 60°K. According to them Tm should be ferromagnetic below 22°K as it shows a hysteresis loop. Jennings, Hill and Spedding[14] have found

a specific heat anomaly at 55°K in Tm metal, presumably connected with magnetic ordering. Koehler, Cable, Wollan and Wilkinson[15] studied by neutron diffraction the magnetic structure of Tm down to very low temperatures and have reported evidence for an oscillatory type antiferromagnetic configuration (spiral or helical type) below 55°K. The structure adopted by Tm at very low temperatures is a type of antiphase domain-type structure in which there is a net moment of 1.0 Bohr magneton, due to incomplete cancellation. For an alloy of 89.4% Tm-10.6% La[16] which is hexagonal close packed, Koehler et al. found that the Néel temperature lowered to 36°K with the Curie point at 31°K. NdTm in the Sm-type structure would appear to be similar to Tm in magnetic behavior in many respects. From the anomaly in the magnetization curve (See Fig. 3) it is deduced that NdTm (Sm-type) orders antiferromagnetically at about 30°K. It exhibits a hysteresis loop at very low temperatures (our data was taken at 1.3°K) and is presumably therefore ferro or ferrimagnetic. The Curie temperature would seem to be near about 10°K. There does not appear to be any susceptibility anomaly indicative of ordering in the dhcp form of NdTm near 30°K and the magnetization curve is quite smooth in this region (See Fig. 4). At very low temperatures (1.4°K) the dhcp form also shows a hysteresis loop which would imply ferrimagnetic or ferromagnetic ordering. The effective moment P^2_{eff} calculated from the susceptibility data in the paramagnetic region for the two forms is near 68 which compares favorably with the theoretical value of 70.8 computed using $g(J(J+1))^{1/2}$ of 3.62 and 7.6 for tripositive Nd and Tm respectively.

Lock[17] investigated the magnetic behavior of Sm-metal and noticed a sharp decrease in the susceptibility,

characteristic of antiferromagnetic ordering at 15°K, and a kink in the curve between 110°K to 150°K. Anomalies in heat capacity have been reported by Jennings et al.[18] at 105° and 13.8°K. Features similar to those observed by Lock were obtained by Jayaraman and Sherwood in the magnetization curve for the normal form of Sm. For the pressure-induced dhcp form there was a much more pronounced kink in magnetization around 100°K. Further, the peak (See Fig. 5) occurring at the lower temperature has shifted to 27°K and is somewhat smaller in magnitude.

McWhan and Stevens[19] have suggested that the double peaks observed in the A.C. susceptibility of Sm-form of Gd, Tb and Dy represent ordering of hexagonal (H) layers and cubic (C) layers at different temperatures, in analogy with the behavior of Nd. In the latter metal neutron diffraction studies[20] in the range 1.6° to 20°K have shown that the hexagonal site layers (H) and the cubic site layers (C) present in the structure order at different temperatures, the former (H) at 19°K and the latter (C) at 7.5°K. McWhan, Jayaraman and Sherwood (to be published) suggest that in the Sm-metal also, the cubic and hexagonal layers order at different temperatures. The kink in the magnetization curve at the higher temperature (100°K-120°K) we believe is due to ordering of the (C) layers and the low temperature peak (27°K and 14°K) associated with the ordering of (H) layers. The specific heat measurements of Jennings et al. give a considerably higher entropy under the 105°K maximum in the C_P than that under the low temperature maximum, which would seem to suggest the opposite sequence for the ordering. Our suggestion is based on the following facts. In the normal form (rhombohedral structure) the hexagonal to cubic layer ratio is 3 to 1 while in the dhcp it is 1 to 1. Since the kink in the

magnetization curve at the higher temperature is much more pronounced for the dhcp form, it must be associated with the ordering of the cubic layers for, the ratio of (C) to (H) layers increases in going from the normal form to the dhcp form of Sm. It would also follow that in the dhcp form the peak associated with ordering of (H) layers should diminish. This is precisely what is observed.

We wish to thank D. B. McWhan, T. H. Geballe and H. J. Williams for discussions and R. G. Maines for technical assistance in the high pressure experiments.

REFERENCES

1. A. Jayaraman and R. C. Sherwood, Phys. Rev. 134A, 691, (1964).
2. "The Rare Earths" Editors, F. H. Spedding and A. H. Daane, John Wiley and Sons (1961).
3. "Rare Earth Alloys", K. A. Gschneidner Jr., Van Nostrand (1961).
4. F. Nachman, C. E. Lundin and G. Rauscher, Technical Report No. 1 Contract No. Nonr- 3661 (02) (1963).
5. C. E. Lundin and J. G. Nachman, Technical Report No. 2, Contract No. Nonr- 3661 (02) (1964).
6. R. M. Bozorth, H. J. Williams and D. E. Walsh, Phys. Rev. 103, 572 (1956).
7. R. Valetta (A. Daane), Dissertation Abstr., 20, 3539 (1960).
8. K. A. Gschneidner Jr., R. O. Elliott and R. R. McDonald, J. Phys. Chem. Solids 23, 1201, (1962).
9. K. A. Gschneidner Jr. and R. Smoluchowski, Jour. Less. Comm. Met. 5, 274, (1963).
10. A. W. Lawson and T. Tang, Phys. Rev. 76, 301, (1949).
11. A. Jayaraman and R. C. Sherwood, Phys. Rev. Letters 12, 22 (1964).

12. W. C. Thoburn, S. Legvold and F. H. Spedding, Phys. Rev. 110, 1298, (1958).
13. D. D. Davis and R. M. Bozorth, Phys. Rev. 118, 1543, (1960).
14. L. D. Jennings, E. Hill, and F. H. Spedding, J. Chem. Phys. 34, 2082, (1961).
15. W. C. Koehler, J. W. Cable, E. O. Wollan and M. K. Wilkinson, Phys. Rev. 126, 1672, (1962), J. Appl. Phys., 33, 1124 (1962).
16. W. C. Koehler, J. Appl. Phys. 36, 1078, (1965).
17. J. M. Lock, Proc. Phys. Soc. (London) B70, 566, (1957).
18. L. D. Jennings, E. D. Hill and F. H. Spedding, J. Chem. Phys. 31, 1240, (1959).
19. D. B. McWhan and A. L. Stevens, Phys. Rev., to be published.
20. R. M. Moon, J. W. Cable, and W. C. Koehler, J. Appl. Phys. Suppl. 35, 1041, (1964).

VALENCE BOND FORMATION IN THE CLOSE-PACKED RARE EARTH METALS

Forrest L. Carter

U.S. Naval Research Laboratory, Washington, D. C.

ABSTRACT

A modified Valence Bond treatment of the close-packed metals has been developed subject to the restrictions that: 1) all near neighbors are bound simultaneously, 2) equivalent atoms form equivalent bonds, and 3) certain periodic boundary conditions. The use of bidirectional orbitals having the general characteristics $ap_x + \sqrt{1-a^2}\, d_{xy}$ give rise to various 'phase structures' involving 'cycles' of old VB theory. In the ccp and hcp structures this leads to a natural division of the electrons and orbitals into those associated with 1) a band of covalent bonds, 2) a MO band having s-character for free electrons and 3) localized orbitals not directed toward near neighbors and suitable for containing unshared electrons.

In the ccp structure the pertinent orthonormal set of bonding orbitals contain 50% d character ($a = \frac{1}{\sqrt{2}}$) whereas in the hcp the p and d character of the bidirectional orbital can change, giving rise to a variation of C/A with d character. At d character of ca. 58% the C/A value has a minimum of approximately 1.54 and rises to the ideal C/A = 1.63 at a d character of 50% and 67%.

The trivalent rare earth metals form a near ideal system to test these ideas inasmuch as the local states of s, p, or d character are unoccupied and the three electrons per atom appear to be involved primarily in the covalent band rather than a free electron band.

The presence of both hexagonal and cubic closest packing in the light (Ce $\rightarrow$ Sm) rare earth metal structures is in accord with the observed C/A of ca. 1.62 and percent d character of ca. 50% in the bifurcated bonding orbitals. Thereafter the observed C/A drops to a minimum near Er and starts to rise again at Lu. The general behavior is the same as indicated by the theory for increasing amounts of d participation in the bonding orbitals. The latter is expected to occur with increasing atomic number because the d energy levels fall more rapidly than the p levels and are accordingly used to a greater extent in (shared electron) orbital occupation.

Introduction

Valence Bond treatments of metals occur rather infrequently and are becoming less popular, with the possible exception of Paulings's semi-empirical discussion of the metallic radii.[1] The reason for the decline is due in part to the immense computational difficulties of a VB treatment of a solid. However the decline may be attributed primarily to the success of band treatments which not only are computationally simpler but also provide an energy estimate for excited states; information of considerable import for those interested in transport problems. Nevertheless the VB treatment of molecules results in ground state calculations which are significantly better than the MO (or 'molecular' band) treatment as a direct consequence of permitting greater correlation between electrons.

Accordingly we might renew our faith in the directed bond of VB theory and take courage, as some chemists[2] have, from the belief that the glue that holds together the carbon atoms of diamond is also responsible for cohesion in metals. To this end we note that in terms of the simpler concepts of VB theory in combination with the bidirectional bond introduced[3] previously that we can give a simple qualitative explanation of the observed variation of C/A in the hcp rare earth metals. In short the variation of C/A is a result of the increasing stability of the 5d orbital relative to the 6p orbital as a function of increasing atomic number.

Electron Classes - Although proper quantum theory forbids the labeling or identifying of individual electrons or electron groups, it is a wide spread practice and conceptually a very useful one to talk about the "core electrons" or the "valence electrons", etc. Accordingly the total energy of a crystalline solid may be similarly divided as in Eqn. 1.

$$E_{Total} = \begin{matrix} E_{\text{Rare Gas Core}} + E_{\text{Local Unshared Electrons}} \\ + E_{\text{Bonds}} + E_{\substack{\text{Bands} \\ \text{(Free Electrons)}}} + E_{\text{Magnetic}} + E_{\text{etc.}} \end{matrix} \quad (1)$$

The first term of the equation is obvious and needs no discussion. The second, third, and fourth terms, however, are of particular interest in that they are intimately interconnected (as we shall see) via the orthogonality conditions occuring in the formation of bidirectional bonding orbitals. The second term will, in the rare earth metals, be related primarily to the electrostatic energy of unshared, paired and/or unpaired, electrons of the f orbitals because the two

localized orbitals of d-p character will not be occupied. These localized orbitals will have unfavorable directionality for bonding or will have small radial extension.

The bond orbitals of the present discussion are bidirectional and accordingly have lobes directed simultaneously to two near neighbors. We may expect crude measures of strength, such as melting point, etc. to be related to the overlap and promotion energy of such orbitals. Another feature of the present treatment is that in addition to the localized orbitals and bonding orbitals, other orbitals largely of s character remain. With these we are free to construct Bloch type wave functions for development of a modified free electron treatment.

The $E_{(magnetic)}$ term is considered to arise from the interaction of clouds of diffuse magnetic dipole distribution of primarily localized electrons and not to the electron repulsion effects that are the source of the magnetic dipole. While these terms are of considerable interest they will not be discussed further here.

It is clear that the fourteen rare earth metals are going to constitute a very important testing ground for numerous physical theories. Further we believe that this series constitutes a unique test for a theory of chemical bonds in metals. That uniqueness resides in the following features of the rare earth metals: 1. In general the three valence electrons are only weakly interacting with the unshared electrons, a situation which is not true in the transition metals. 2. A gradual change takes place in the relative energies of atomic levels involving 5d, 6s, and 6p states. 3. Most important, the three valence electrons (excluding Ce, Eu) are primarily involved in bond formation, in contradistinction to being involved in a free electron type role. In support of the last item we note the following: (a) The rare earth metals are metallic conductors of unusually high resistivity.[4] Speaking loosely we might say that the conducting electrons are very much involved in the local picture (or are frequently scattered compared to the free electron treatment). (b) Augmented plane wave calculations are in distinct disagreement with the free electron model.[5] (c) Heats of atomization for the elements at STP are fully consistent with the involvement of three electrons per atom in strong bond formation.[2]

Bonding in the Close-Packed Metal Structures - Bidirectional bonds of the same form can be used to discuss the bonding in both the cubic and hexagonal structures. This discussion presumes that the 6s, 6p, and 5d orbitals are sufficiently close in energy to permit bond hybridization, however, let us defer the consideration of f orbitals till later.

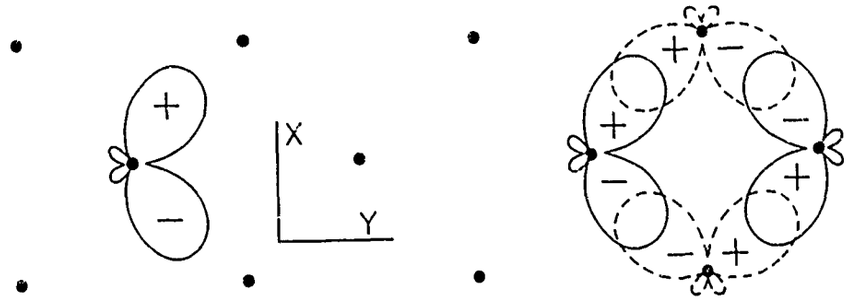

Fig. 1. A C-orbital of the form $1/\sqrt{2}\ p_x + 1/\sqrt{2}\ d_{xy}$ is shown in the (001) plane of the fcc structure. In part b we see how such C-orbitals on nearby atoms can be used to form a cycle involving four atoms with good overlap between them.

Cubic close-packed bonding. In the ccp structures each atom has 12 near neighbors, with four of these forming a square array in each principle plane. This is illustrated in Fig. 1a where a bidirectional bond of the form $ap_x + \sqrt{1-a^2}\ d_{xy}$ is used to bond the two atoms to the right. If $a = \frac{1}{\sqrt{2}}$ a second orbital equivalent and orthogonal to the first may be used to form bonds to the two atoms on the left. Similar and mutually orthogonal bonds may be formed in the two other perpendicular planes for bonding the other eight near neighbors. Such orbitals correspond to an electron density distribution of C_{2v} symmetry and have been indicated by the term C-orbital in a discussion of the rare earth chalcogenides having the Th_3P_4 structure.[3] The six C-orbitals of the ccp structure have been also used in a consideration of bonding in the distorted icosahedral coordination of the β-tungsten structure.[6]

If the six C-orbitals comprise the bonding orbitals employing the d_{xy}, d_{xz}, d_{yz}, p_x, p_y, and p_z atomic orbitals in hybrid formation, then the remaining orbitals are the $d_{x^2-y^2}$, d_{z^2}, and s states.

The $d_{x^2-y^2}$ and d_{z^2} orbitals are local in character in that they are directed away from all near neighbors. The s orbital is of course non-directional and may be used as a basis for a Bloch function which, at the atomic sites, is orthogonal to the bonding orbitals in the first approximation.

Hexagonal close-packed bonding. The same general situation obtains in the hexagonal close packed structures. Six C-type orbitals (somewhat distorted from C_{2v} symmetry) are used to bond the twelve near neighbors, two per C-orbital, one neighbor in the basal plane and one neighbor above or below the basal plane. These orbitals cannot

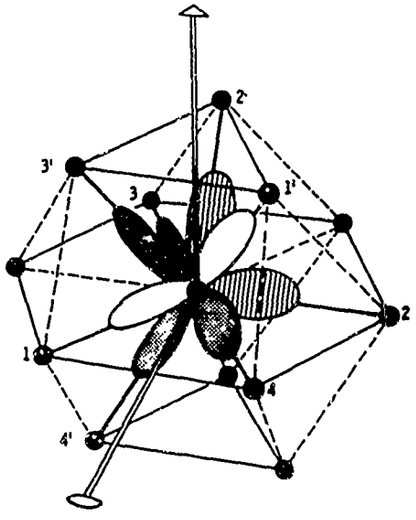

Fig. 2. This shows the 12 nearest neighbors of the central atom in the hcp arrangement; 6 in the basal plane, three above, and three below. The C-orbitals are represented schematically by the shape of their large lobes in the plane containing the central atom and the lobe maxima; the small lobes are not indicated. Each of the six orthogonal C-orbitals binds two atoms which are at right angles at the central atom, e. g. No. 1 and No. 1'.

be obtained by inspection however, as can those of the cubic structure, and we must use more general methods. Let us take a function of the form Eqn. 2 and from it

$$\text{Ⓗ} = A\,s + Bp_x + Cp_y + Dp_z + Ed_{xy} + Fd_{xz} + Gd_{yz} + Hd_{x^2-y^2} + Id_{z^2} \tag{2}$$

obtain five others according to the point symmetry 32. If these six general orbitals are to be mutually orthogonal and normalized the above coefficients must satisfy the following conditions:

$$A^2 + I^2 = D^2 = 1/6 \tag{3}$$

$$B^2 + G^2 + H^2 = 1/3 \tag{4}$$

$$C^2 + E^2 + F^2 = 1/3 \tag{5}$$

$$BC = EH + FG \tag{6}$$

Inasmuch as the 3 fold axis is taken along the Z direction we see that except for sign the p_z component will be the same for each of the 6 orbitals (the same will be true for the s and d_{z^2} orbitals). Accordingly the p_z orbital will be employed in its entirety in the formation of the orbitals corresponding to the point group 32. At our current level of approximation the same will be roughly true of the d_{z^2}

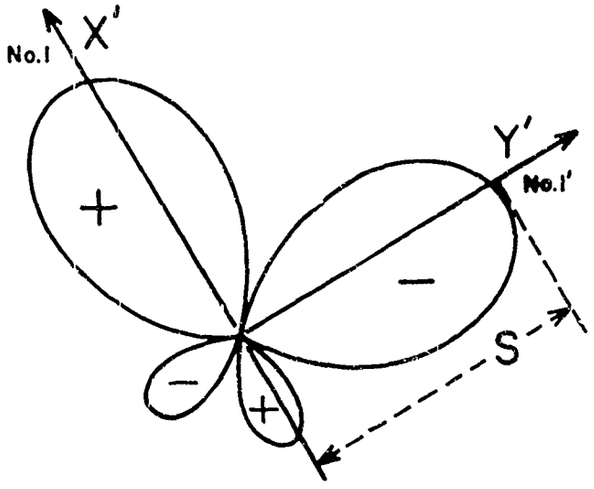

Fig. 3. This indicates the shape of a C-orbital in the plane of its lobe maxima. This orbital contains 66.6% d character and can be used for bonding in the hcp structure. The coefficients, in terms of Eqn. 2, are A=0, B=-C =-F=-G=1/$\sqrt{12}$, D=E=-H-I =-1/$\sqrt{6}$.

orbital. This follows from Eqn. 3 and the fact that s character in the bond will be small because it is spherical and has small directed radial extension; therefore overlap will fall off with large amounts of s character.

In Fig. 2 we have schematically illustrated the relationship of the various C-orbitals of Eqns. 2 to 6 to one another and the twelve nearest neighbors in the hcp structure. For example, atom No. 1 of the basal plane and atom No. 1' of the upper three atoms are joined by a C-orbital. This orbital is related to the orbital joining atoms No. 2 and 2' by a 120° rotation about the 3 fold axis (z direction). The orbitals joining atoms No. 2 and 2' and No. 3 and 3' are similarly related. The C-orbital whose lobes are directed toward atoms No. 4 and 4' is related to C-orbital 1-1' by a 2 fold rotation about the x axis. The two remaining orbitals not shown are related to C-orbital 4-4' by the 3 fold rotation axis.

If we inspect a C-orbital of the hcp structure in the plane containing the origin and the two maxima of the lobes as in Fig. 3 we see that indeed it is very similar to the C-orbital of the ccp structures, Fig. 1. There is another important point to note in Fig. 3, i.e., the atoms joined by the C-orbital form a right angle; hence this is true in both the hcp and ccp structures.

Having formed six C-orbitals for bonding, from a basis of nine atomic orbitals, it is clear that three orbitals remain. One of these, composed of 6s plus $5d_{z^2}$ character, will be suitable for the atomic part of a Bloch function. The d_{z^2} character here will be small, of course, if little s character is used in the C-orbitals. The other two

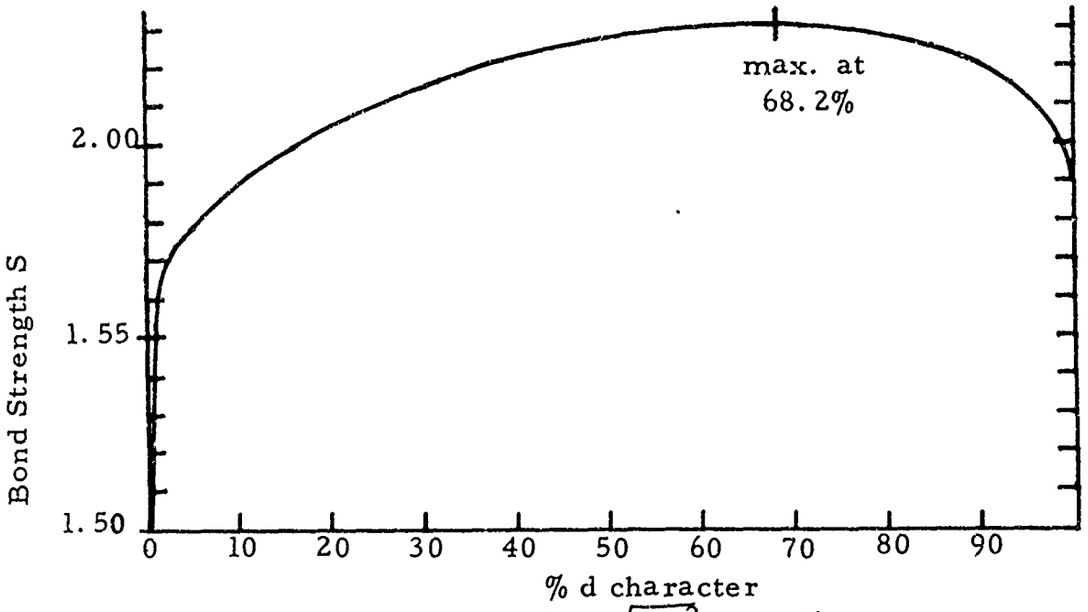

Fig. 4. Bond strength S vs $\sqrt{1-a^2}$ x 100 % for an angle between bonds of 90°

orbitals, of 5d and 6p character, may be expected to have small overlap with neighboring atoms and hence can be described as local in character.

We have argued above on the basis of electrical conductivity, heats of atomization, etc., that small occupation is expected of a band (composed here of 6s + $5d_{z^2}$ character) having a free electron aspect. In addition there is even less reason to suppose that the localized orbitals would be occupied.

We may then suggest that since the bonding electrons of the heavier rare earths will have small interaction with either the localized electrons or the Bloch electrons these metals constitute an excellent testing ground for the theories of bonding in metals.

Variation of Bond Strength with d character - Earlier it was noted that the two atoms bound by the C-orbitals form a right angle. Using a generalized notion[5b] of Pauling's concept of the bond 'strength' S of an orbital we may examine the effect of varying the amount of d character of a C-orbital. This amounts to taking the maximum projection of the angular component of the lobe on the pertinent internuclear axis as is indicated in Fig. 3. For an orbital of pure C_{2v} symmetry this variation is illustrated in Fig. 4. We note that only for small and large amounts of d character does the strength S fall off drastically. Therefore it remains to determine the direction of the non-basal plane lobe with variation in d character.

Variations of C/A with d-character - An approximation to the variation of the hexagonal C/A ratio with the amount of d character in the C-orbital is obtainable from the following stratagem. An orbital of the type $ap'_x + \sqrt{1-a^2}\, d'_{xy}$ is rotated about the z' axis by an angle ω ($\omega \cong -45°$) until the maximum of the positive lobe is a little past the x' axis. The negative large lobe then lies along the +y' direction (see Fig. 3). The orbital is then rotated about the x' axis by an angle γ which then directs the negative lobe toward one of the atoms above the basal plane. The angle γ is related to the C/A ratio by Eqn. 7.

$$\tan \gamma = \left(\frac{C}{A}\right) \frac{\sqrt{3}}{2} \tag{7}$$

This C-orbital is then in the same relationship to the near neighbors as is C-orbital 1-1' of Fig. 2 if we take the x' axis as the internuclear axis between the central atom and atom No. 1 and the Z and Z' axes as the same. If the coefficients of p'_z and d'_{z^2} are expressed in terms of the angles ω and γ and set equal to $\frac{1}{\sqrt{6}}$ then ω can be eliminated to give an expression, Eqn. 8, between γ and a^2, the amount of p character.

$$\sin^2 \gamma = \frac{a^2}{3}\left(\frac{1}{1-a^2} + \frac{1}{2a^4}\right) \tag{8}$$

By combining Eqns. 7 and 8 we plot C/A as a function of d character in Fig. 5. Three points are important: (1) a given C/A does not correspond to a unique value of d character in the C-orbital; (2) large amounts of p character ($>50\%$) and small amounts of p character ($<33\%$) correspond to high C/A ratios and are not pertinent to a C-orbital description since the lobes become quite disimilar; (3) a minimum C/A value is observed at 58% d character. C-orbitals satisfying all the orthogonality conditions (Eqns. 3-6) do not rise as fast as does the curve of Fig. 5 near high values of d character. Similar curves will be presented at the conference for various ratios of the projected maxima of the two lobes according to bond order-bond length considerations.

C/A in the Rare Earth Metals - As the atomic number of the rare earth metal increases we may expect the 5d orbitals to become increasingly stable relative to the 6s orbital while the 6p state will be relatively constant; this is schematically illustrated in Fig. 6. In view of our arguments concerning the (non) use of the 6s orbital in bond formation, we are really interested in the increasing separation between 6p and 5d levels. As this separation increases with atomic number more d character will be involved in the C-orbital bonding at the expense of p character. According to Fig. 5 we may expect the C/A ratio to

decrease to a minimum and then to increase again as the d character approaches 67%. Such a variation of C/A is observed in the heavier trivalent rare earths (see Fig. 7).

Another point of interest is that at 50% d character Fig. 5 shows the C/A to be ideal (i.e., 1.63) which is the same value as occurs in the ccp structure. However since orthogonality conditions require the C-orbital to also have 50% d character in the cubic structures we have a continuous transition from the ccp to hcp structures in terms of the composition of the C-orbital. This is essentially observed in the layer phases of the lighter rare earths (Fig. 7) which contain both cubic and hexagonal close packing with a C/A just a little below the ideal value of 1.63. In the heavier rare earth metals we may expect less participation in layer structures because then a larger promotion energy would be associated with the cubic sites.

F Orbital Participation in Bonding - In Fig. 6 we note that the energies of the 6p, 6s, 5d, and 4f orbitals are rather close in the lighter rare earths. It would not be surprising then if f orbitals played a role in the bonding. In particular we remark here that the f orbitals are of odd symmetry like the p orbitals and can be employed in a similar fashion in the formation of C-orbitals. In fact they can be used in combination with d_{xy} type orbitals to give lobes whose maxima make an angle of 90° or somewhat less, whereas the p orbital does not have this property. In this possibility may reside the explanation for the C/A not declining with atomic number before Sm. In the heavier rare earths however we may presume that the radial part of the f orbital is so concentrated that it no longer is able to make a contribution to the bonding.

Final Remarks - The bidirectional nature of the C-orbital permits the atom in question to bind two neighbors per C-orbital if the signs (or phases) of the overlapping lobes are the same. By requiring the matching of phases, atoms are linked together in chains or rings of even number of atoms. Rings or cycles involving four atoms could be formed in the ccp structures (Fig. 1b) and would lead to strong bond formation. Such rings can also be formed in the hcp structures but appear to have somewhat less overlap. Cycles, as rings or chains, can be used to form 'phase structures'[3),6)], in which all atoms are consistently bonded and which may or may not have the same periodicity of the lattice.

It is necessary to say something about the symmetry of the C-orbitals in relation to the higher symmetry we expect for electron bond density. We note that the C-orbitals in Fig. 2 are related by point symmetry 32 whereas the atom site in the crystal has higher symmetry due to the presence of mirror planes. This symmetry is

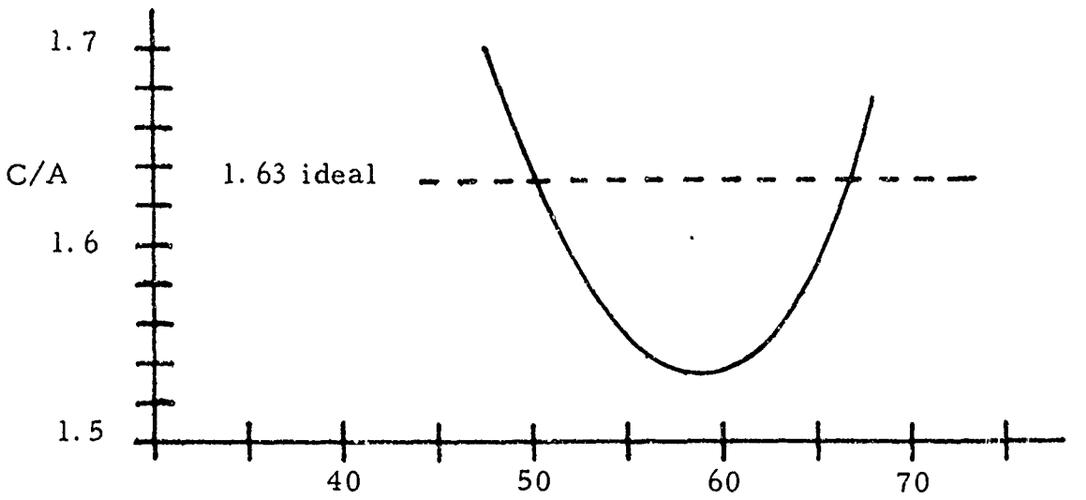

Fig. 5. % d-character vs C/A

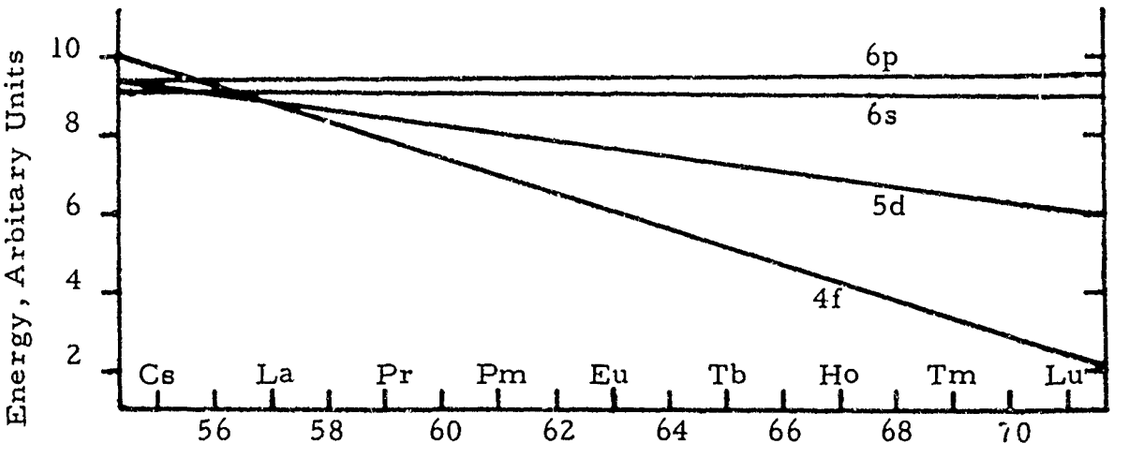

Fig. 6. Schematic energy levels of 6s, 6p, 5d, 4f orbitals versus atomic number (after Ref. 4).

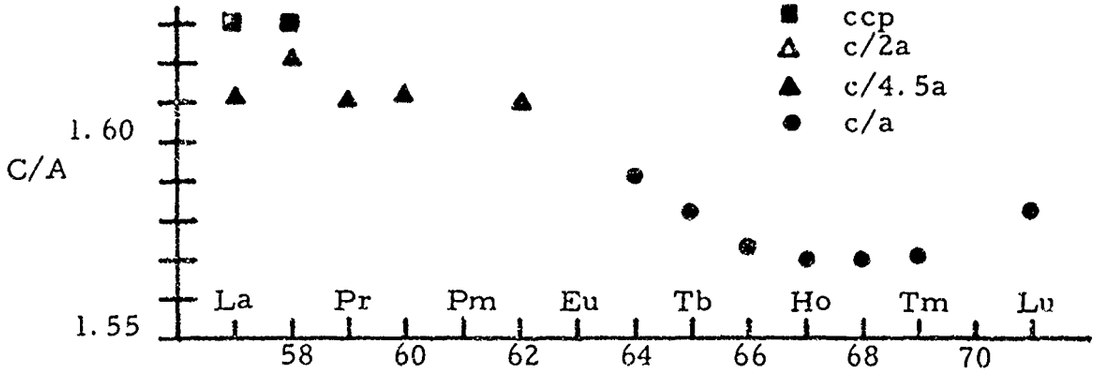

Fig. 7. Observed C/A ratio vs atomic number (after Ref. 4) for the trivalent rare earth metals

restored if we consider the mirror image of Fig. 2 is equally likely. Phase structures containing one or both enantimorphic forms of Fig. 2 can be devised. The same situation applies to the C-orbitals in ccp positions. It is worth noting further that transitions between hcp and ccp layers can be discussed by means of cycles and phase structures where each atom is consistently bonded (in terms of phase signs and orientation of lobes) to all its neighbors.

Finally we note that the use of this form of covalent binding does not deny these metals their electrical conductivity since the number of electrons per atom is insufficient to fill these 'covalent bands'[3].

References

1. L. Pauling, "The Nature of the Chemical Bond", 3rd Ed., Cornell University Press, Ithaca (1960)

2. L. Brewer, "Electronic Structure and Alloy Chemistry of the Transition Elements", (Edit. by P.A. Beck, Interscience Publishers, New York, 1963) p. 221 ff.

3. F.L. Carter, "Rare Earth Research" (Vol. III, Edit. by L. Eyring, Gordon and Breach Science Publishers, New York, 1965)

4. A.H. Daane, "The Rare Earths" (Edit by F.H. Spedding and A.H. Daane, John Wiley, New York, 1961) p. 177 ff; K.A. Gschneidner, p. 190 ff.

5. A.J. Freeman, Spring Meeting of Amer. Phys. Soc., Wash., D.C., 26-29 April 1965

6. F.L. Carter, 'Valence Bonding in Alloys Having the β-Tungsten Structure', to be published, Acta. Cryst.

UNCLASSIFIED
Security Classification

DOCUMENT CONTROL DATA – R&D

(Security classification of title, body of abstract and indexing annotation must be entered when the overall report is classified)

1 ORIGINATING ACTIVITY (Corporate author)
Iowa State University
Department of Physics
Ames, Iowa

2A REPORT SECURITY CLASSIFICATION
☒ Unclassified
☐ Other — Specify

2B. GROUP

3 REPORT TITLE
Rare Earth Research Conference 5th Ames, Iowa 30 Aug-1 Sep 1965 Books 1-6. Spectra Bk 1; Solid State bks 2,4 & 6; Chemistry Bk 3; Metallurgy Bk 5

4 DESCRIPTIVE NOTES (Type of report and inclusive dates)
☐ Scientific Report ☒ Final Report ☐ Journal Article ☐ Proceedings ☐ Book

5. AUTHOR(S) (Last name, first name, initial)
(Legvold Sam Dr (PI)

6 REPORT DATE AS PRINTED	7A. TOTAL NO. OF PAGES	7B. NO. OF REFS
September 1965	718	811

8A. CONTRACT OR GRANT NO. AF-AFOSR-812-65
B. PROJECT NO. 9760-01
C. 61445014
D.

9A. ORIGINATOR'S REPORT NUMBER(S) (If given)

9B. OTHER REPORT NO.(S) (Any other numbers that may be assigned this report)
AFOSR 65-1917
AD

10 AVIALABILITY/LIMITATION NOTICES
Distribution of this document is unlimited

☒ Available from DDC
☒ Available from CFSTI
☐ Available from Source
☐ Available Commercially

11. SUPPLEMENTARY NOTES (Citation)

12. SPONSORING MILITARY ACTIVITY
AF Office of Scientific Research (SRC)
Office of Aerospace Research
Washington, D. C. 20333

13 ABSTRACT

A total of 69 papers were presented at the Rare Earth Research Conference. The papers, with abstracts, are contained in 6 volumes. Book 1 deals with spectra; Books 2, 4, and 6, solid state; Book 3, chemistry; and Book 5, metallurgy. (U)

DD FORM 1473
1 JAN 64

UNCLASSIFIED
Security Classification

14 KEY WORDS	LINK A		LINK B		LINK C	
	ROLE	WT	ROLE	WT	ROLE	WT
Metallurgy Rare Earth Elements Solid States Spectra Symposia						

INSTRUCTIONS

1. ORIGINATING ACTIVITY: Enter the name and address of the contractor, subcontractor, grantee, Department of Defense activity or other organization *(corporate author)* issuing the report.

2a. REPORT SECURITY CLASSIFICATION: Enter the overall security classification of the report. Indicate whether "Restricted Data" is included. Marking is to be in accordance with appropriate security regulations.

2b. GROUP: Automatic downgrading is specified in DoD Directive 5200.10 and Armed Forces Industrial Manual. Enter the group number. Also, when applicable, show that optional markings have been used for Group 3 and Group 4 as authorized.

3. REPORT TITLE: Enter the complete report title in all capital letters. Titles in all cases should be unclassified. If a meaningful title cannot be selected without classification, show title classification in all capitals in parenthesis immediately following the title.

4. DESCRIPTIVE NOTES: If appropriate, enter the type of report, e.g., interim, progress, summary, annual, or final. Give the inclusive dates when a specific reporting period is covered.

5. AUTHOR(S): Enter the name(s) of author(s) as shown on or in the report. Enter last name, first name, middle initial. If military, show rank and branch of service. The name of the principal author is an absolute minimum requirement.

6. REPORT DATE: Enter the date of the report as day, month, year; or month, year. If more than one date appears on the report, use date of publication.

7a. TOTAL NUMBER OF PAGES: The total page count should follow normal pagination procedures, i.e., enter the number of pages containing information.

7b. NUMBER OF REFERENCES: Enter the total number of references cited in the report.

8a. CONTRACT OR GRANT NUMBER: If appropriate, enter the applicable number of the contract or grant under which the report was written.

8b, 8c, & 8d. PROJECT NUMBER: Enter the appropriate military department identification, such as project number, subproject number, system numbers, task number, etc.

9a. ORIGINATOR'S REPORT NUMBER(S): Enter the official report number by which the document will be identified and controlled by the originating activity. This number must be unique to this report.

9b. OTHER REPORT NUMBER(S): If the report has been assigned any other report numbers *(either by the originator or by the sponsor)*, also enter this number(s).

10. AVAILABILITY/LIMITATION NOTICES: Enter any limitations on further dissemination of the report, other than those imposed by security classification, using standard statements such as:

(1) "Qualified requesters may obtain copies of this report from DDC."

(2) "Foreign announcement and dissemination of this report by DDC is not authorized."

(3) "U. S. Government agencies may obtain copies of this report directly from DDC. Other qualified DDC users shall request through _____."

(4) "U. S. military agencies may obtain copies of this report directly from DDC. Other qualified users shall request through _____."

(5) "All distribution of this report is controlled. Qualified DDC users shall request through _____."

If the report has been furnished to the Office of Technical Services, Department of Commerce, for sale to the public, indicate this fact and enter the price, if known.

11. SUPPLEMENTARY NOTES: Use for additional explanatory notes.

12. SPONSORING MILITARY ACTIVITY: Enter the name of the departmental project office or laboratory sponsoring *(paying for)* the research and development. Include address.

13. ABSTRACT: Enter an abstract giving a brief and factual summary of the document indicative of the report, even though it may also appear elsewhere in the body of the technical report. If additional space is required, a continuation sheet shall be attached.

It is highly desirable that the abstract of classified reports be unclassified. Each paragraph of the abstract shall end with an indication of the military security classification of the information in the paragraph, represented as *(TS), (S), (C), or (U)*

There is no limitation on the length of the abstract. However, the suggested length is from 150 to 225 words.

14. KEY WORDS: Key words are technically meaningful terms or short phrases that characterize a report and may be used as index entries for cataloging the report. Key words must be selected so that no security classification is required. Identifiers, such as equipment model designation, trade name, military project code name, geographic location, may be used as key words but will be followed by an indication of technical context. The assignment of links, roles, and weights is optional.